Volatile metal mobility and fluid melt partitioning: Experimental constraints and applications to degassing magmas

by

Jason MacKenzie
MSc., University of Victoria, 1999
BSc., Acadia University, 1996

A Dissertation Submitted in Partial Fulfillment
of the Requirements for the Degree of

DOCTOR OF PHILOSOPHY

in the School of Earth and Ocean Sciences

Supervisory Committee

Volatile metal mobility and fluid melt partitioning: Experimental constraints and applications to degassing magmas

by

Jason MacKenzie
MSc., University of Victoria, 1999
BSc., Acadia University, 1996

Supervisory Committee

Dr. Dante Canil (School of Earth and Ocean Sciences)
Supervisor

Dr. Kevin Telmer (School of Earth and Ocean Sciences)
Departmental Member

Dr. Laurence Coogan (School of Earth and Ocean Sciences)
Departmental Member

Dr. Alexandre Brolo (Department of Chemistry)
Outside Member

Abstract

Supervisory Committee
Dr. Dante Canil (School of Earth and Ocean Sciences)
Supervisor
Dr. Kevin Telmer (School of Earth and Ocean Sciences)
Departmental Member
Dr. Laurence Coogan (School of Earth and Ocean Sciences)
Departmental Member
Dr. Alexandre Brolo (Department of Chemistry)
Outside Member

Volatile trace metals are variably enriched in volcanic gases. Metal concentrations in sub-aerially erupted magmas are also depleted in many of these metals. The causes of variable metal enrichment in volcanic gasses, however, remain enigmatic. The objective of this work is to place experimental constraints on kinetic and thermodynamic factors that influence the concentrations of trace metals in volcanic gases. To measure metal mobility in silicate melts, Pt crucibles packed with metal doped glasses of broadly basaltic composition were equilibrated with air and mixed gases at atmospheric pressure. The metals in the melt diffused to the gas/melt interface where they were released as a volatile species. The experiments produced concentration-distance profiles from which diffusivity was derived. Experiments were also conducted in a piston-cylinder apparatus at 1 GPa pressure. In these experiments, melts were equilibrated with Cl-bearing fluids at high temperature and pressure. At equilibrium, trace metals partitioned between the melt and fluid phase as a function of temperature and fluid composition. The diffusivity of Re in melts of natural basalt, andesite and a synthetic composition in the CaO-MgO-Al_2O_3-SiO_2 (CMAS) system has been investigated at 0.1 MPa and 1250-1350°C over a range of fO_2 conditions from log fO_2 = -10 to –0.68. Re diffusivity in natural basalt at 1300°C in air is $\log D_{Re}$ = -7.2 ± 0.3 cm^2/sec and increases to $\log D_{Re}$ = -6.6 ±0.3 cm^2/sec when trace amounts of Cl were added to the starting material. At fO_2 conditions below the nickel-nickel oxide (NNO) buffer Re diffusivity decreases to $\log D_{Re}^{reducing}$ = -7.6±0.2 cm^2/sec and to $\log D_{Re}^{andesite}$ = -8.4 ± 0.2 cm^2/sec in andesite melt. Cd, Re, Tl, Pb, Sb and Te diffusivity in CMAS and Na_2O-MgO-Al_2O_3-SiO_2 (NMAS) melts were also determined at 0.1 MPa and 1200-1350°C. In the CMAS composition at 1300°C, the fastest diffusing element was Cd having a $\log D_{Cd}$ = -6.5 ± 0.2. The slowest element was Re with $\log D_{Re}$ = -7.5 ± 0.3. Diffusivities of Sb, Te, Pb and Tl have intermediate values where $\log D_{Sb}$ = -7.1 ± 0.1, $\log D_{Te}$ = -7.2 ± 0.3, $\log D_{Pb}$ = -7.1 ± 0.2, $\log D_{Tl}$ = -7.0 ± 0.2 cm^2/sec. In the NMAS composition, $\log D_{Re}$ = -6.5 ± 0.2, $\log D_{Sb}$ = -6.0 ± 0.2, $\log D_{Pb}$ = -6.1 ± 0.1, $\log D_{Tl}$ = -5.8 ± 0.2 cm^2/sec. Fluid/melt partition coefficients ($Kd_x^{f/m}$) of Re, Mo, W, Tl and Pb between fluid (H_2O + Cl) and a haplobasaltic melt in the CMAS system were

measured between 1200 and 1400°C at 1 GPa and fluid chlorine molarities from 7.7 to 27 mol/L. At 1300°C and fluid molarity of 7.7 mol/L, $Kd_{\mathrm{Re}}^{f/m}$ = 9.8±1.8, $Kd_{Mo}^{f/m}$ = 11.8±1.6, $Kd_{W}^{f/m}$ = 3.7±1.6, $Kd_{Tl}^{f/m}$ = 4.5±1.4 and $Kd_{Pb}^{f/m}$ = 2.4 ±1.8. Both Mo and Re were shown to partition most strongly into the fluid at all temperatures and fluid chlorinities. Differences in diffusivity of volatile heavy metal ions to a lead to significant fractionation between these metals in magmas during degassing. Given the observed differences in Cd and Re diffusivities, an increase in the normalized Cd/Re ratio in the gas phase with increasing bubble growth rate is predicted. Monitoring of the Cd/Re ratios in aerosols from degassing volcanoes may provide a tool for predicting volcanic eruption. Modeling of Re using the values measured here support the contention that subaerial degassing is the cause of lower Re concentrations in arc-type and ocean island basalts compared to mid-ocean ridge basalts. The model results were also compared with emanation coefficients for trace metals from natural volcanoes. The magnitudes of the modeled Re/Tl and Re/Pb in fluids at 1300°C and the lowest fluid chlorinities were less than that observed from their emanation coefficients. Re and Pb are more sensitive to fluid chlorinity than Tl. The ratios of Re/Tl and Re/Pb expected from emanation coefficients are closely matched if partitioning values for experiments having fluid chlorinities of ~16-20 *M*Cl at 1300°C are used.

TABLE OF CONTENTS

LIST OF TABLES

LIST OF FIGURES

ACKNOWLEDGMENTS

Above all, I wish to thank Dr. Dante Canil for providing the opportunity to study under his mentorship. His leadership and knowledge proved invaluable during the course of this study. I am exceptionally grateful for his patience and understanding, his ability to challenge, and willingness to let me find my own way and make my own mistakes. I also appreciated Dante's open door and generous contributions of time and equipment. I could not have done this study without him and would not have become the person I am without him. I am proud to have learned under his tutelage and call him a friend.

I am grateful to Dr. Mati Raudsepp (UBC) for his continued help with microprobe work. Mati taught me everything about electron microscopy and his attention to detail and value cannot be understated. Visits to UBC always put a smile on my face and his time was appreciated.
Many thanks to Dr. Jody Spence (UVIC) for his assistance with ICPMS and help making solution standards and calibrations. Thanks also to Dr. Abigail Barker (UVIC) for showing me how to do acid digestions without killing myself and Dr. Adam Monahan (UVIC) for his help with modeling and mathematical treatment of my data.

During my time in the lab at UVIC I was fortunate to have worked with many other students. I want to thank Dr. Yana Fedortchouk (Dalhousie) for calibrating the piston-cylinder and helping with experimental design. I enjoyed our discussions regarding science, careers and parenting. I had a lot of laughs and good times with T-Knuckles and thank him for his help with calculating fO2. Thanks also to Zhihuan Wan and J-Rock for helping make the lab fun. I also want to thank all the undergraduate students that have come and gone through the years for their interest and questions. They made my time at UVIC very rewarding.

This work would not have been possible without the unwavering support of my beautiful wife, Melissa MacKenzie. I want to sincerely thank her for her patience, belief in me, and for going the extra mile raising our son during the many hours I spent away from home. Her love and strength were a constant source of inspiration.

I also want to thank Mary Widmer for helping myself and my family during the course of this study. Finally, I want to thank my son Spencer for keeping me aware of what is truly important; playing.

I dedicate this thesis to my grandfather
CLIFFORD MCMULLEN
who was one of the most inquisitive people I have ever known
and my parents
MILLARD and SANDRA MACKENZIE
who supported me throughout my education

CHAPTER 1.

INTRODUCTION

All magmas contain small amounts of dissolved volatiles (H_2O, CO_2, SO_2). As magmas rise and decompress from their source regions to the Earth's surface, they release volatile species into a fluid or gas phase due to decreasing solubilities in the silicate melts with decreasing pressure (Carroll and Holloway, 1994). This exsolved fluid/gas phase feeds persistent quiescent and active volcanic degassing.

The study of volcanic gases has largely focused on the most abundant major volatiles including H_2O, CO_2 and SO_2 (Carrol and Blank, 1997; Pineau et al., 1998; Winther et al., 1998; Morizet et al., 2002; Freda et al., 2003; Nowack et al., 2004; Freda et al., 2005; Aiuppa et al., 2007) with lesser studies on halogens (Cl, F, Br and I) (e.g., Signorelli and Carrol, 2000; Webster and De Vivo, 2002; Bureau and Metrich 2003; Aiuppa and Federico, 2004; Botcharnikov et al., 2004; Giordano et al., 2004). The reasons for studying the major volatiles in magmas are rooted in their impact on melt structure, vesiculation, complexing in metal transport and volcanic eruption.

The trace metal contents of volcanic gases have received much less attention even though volcanic gases may account for up to 50% of the natural sources of these metals (including cadmium and lead) in the environment (Nriagu, 1989). Much of the lack of interest in metal contents of volcanic gases was related to the overwhelming evidence that metals are primarily transported by low temperature aqueous fluids and not by a primary volcanic fluid or an evolved gas phase (Williams-Jones et al., 2002). Metal transport in a gas phase has received renewed attention in recent years by ore deposit

researchers (e.g., Williams-Jones et al., 2002) who recognized that vapour may indeed be an important metal transport agent. High concentrations of rare metals and the discovery of economically viable metallic mineral deposits in volcanic vents (e.g., Korzhinsky et al., 1994; Taran et al., 1995) also suggest volcanic gases may be important transport mediums.

Volcanic gases are sampled from lava lakes and fumaroles (Stoiber, 1995) and only recently have become monitored at active volcanoes (Aiuppa et al., 2007) by flying aircraft through volcanic plumes. Advances in spectrographic techniques allow for characterization of gases at a safe distance away from an actively erupting volcano. Gases are collected in evacuated vessels and allowed to pass through filters, forming condensates, and also through spectroscopic detectors and sensors designed for the analysis of a specific gas (Giggenbach, 1975). Volcanic eruptions are notoriously difficult to predict thus these measurements are limited to but a few active volcanoes that show more frequent and regular activity (e.g., Kilauea, Hawaii; Mt. Etna in Italy).

The major drawback of sampling gases at the surface is, invariably, secondary processes have modified such samples. Mineral condensation on to conduit walls and dilution and interaction with meteoric water and hydrothermal systems(Hinkley et al., 1994) all act to change the primary composition. As such, volcanic gases measured at the surface likely do not unambiguously represent equilibrium values with the melt from which they are sourced. The modified nature of volcanic gases influences models that estimate the flux of these metals across geochemical reservoirs.

The danger and cost associated with monitoring gases in volcanoes combined with the unpredictable nature of eruptions highlights the utility of experimental studies in

understanding the evolution of volcanic gases. Experiments in controlled environments provide an effective means to constrain many aspects of magma degassing including controls on the composition of gases. Experimental studies can also be compared with natural data, and perhaps, find utility in guiding field studies that measure such data. Experimental studies also do not suffer from secondary processes affecting measurements of natural samples. However, because natural systems are always altered by some secondary process and experimental studies are conducted under a limited range of conditions, comparing experimental data with natural data must always be viewed with caution.

Volcanic aerosols, plumes and fumarolic gasses are variably enriched in volatile metals (Lambert et al., 1986; Crowe et al., 1987; Pennisi et al., 1988; Hinkley et al., 1994; Allard et al., 2000; Nriagu and Becker, 2003; Norman et al., 2004). Furthermore, volcanic gases can significantly fractionate families of trace metals from one another during degassing (Hinkley et al., 1994) but our knowledge of the underlying causes of element fractionation remain poor. For example, in a sample set of volcanic gases from Kilauea, Crowe et al. (1987) showed that chalcophile metals Cd and Cu have enrichment factors that vary by over four orders of magnitude.

From an empirical evaluation of volcanic gas data Aiuppa et al. (2007) have shown that quantitative forecasting of volcanic eruptions is possible by real-time monitoring of the CO_2/SO_2 ratio. Alletti et al. (2007) have shown that differences in sulphur and halogen mobilities cause them to fractionate and monitoring S/F, Br/F, Cl/F ratios may also be useful in predicting eruptions. Finally, Crowe et al. (1987) suggested

that monitoring trace metal ratios, specifically the Cd/Re ratio, in volcanic fumes during passive degassing could provide a tool for predicting volcanic eruptions.

Volatile depletion and vapour transport of metals out of silicate liquids requires: 1) the exsolution of volatile species from the melt during depressurization and formation of fluid bubbles, 2) diffusion of metal to a melt/fluid interface (bubble wall) and 3) partitioning of a metal species into the bubble followed by release of this fluid. Melt viscosity, oxidation state and speciation potentially affect all three of these processes as well as the speciation of an element in both the melt and gas phases. The major volatiles (H_2O, CO_2, SO_2, HCl) act as solvents for the metals or as ligands with which the metals complex. With a fluid/gas phase present, metals in the melt must diffuse through the melt to reach a melt/fluid interface that can be measured as a diffusion rate. Once a metal arrives at a melt/fluid interface, its concentration in the fluid is governed by its partition coefficient between the melt and fluid.

The overall goal of this thesis is to provide constraints on the kinetic and thermodynamic factors that affect the evolution of trace metals in degassing magmas and to address the scarcity of experimental information on which to quantify and predict true metal behaviour in magmas and magmatic gases. The findings of this dissertation are presented in three manuscripts (Chapters 2, 3 and 4).

Chapter two entitled “Experimental constraints on the mobility of rhenium in silicate liquids.” uses experimentally derived diffusion coefficients to address models of Re depletion in basalts from different tectonic settings. The Re contents of ocean-island basalts (OIB), arc-type basalts or MORB are governed by the behaviour of this element in their mantle source region and its mobility during ascent and emplacement of magma.

The differences in Re contents in basalts from different tectonic environments may be caused by volatile release during the emplacement of arc magmas and OIB (Lassiter, 2003; Sun et al., 2003a) or reflect Re partitioning into garnet and/or residual sulphides in the source regions. Twenty nine experiments using three natural and synthetic basalt compositions and a single andesitic composition were carried out. The experiments were performed in one atmosphere furnaces at magmatic temperatures and varying oxygen fugacity (fO_2) conditions. This work provided composition-distance profiles from which diffusivity could be derived and the influence of fO_2, composition and temperature evaluated. The resulting data provided a basis from which the above models could be addressed.

Chapter three applies the experimental method outlined in Chapter 2 to several volatile metals including Re. The paper "Volatile heavy metal mobility in silicate liquids: Implications for volcanic degassing and eruption prediction" evaluates differences in metal diffusivities in silicate liquids. Thirteen experiments in two synthetic compositions were performed and diffusivities of Re, Pb, Tl, Sb, Cd and Te were determined as functions of melt composition and temperature. The results of this study were modelled using a 1-D bubble growth model to evaluate the changes in the concentration of trace metals in bubbles as functions of changing bubble growth rate, temperature and radius assuming some partition coefficients for the metals involved. Attributable to differences in trace metal diffusivities, the model predicts an increase in the Cd/Re ratio in pre-eruptive volcanic gases; a prediction supported by natural data. The modeling not only confirms that monitoring the Cd/Re ratio may provide a tool for predicting eruptions (Crowe et al., 1987) but also addresses the underlying mechanism for changes in the

Cd/Re ratio over an eruption cycle. Understanding and providing a method to quantify the fundamental underlying mechanisms of trace metal enrichment in volcanic gasses provides a framework for future investigations.

Chapter 4 entitled “Fluid/melt partitioning of Re, Mo, W, Tl and Pb in the system haplobasalt -H_2O-Cl and the volcanic degassing of trace metals” builds on the findings of Chapters 2 and 3 in an effort to constrain the partition coefficients between melt and fluid for the metals). Consisting of 17 experiments in four different compositions partition coefficients were determined using mass balance. Combining the partition coefficients with diffusion measurements from the previous studies facilitates model refinement and provides information related to speciation of metals in the fluid phase.

Metal mobility and partitioning control the metallic composition of primary volcanic fluid/gas phases and the evolution of volcanic gases en-route to the surface where they are ultimately sampled. Aiuppa et al. (2007) note, “It is generally accepted, but not experimentally proven, that a quantitative prediction of volcanic eruptions is possible from evaluation of volcanic gas data”. This dissertation is a major step towards providing the missing experimental proof and provides a framework for further investigation.

Contribution of the authors:

I carried out all the experiments, data collection and interpretation. I wrote all the chapters and Dr. Dante Canil reviewed and suggested editorial changes. Two of the papers have undergone peer review and are published in international journals including Chapter 2 (MacKenzie, J.M. and Canil, D. (2006) Experimental constraints on the

mobility of rhenium in silicate liquids. *GEOCHIMICA ET COSMOCHIMICA ACTA*, Volume 70, Issue 20, pp 5236-5245) and Chapter 3 (MacKenzie, J.M., and Canil, D. (2008) Volatile heavy metal mobility in silicate liquids: Implications for volcanic degassing and eruption prediction. *Earth and Planetary Science Letters, Volume 269, Issues 3-4*,p *488-496)*. Chapter 4 is submitted for publication as of this writing.

CHAPTER 2.

EXPERIMENTAL CONSTRAINTS ON THE MOBILITY OF RHENIUM IN SILICATE LIQUIDS

Jason M. MacKenzie

Dante Canil

University of Victoria School of Earth and Ocean Sciences

Victoria, BC, Canada,V8W 3P6

2.1 ABSTRACT

The volatization of Rhenium (Re) from melts of natural basalt, andesite and a synthetic composition in the CaO-MgO-Al_2O_3-SiO_2 (CMAS) system has been investigated at 0.1 MPa and 1250-1350°C over a range of fO_2 conditions from log fO_2 = -10 to -0.68. Experiments were conducted using open top Pt crucibles doped with Re and Yb. Analysis of quenched glasses by laser ablation inductively coupled plasma mass spectrometry (LA-ICP-MS) normal to the melt/gas interface showed concentration profiles for Re, to which a semi-infinite one-dimensional diffusion model could be applied to extract diffusion coefficients (D). The results show Re diffusivity in basalt at 1300°C in air is $\log D_{Re} = -7.2 \pm 0.3$ cm^2/sec and increases to $\log D_{Re} = -6.6 \pm 0.3$ cm^2/sec when trace amounts of Cl was added to the starting material. At fO_2 conditions below the nickel-nickel oxide (NNO) buffer Re diffusivity decreases to $\log D_{Re}^{reducing} = -7.6 \pm 0.2$ cm^2/sec

and to $\log D_{Re}^{andesite} = -8.4 \pm 0.2$ cm^2/sec in andesite melt. In the CMAS composition, $\log D_{Re}^{CMAS} = -7.5 \pm 0.1$. The diffusivity of Re is comparable to Ar and CO_2 in basalt at 500 MPa favoring its release as a volatile. Our results support the contention that subaerial degassing is the cause of lower Re concentrations in arc-type and ocean island basalts compared to mid-ocean ridge basalts.

2.2. INTRODUCTION

Rhenium is a moderately incompatible element whereas Osmium is a highly compatible element retained in the mantle during melt extraction to form the crust (Shirley and Walker, 1998). These unique geochemical properties highlight the utility of the Re-Os isotopic system in studies of magma genesis (Righter and Hauri, 1998), crustal recycling (Becker, 2000; Sun et al., 2003a) and mantle evolution (Brenan et al., 2003).

The Earth's major geochemical reservoirs include mid-ocean ridge basalts (MORBs), depleted MORB mantle, continental crust and the primitive mantle. Constraints regarding Re and Os abundances and isotopic ratios in these reservoirs are continually evolving, but experimental data on the behaviour of Re and Os at high P and T are limited, creating uncertainty in models for the distribution of these elements in the solid earth system. For example, in numerous geochemical studies, Re has been shown to exhibit a range of behaviours from volatile (Lassiter, 2003) and chalcophile (Alard et al., 2002), to siderophile and moderately incompatible lithophile (Righter and Hauri, 1998, Brenan et al., 2003, Sun et al., 2003a).

Sun et al. (2003a) suggested that the mantle-crust reservoirs are not balanced with respect to their Re contents and Re/lithophile-element ratios. Yb and Re are similarly

incompatible during formation of MORB, as evidenced by their restricted Re contents, (~0.926 ppb; Righter and Hauri, 1998) and Re/Yb ratios (~280 ppt/ppm; Hauri and Hart, 1997). In the depleted MORB mantle however, Re is strongly depleted relative to Yb. A mass balance between continental crust, depleted MORB mantle and primitive mantle indicates that the crustal abundance of Re is too low to balance the Re depletion estimated for depleted MORB mantle (Hauri and Hart, 1997) creating a paradox for the processes responsible for Re depletion in the mantle-derived melts.

The Re contents of ocean-island basalts (OIB), arc-type basalts or MORB are governed by the behavior of this element in their mantle source region and its mobility during ascent and emplacement of magma. The average Re concentrations in MORBs are 0.956 ± 0.349 ppb, considerably higher than in OIB (0.414 ± 0.235 ppb). The Re concentration in arc-type basalts is generally lower (0.233 ± 0.170 ppb) than both MORB and OIB but varies significantly from <1 to 800 ppt (Woodhead and Brauns, 2004) (Figure 2.1). The variability in the Re content of arc-type basalts could reflect complex interactions between melting and fluid release of subducted slabs and the overlying mantle wedge, or volatile release during the emplacement of arc magmas.

Righter and Hauri (1998) attributed differences in the Re contents between MORB and OIB to the presence of garnet in the mantle source of the latter magma type. In this model, the missing Re required to balance the crustal and mantle reservoirs is retained in garnet residual from partial melting. Alard et al. (2002) found elevated concentrations of Re in residual sulphides in peridotite xenoliths hosted in alkali basalts. This observation suggests residual sulfide phase can serve as a sink for the missing Re

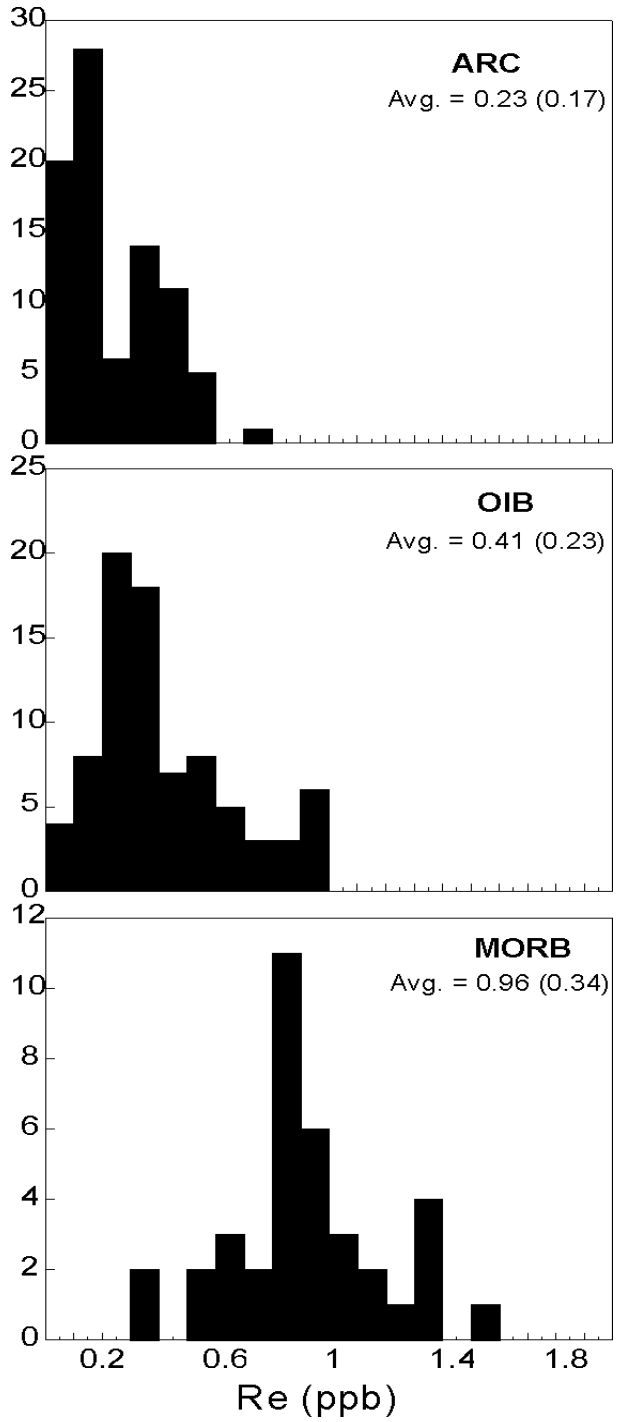

Figure 2.1. Histogram of Re contents from MORB, OIB and arc-type basalts showing arithmetic mean and 1σ standard deviation in brackets. Data sources are: MORB - (Roy-Barman and Allègre, 1994, Schiano et al., 1997, Woodhead and Brauns, 2004), OIB - (Widom and Shirey, 1996, Hauri and Kurz, 1997, Lassiter and Hauri, 1998, Bennett et al., 2000, Schiano et al., 2001, Lassiter, 2003), ARC - (Alves et al., 1999, Borg et al., 2000, Alves et al., 2002, Chesley et al., 2002, Woodhead and Brauns, 2004).

between OIB and MORB, but not all magmas are necessarily sulphide-saturated at their source.

Arc magmas are generally considered to be the major building blocks of continental crust (Sun et al., 2003a). As such, the Re contents of arc magmas should provide a good estimate of Re transfer from partial melting of the mantle to form the continental crust. Problematically, most Re analyses of arc magmas are from subaerially erupted samples (Lassiter, 2003; Sun et al., 2003a) which, if Re exhibits volatile behaviour, could serve to underestimate their Re contents and the resulting magnitude of Re transfer from the mantle to the continental crust.

There is convincing evidence that Re is volatile at volcanic edifices. Crowe et al. (1987) noted high Re concentrations in volcanic gasses from Kilauea volcano, Hawaii and established a Re flux of 2.4×10^{-2} mg/m^3. Re enrichment and pure Re-sulphide condensates have been observed in fumaroles from the Kudryavy volcano in Russia (Korzhinsky et al., 1994; Taran et al., 1995). Lassiter (2003) measured Re concentrations in lava sequences from drill core from the Mauna Loa volcano and found lower Re levels in those lavas calculated to have erupted subaerially. Further quantification of Re volatility and degassing from volcanic edifices requires knowledge of the behavior of Re in silicate liquids and its partitioning and transport behavior to and across melt/gas interfaces. Towards this end, the goal of this study is to measure the diffusivity of Re as a volatile element from silicate liquids as well as to establish the role of intensive variables (e.g., melt composition (X), T and fO_2) that control its mobility.

2.3 EXPERIMENTAL METHODS

To measure diffusion rates, we used Re-doped melts in contact with a gas phase. The technique uses the volatility of this element (Borisov and Jones, 1999) to establish a concentration gradient where Re in the melt must equilibrate with the atmosphere above it. The concentration gradients resulting from volatilization of Re were measured to investigate its chemical diffusivity in melts of different compositions and under different ambient fO_2 conditions. A similar experimental design was used to measure F diffusion in silicate liquids (Dingwell and Scarfe, 1985).

Starting materials were natural basalt (MIC99-8) from the Eocene Metchosin Igneous complex (Vancouver Island, BC), andesite (WP-1) from the Quaternary Watts Point lava dome (Squamish, BC) and a synthetic CaO-MgO-Al_2O_3-SiO_2 (CMAS) composition (Table 2.1). To prepare starting materials, basalt or andesite powder was ground in an agate mortar and dried at 100°C in air for one hour. Once dried, 1000 ppm NIST certified Re standard solution was added to each powder using a micropipette. The powder and solution were subsequently ground under alcohol for 10 minutes to homogenize the mixture. After drying, the mixture was loaded into a 25 mm diameter Pt crucible and fused in air at 1500°C for 24 hours prior to quenching to a glass. A fourth composition composed of MIC99-8 powder doped with 1000 ppm Re standard solution and 1000 ppm Cl (added as NaCl) was also prepared in this fashion.

For the CMAS composition, reagent grade SiO_2, Al_2O_3, MgO and $CaCO_3$ were mixed and ground as noted above. The mixture was decarbonated at 1000°C for 3 hours and then fused at 1500°C for 4 hours prior to quenching to a glass. Quenched glasses were crushed, re-ground and re-melted three times to homogenize the major elements

prior to adding 200µl of a 1000 ppm Re standard solution before the fourth and final melt/quench cycle.

All final starting glasses were crushed and ground to a powder. The glass is nearly completely oxidized at 1500° C in air over 24 hours and, in the Fe-bearing compositions, most Fe is present as Fe^{3+} as reported in Table 2.1 (MIC99-8 Fe^{3+}/Fe^{total} = 0.88, WP-1 Fe^{3+}/Fe^{total} =0.79). There is negligible Fe loss to the Pt crucible in an air atmosphere. Analyses of random chips of starting glasses indicate homogeneity in their major and trace element compositions (Table 2.1).

Powdered starting glass was loaded into 10 mm long 4 mm diameter Pt crucibles. For experiments in air, the crucible was held in a 4 x 4 x 3 cm ceramic carrier and placed in the pre-heated box furnace. For experiments at more reducing conditions, the crucible was suspended in a Deltech DT-31-V-OT vertical tube gas-mixing furnace. The crucible was introduced to the gas-mixing atmosphere, the furnace sealed, and the desired fO_2 was achieved after approximately 5 minutes. Oxygen fugacities were imposed using CO-CO_2 gas mixtures at total gas flow rates of 200 standard cubic cm/min, and continuously monitored using a solid zirconia electrolytic cell. Fluctuations in cell voltage were less than ± 10 mV during each experiment corresponding to ± 0.10 log fO_2 units. Temperature was measured using a type S ($Pt/Pt_{90}Rh_{10}$) thermocouple immediately above the crucible. Temperature fluctuations were ± 1°C in the box furnace and ± 3°C in the gas-mixing furnace. Experiments for variable run durations were quenched in a stream of dry air (Table 2.2). After each experiment, the charges, composed entirely of quenched glass, were sectioned axially into two pieces. One half was mounted in epoxy, polished and examined in reflected light.

2.4. ANALYTICAL METHODS

2.4.1. Electron microprobe

Major and minor elements in the run products were determined using a CAMECA SX50 electron microprobe (EMP) at the University of British Columbia at 15 kV acceleration voltage and a beam current of 20 nA with peak counting times of 30 seconds for Na, Mg, Al, Si, Ca, K, Ti, Cr, Mn and Fe. Chlorine and sulphur contents were below detection (500 ppm and 350 ppm, respectively) even with 300 second counting times at 10 kV acceleration voltage and a beam current of 50 nA. Major element profiles were collected perpendicular and parallel to the melt/gas interface as well as adjacent to the capsule walls (Figure 2.2). Major element concentrations were homogenous throughout the entire charge.

2.4.2. Laser ablation-inductively coupled plasma-mass spectrometry (LA-ICP-MS)

Line profiles of trace element concentrations were collected perpendicular to the melt/gas interface by LA-ICP-MS at the University of Victoria using a VG Elemental PQ II S+ ICP-MS. Laser ablation was conducted using a Merchantek solid-state, frequency quadrupled 266 nm Nd:YAG UV laser pulsed at a frequency of 20 Hz with an energy of ~1.8 mJ. NIST 613 SRM glass containing 6.57 ppm Re (Sylvester and Eggins, 1997) was used as a standard. The spot size and line scan traverse rate were 20 μm and 0.008 mm/sec, respectively. The detection limit for Re was 53 ppb. Data was collected in peak jumping mode with a dwell time of 10 milliseconds at one point per peak. ^{43}Ca was used as the internal standard for NIST SRM and experimental run products. Each block of

analyses consisted of measuring the NIST glass twice followed by <10 separate line scans before measuring the NIST glass twice again. Data was recorded as time resolved spectra in counts per second, collected over 360 seconds with 50 seconds allotted to collecting background concentrations. The spectra were then subdivided into 50 time slices, each representing ~50 μm of scan length. The individual time slices were reduced to concentrations using the PlasmaLab© data reduction software.

Trace element concentration profiles were collected perpendicular to the melt/gas interface (Figure 2.2) and at different locations along the interface. No distortions in the profiles by the presence of a meniscus at the glass/air interface were observed (Figure 2.3). We conducted similar line scans across the charge into the Pt crucible walls and observed no change in Re concentration within the glass at or near this boundary. We therefore conclude that Re diffusion was uni-directional to the melt/gas interface during the experiments. The thermal gradient along the length of our Pt crucibles is less than 1 °C as measured with a thermocouple. The Rayleigh number for the least viscous melt composition (MIC99-8) is less than 100 assuming planar geometry, a thickness of 1 cm and boundary conditions of $\Delta T = 1$ °C (Philpotts, 1990). The trivial thermal gradient and low Rayleigh number indicate that convection is negligible in our experimental design.

2.5. DATA REDUCTION

The volatility of Re from magma is a diffusion-controlled process limited by its diffusivity in silicate liquids (D_{Re}) and transport across a reacting interface (melt/gas). In practice, measuring D involves determining the actual transport distance and concentration gradients.

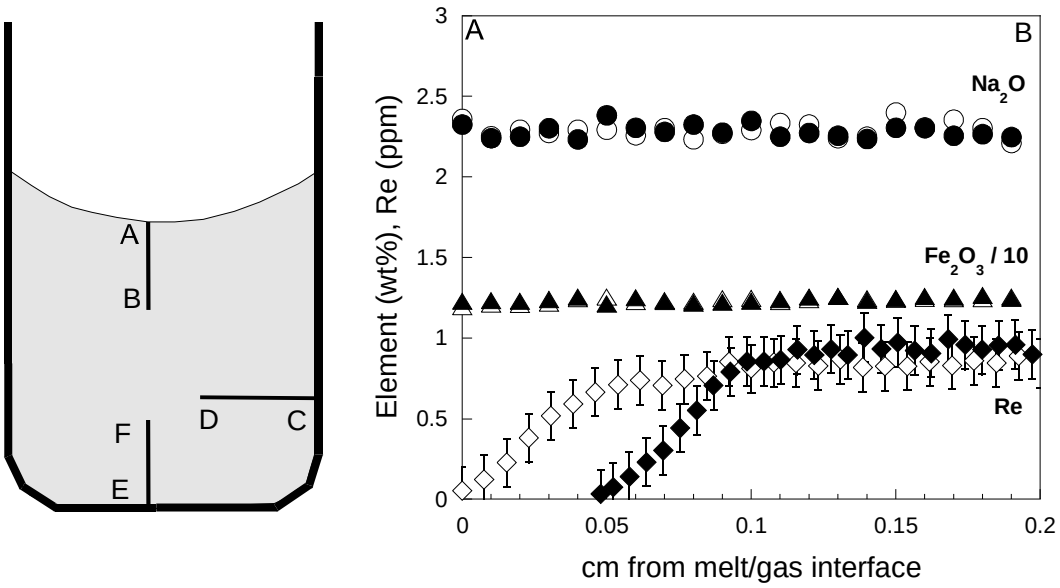

Figure 2.2. Left: schematic drawing of an experimental run product and locations of line scans (ICPMS (Re,Yb), EMP (major elements)). Charge diameter is 4 mm; height is 10 mm. Right: Rhenium and major element concentration profiles along transect A-B from melt/gas interface into glass. Rhenium profiles are shown for 6- (open diamonds) and 12-hr runs (solid diamonds). Na_2O and Fe_2O_3/10 profiles are shown for the same 6- (open circles/triangles) and12-hr runs (solid circles/triangles). Error bars for Re are calculated using 1σ counting statistics from ICPMS analysis. For Na_2O and Fe_2O_3 the size of symbols span the 1σ counting statistics from EMP analysis. No major element or Re concentration profiles were observed along transects C-D or E-F.

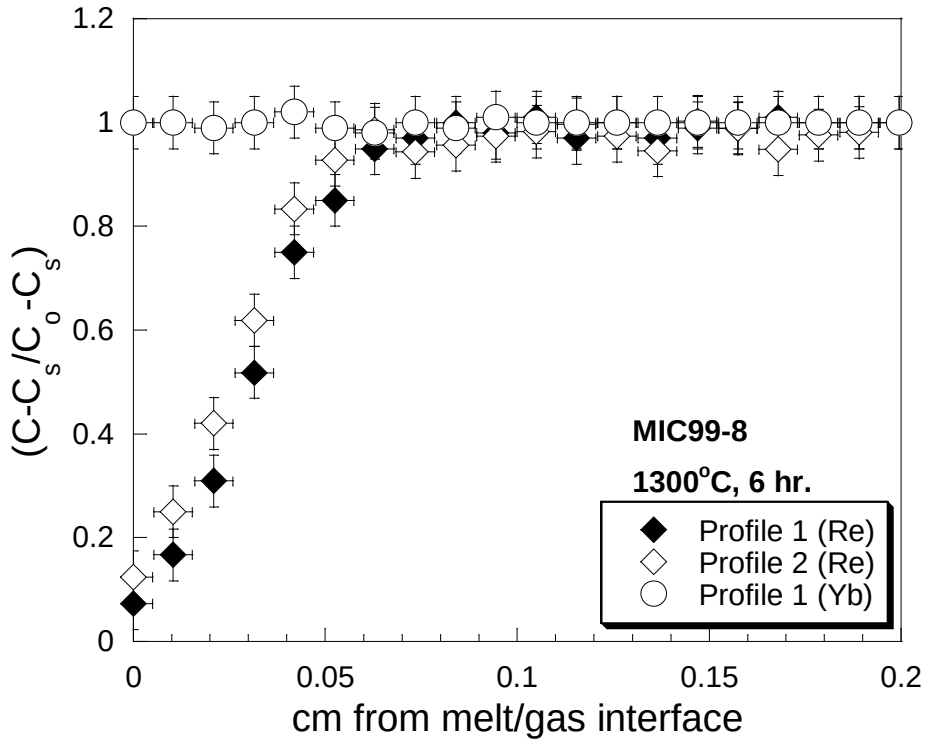

Figure 2.3. Normalized Re and Yb concentration versus distance from the melt/gas interface measured at two positions normal to the melt/gas interface for basalt composition MIC99-8. ($C-C_s/C_o-C_s$) error bars calculated at 1σ based on counting statistics. Distance error bars correspond to the scan distance for each time slice (~50 μm).

The ideal experimental design generally is such that the sample can be treated as a one-dimensional, semi-infinite medium (Chakraborty, 1995). In the geometry of our

experiments, which utilize open Pt crucibles, we assume the melt can be treated as a semi-infinite medium and the flux of species out the top as one-dimensional.

Crank (1975) derived mathematical relationships for diffusion in a one-dimensional, semi-infinite medium:

$$\frac{C - Cs}{Co - Cs} = erf\,\frac{x}{2\sqrt{(Dt)}} \qquad \text{(eqn. 2.1)}$$

The chemical gradient that serves as the driving force for chemical diffusion is quantified by the concentration term ($C\text{-}C_s/C_o\text{-}C_s$) where C is the measured concentration along the profile, C_o is the initial concentration and C_s is the equilibrium surface concentration (Figure 2.3). In the case of concentration-independent diffusion, the equation relating the diffusion coefficient (D), distance from the interface (x) and time (t) is:

$$x/(2\sqrt{Dt}) = erf^{-1}(C - Cs/Co - Cs) \qquad \text{(eqn. 2.2)}$$

where erf^{-1} is the inverse error function.

Plots of erf^{-1} ($C\text{-}C_s/C_o\text{-}C_s$) versus the distance ($x$) from the melt/gas interface yield straight lines with slopes equal to $1/2\sqrt{Dt}$ (Figure 2.4), from which D can be derived.

2.6. RESULTS

The experimental results are summarized in Table 2.2 and plotted versus reciprocal temperature in Figure 2.5. LogD varies in a linear fashion with reciprocal T assuming there are no changes in Re speciation in silicate liquids with temperature. The temperature dependence of Re diffusion may be fitted to Arrhenius equations of the form:

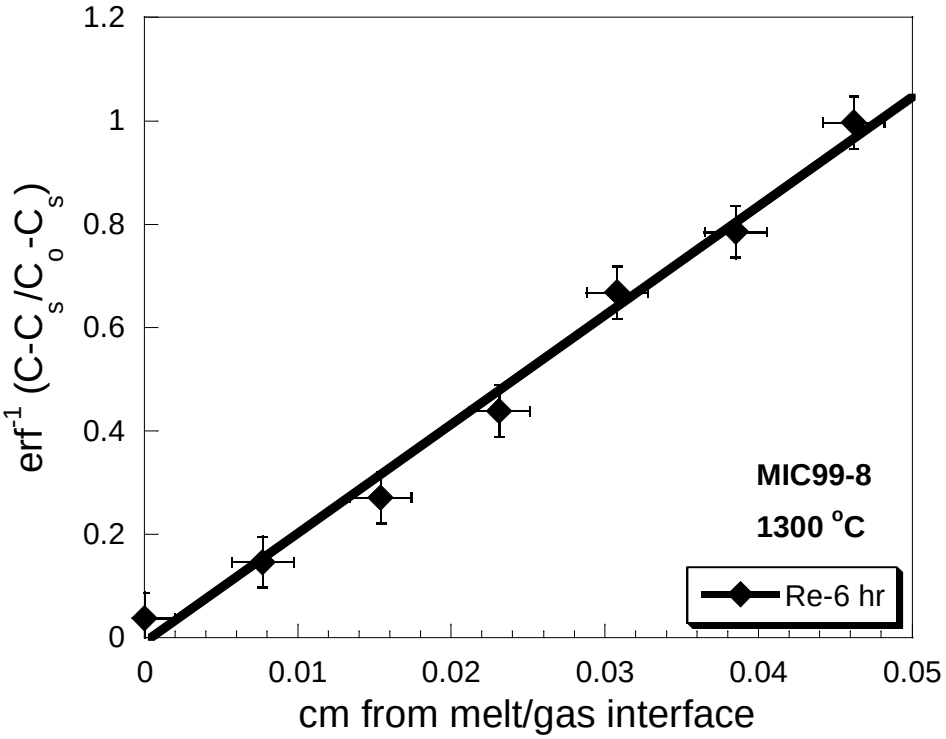

Figure 2.4. Inverse error function (erf^{-1}) for normalized Re concentration ($C-C_s/C_o-C_s$) versus distance from melt/gas interface for an experiment in basalt composition MIC99-8 shown in figure 2.3. Slope of line is equal to $1/2\sqrt{Dt}$ ($R^2 = 0.98$). ($C-C_s/C_o-C_s$) error bars calculated at 1σ based on counting statistics. Distance error bars correspond to the scan distance for each time slice (~50 μm).

$$LogD = LogD_0 - E_a/2.303RT \qquad \text{(eqn. 2.3)}$$

where D is the diffusivity at temperature T (K), D_0 is the pre-exponential or frequency factor, R is the gas constant and E_a is the activation energy for Re diffusion. The

activation energies of Re diffusion are extracted from the slopes of the lines in Figure 2.5 and vary from 473 ± 4 kJ/mol in MIC99-8 melt to 202 ± 46 kJ/mol in WP-1 melt. The calculated frequency factors (D_0) for the basalt MIC99-8 is 8.5 ± 0.3 cm^2/sec and –1.5 ± 4.1 cm^2/sec for the andesite WP-1 composition.

In the basalt composition, runs conducted over one-, three- and six-hour durations show a Re concentration gradient that is well described using the D_{Re} values listed in Table 2.2. Over extended run durations (12 to 24 hours), however, the shape and position of the Re concentration curves deviates strongly from our model calculations (Figure 2.6). At a given temperature, the shape of the Re concentration curves are approximately uniform after six hours, but the position of the curves (e.g., where Re concentration ~ zero) is progressively displaced away from the melt/gas interface, leading to a region containing essentially no Re, that grows in thickness away from melt/gas interface with time.

We are unaware of this phenomena being reported previously in any literature on diffusion or evaporation. Most importantly, this layer of Re depletion only occurs in the basaltic composition (MIC99-8) containing substantial Fe, and only under oxidizing conditions (e.g., log fO_2 > -2) in experiments of over more than 6 hours run duration. The layer of Re depletion does not develop in runs conducted at reducing conditions (e.g., log fO_2 < -2), or in the CMAS and andesitic (WP-1) compositions. In the Fe-bearing andesite

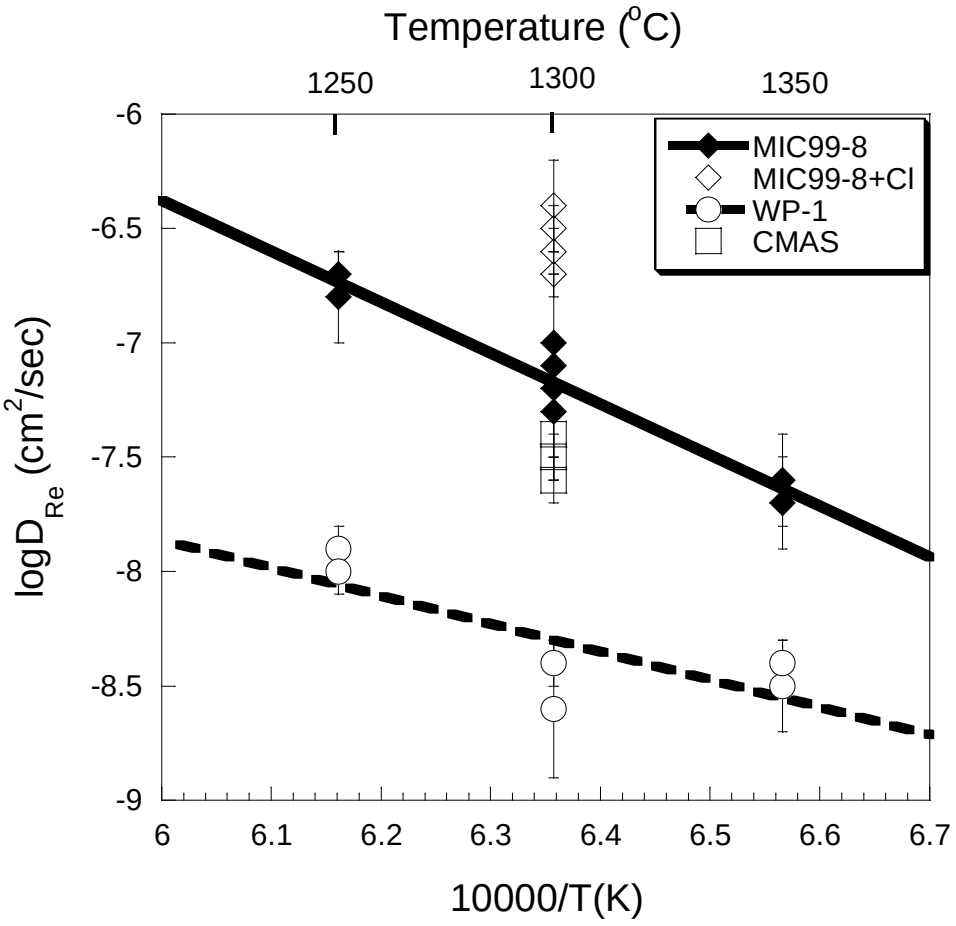

Figure 2.5. Experimental data plotted as Arrhenius functions of absolute temperature. Error bars calculated at 1 σ for each experiment based on linear regression statistics of erf^{-1} versus distance from melt/gas interface (Figure 2.4, Table 2.1).

composition, we cannot rule out growth of the depletion zone over much longer times given the lower Re diffusivity in this composition.

Initially, it might appear this moving interface in experiments performed in air is the well-known Stefan problem for moving boundary problems (e.g.,, Chebbi and Selim, 2006), but we emphasize it is not an actual physical movement of the melt/gas interface, only the shift in a chemical gradient away from that interface.

The causes of this Re depletion layer may include: 1) vigorous convection within this layer, 2) compositional change (Re, Na and/or Fe loss) within this layer or 3) oxidation of the melt near the melt/gas surface causing a change in melt structure or valence state of Re leading to increased Re diffusivity. Based on the calculated Rayleigh number for our experimental design, convection is not predicted. Furthermore, the CMAS composition has a viscosity similar to the MIC99-8 composition ($\log\eta$ = 2.32 and 2.24, respectively), thus convection in a depleted layer would be the same for both compositions, yet a Re depletion layer only develops in the Fe-bearing one. A compositional change in or near the Re depletion layer is untenable, as we observe no change in Fe or Na loss near the melt/gas interface (Figure 2.2) or the walls of the crucible either within or below the depleted layer

As noted previously, all starting compositions were synthesized at 1500°C. At these conditions, the Fe^{3+}/Fe^{total} in MIC99-8 calculated using the Kress and Carmichael (1998) algorithm is 0.88. At the lower T of our volatilization experiments in air, however, the equilibrium Fe^{3+}/Fe^{total} for MIC99-8 calculated using this algorithm is 0.98, requiring a slight amount of oxidation of the melt (increase in Fe^{3+}/Fe^{2+}). For this reason, we hypothesize that for experiments in air, higher valence states of Re in the melt are being

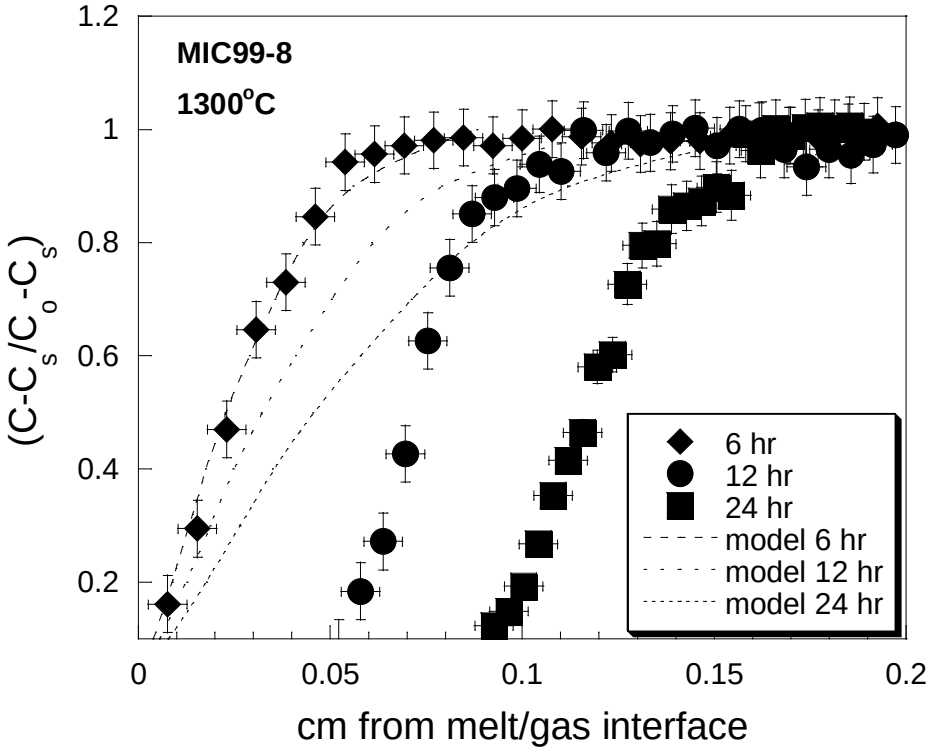

Figure 2.6. Normalized Re concentration profiles for experiments performed in air as a function of run duration. Dashed lines are modeled diffusion curves (after Equation 2.1) using $\log D_{Re} = -7.2$ cm^2/sec. Note the shape of the Re profile remains constant after 6 hours, and the deviation of position of the curves relative to the model curves.

reduced in the outermost layer to oxidize Fe^{2+} within this layer via a homogeneous equilibrium such as:

$Re^{7+} + Fe^{2+} = Re^{6+} + Fe^{3+}$ (eqn. 2.4)

We suspect lower valence species of Re (e.g., Re^{6+}) diffuse faster than higher valence species Re^{7+}, and thus leaves a 'layer' impoverished with Re.

Although the growth of a zone of Re depletion near the melt/gas interface and the displacement of the Re concentration gradient away from this interface is puzzling, we emphasize its existence only in the oxidizing experiments on basalt conducted over more than 6 hours. The Re depletion layer does not affect the outcome of our extracted D values, or the conclusions of our study.

2.6.1 Effect of composition

In one set of experiments, the MIC99-8 basalt powder was initially doped with Cl to a level of 1000 ppm, but analysis of this composition after synthesis showed it to contain Cl levels below detection (500 ppm). Preliminary results from Cl diffusion experiments in hawaiite melt (± H_2O) from Etna at 0.5 and 1.0 GPa and temperatures between 1250 and 1450°C show $\log D_{Cl} = -4.8$ to -5.9 cm^2/sec (Alletti et al., 2006). Because Cl is volatile, some was likely lost during synthesis and during the experiments but using the D_{Cl} values listed above, Cl would still be present albeit below detection. Nonetheless, the experiments conducted using the MIC99-8 composition doped with Cl yield a $\log D_{Re} = -6.6 \pm 0.3$ cm^2/sec at 1300°C (Table 2.2), almost an order of magnitude higher than that in the undoped composition at the same temperature ($\log D_{Re} = -7.2 \pm 0.3$

cm^2/sec). The result indicates that Re diffusion is increased if Cl is present, even in trace amounts.

Experiments performed in the andesite (WP-1) and CMAS compositions at 1300°C yield a $logD_{Re}^{andesite} = -8.4 \pm 0.2$ cm^2/sec and $logD_{Re}^{CMAS} = -7.5 \pm 0.2$ cm^2/sec (Table 2.2). Re diffusivity in andesite liquid is more than an order of magnitude lower than the corresponding basaltic composition at the same temperature whereas the basalt and CMAS compositions have similar diffusivities.

2.6.2. Effect of changing oxygen fugacity

Experiments were performed to examine Re diffusion under the range of fO_2 conditions characteristic of most natural magmas (Christie et al., 1986, Carmichael, 1991). In a set of experiments on MIC99-8 basalt, temperature and run duration were held constant at 1300°C and 24 hours respectively while fO_2 was varied between $log fO_2$ = -2 to -10. At conditions near the fayalite-magnetite-quartz buffer (FMQ), $logD_{Re}^{reducing} = -7.6 \pm 0.2$ cm^2/sec, only slightly lower than D_{Re} for runs conducted in air ($logD_{Re}^{air} = -7.2 \pm 0.2$ cm^2/sec). The value of $logD_{Re}$ changes with fO_2 in a non-linear fashion (Figure 2.7) and increases at fO_2 above the nickel-nickel oxide (NNO) buffer.

2.7. DISCUSSION

At 1350°C and 0.1 MPa, the diffusivity of Re in our basalt composition MIC99-8 is $logD_{Re} = -6.7 \pm 0.2$ cm^2/sec, not unlike CO_2 and Ar diffusivity in basalt at 500 MPa (

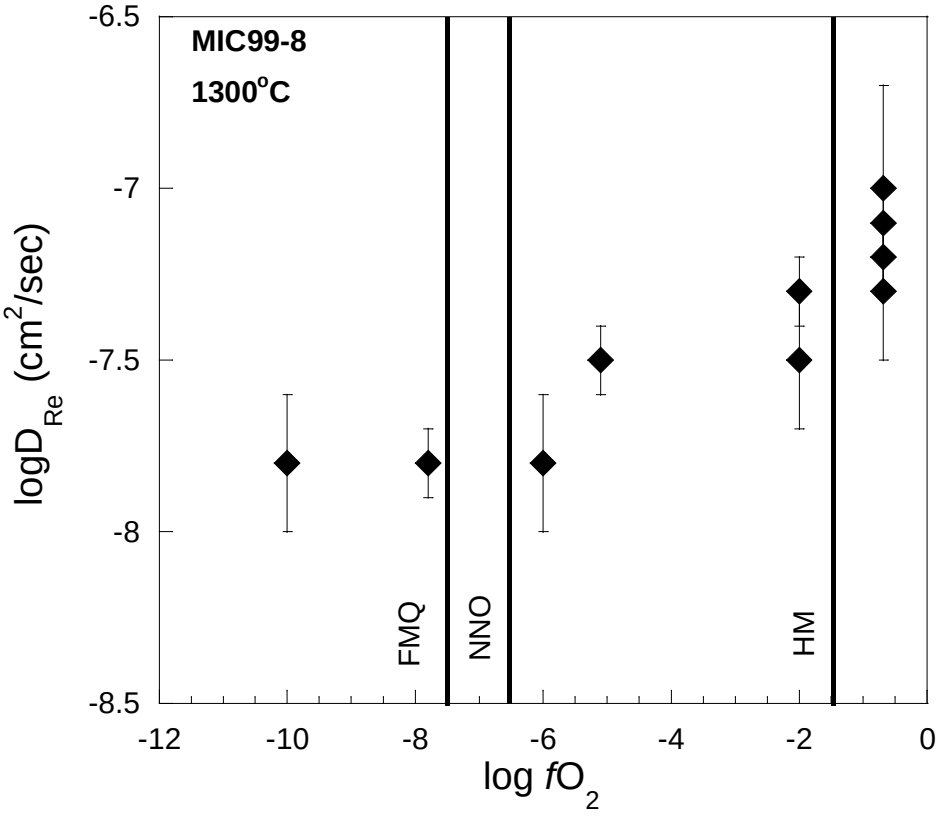

Figure 2.7. $\log D_{Re}$ versus $\log fO_2$ for experiments on MIC99-8 (basalt) composition. Solid lines mark the positions of the fayalite-magnetite-quartz (FMQ), Ni-NiO (NNO) and hematite-magnetite (HM) oxygen buffer assemblages calculated from Frost (1991). Note change in Re diffusivity at conditions above the NNO buffer. Error bars calculated at 1 σ for each experiment based on linear regression statistics of erf^{-1} versus distance from melt/gas interface (Figure 2.4, Table 2.2).

$\log D_{CO2,\ Ar}$ = -7.2 and -6.6 cm^2/sec, respectively; Nowak et al., 2004). If D_{Re} was orders of magnitude lower than that of other volatile constituents in magmas it would be difficult to ascribe to a model of Re degassing as a significant source for Re depletion in subaerially erupted magmas, because Re mobility would restrict transport of Re as a constituent to the melt/gas interface. The similar diffusivities of other volatile constituents and Re indicate there is no kinetic barrier for Re release as a volatile. Ultimately, the release of Re as a volatile is also dependent on its partition coefficient into the (C-H-S-Cl) gas phase, for which there is only empirical evidence from volcanic gas emissions, and currently no experimental constraints.

It has long been recognized that diffusivity is related to differences in melt structure, itself reflected in viscosity (e.g., Glasstone et al., 1941, Einstein, 1956), and sometimes described by the ratio of non-bridging oxygens to tetrahedral cations (NBO/T) in a melt composition (Mysen et al., 1982). In general, diffusivity decreases with increasing tetrahedral network formers (Si, Al) and decreasing network modifiers (Na, H_2O) (e.g., with decreasing NBO/T). Compared to our basalt and CMAS composition, andesite has a higher ratio of non-bridging oxygen to tetrahedral cations (NBO/T) and thus higher viscosity causing lower diffusivity of Re.

Diffusivity of an element may also change according to its speciation in the melt structure. Cotton and Wilkinson (1966) and Knacke et al. (1991) suggest that the species responsible for Re volatility from pure Re metal is Re_2O_7, suggesting a Re^{7+} valence state. Recently, Ertel et al. (2001) showed that the dominant oxidation state of Re in silicate melts is Re^{6+} at fO_2 conditions below ~ NNO. Our results show a measurable increase in D_{Re} above ~ NNO (Figure 2.7). Interestingly, Borisov and Jones (1999) also

showed that evaporation of Re from pure Re wire at 1400°C also increased at fO_2 greater than ~NNO. From these observations, we infer that Re^{6+} is the diffusing species at logfO_2's less than NNO, whereas Re^{7+} is the diffusing species at logfO_2's greater than this buffer.

Xiong and Wood (1999) showed that the dominant oxidation state in hydrothermal fluids was Re^{4+}, with Re present as a ReCl species. Carroll and Webster (1994) note that, similar to F, Cl may dissolve in melts as a metal chloride ($Me^{+}Cl$) species. It is unknown what metal species preferentially complex with Cl and to what extent but Fe and Na have been indicated as potential candidates.

Kiprianov and Karpukhina (2006) show volatile products above fluorine containing melts involve a $Me^{+}Cl$ species and include exotic species such as GeF_4. Given the uncertainty in Cl speciation, at 1300°C, in our basaltic composition logD_{Re} = -7.2 cm^2/sec but this increased to –6.6 cm^2/sec in Cl doped experiments, suggesting that the speciation and complexation of Re with Cl, even in trace amounts, significantly increases its diffusion and volatilization. In trace amounts, Cl is not expected to change the viscosity of the melt significantly (Dingwell and Hess, 1998) and thus melt viscosity is not likely the cause for increased D_{Re} in experiments doped with Cl. Given the evidence above, we instead favor complexation of Re species with Cl species in silicate melts.

2.8. APPLICATION

Differences in Re contents of MORB, OIB and arc-type basalt may be related to the mechanism of degassing. Degassing of magma requires exsolution of constituents from the melt during de-pressurization. The process can occur as either a closed system

(batch degassing) where gasses released by the magma remain in equilibrium with the liquid, or as an open system (fractional distillation) where gases exsolved from the magma are continuously lost from the system. Moreira and Sarda (2000) suggest that MORB and OIB experience different degassing mechanisms. They show noble gas ratios and isotopic compositions of MORB are best explained using a model of batch degassing, whereas a fractional distillation process best describes samples of OIB. This conclusion is challenged by Yamamoto and Burnard (2005) who argue that the He and Ar solubility ratio in MORB would have to be up to 15 times higher to account for the noble gas ratios using a batch degassing model. Alternatively, Burnard (1999), noting the correlation between vesicle size and its trapped volatiles (CO_2 and noble gases), showed that both MORB and OIB degassing can be modeled using a fractional distillation process (Yamamoto and Burnard, 2005). For the purpose of our discussion, we will assume that degassing of MORB, OIB and arc-type basalt results from an open system (fractional distillation) process.

Degassing of magmas occurs mostly within a magma chamber as pressure decreases and gas bubbles form. The most important volatile constituents in silicate magmas are H_2O and CO_2, with minor SO_2 and Cl (Jambon, 1994) all of which are likely to influence volatile release of Re from magma. Evaluating Re concentrations in sub-aerially versus subaqueously erupted magmas requires an estimate of the amount of degassing experienced in each case, which in a general way could be estimated by the volume percent of vesicles (vesicularity).

MORB's are typically erupted at depths of 2 km below sea level and generally have vesicularities of less than 5% by volume (Cashman and Mangan, 1994). In contrast,

subaerially erupted arc-type basalts can have vesicularities approaching 60-70 % depending on the mode of eruption (e.g., effusion) (Cashman and Mangan, 1994). Assuming Re depletion is related to gas loss, the Re abundances should scale with vesicularities. Unfortunately, there is no direct data on the vesicularity for each sample measured for its Re content (Figure 2.1). The differences in vesicularities between subaqueously and subaerially erupted samples would suggest that Re abundances in the former are at least ten times greater than that of the latter. MORB and arc-type basalts have average Re concentrations of 0.956 ppb and 0.233 ppb, respectively. Thus qualitatively, a general correlation between vesicularity and Re contents in basalts exists, but it must be used with caution, as vesicularity may not simply reflect volatile contents, rather the degree of volatile supersaturation and magma ascent rate on vesicle formation and growth need also be considered.

Differences in Re contents among MORB, OIB and arc-type basalts may reflect differences in the source region and/or degrees of partial melting or fractional crystallization. The mineralogy (e.g., garnet presence) and presence of residual sulphide in the source region affect Re contents but these cannot fully account for the differences between all cases in Figure 2.1 (Lassiter, 2003). For example, residual garnet in the source region of OIB and arc-type basalts could account for the lower Re contents in these rocks. However, Yb and Re are similarly compatible in garnet (Righter and Hauri, 1998) and thus, garnet in the source should act to deplete Yb as much as Re, which is not the case; Yb is not as depleted in OIB and arc type basalts as in MORB (Lassiter, 2003). Additionally, among lavas from Kilauea, Re contents do not scale with indices of partial melting or fractional crystallization (Lassiter, 2003).

Several observations are suggestive that Re can be lost from magma as a volatile species. In arc volcanics from Aoba, Vanuatu, Re is enriched in olivine-hosted melt inclusions relative to their host magma (Sun et al., 2003b). Subaerially erupted basalts from Kilauea have lower Re contents than their submarine equivalents within the same volcanic pile (Lassiter, 2003). Re-rich mineral species are recognized at volcanic edifices (Korzhinsky et al., 1994, Taran et al., 1995). Because arc-type basalts are generally enriched in volatile components (0.2 – 6.1 wt% H_2O, 0 - 2100 ppm CO_2 and 500 - 2000 ppm Cl (Wallace; 2005) relative to MORBs (0.1-0.5 wt% H_2O, 100-300 ppm CO_2 and <100 ppm Cl ; Dixon and Stolper, 1995) they likely experience more de-pressurization and gas production upon eruption, and potential Re loss as a volatile.

Re and Cl are strongly correlated in gas compositions measured from Kilauea (Crowe et al., 1987; Miller et al., 1990) suggesting the formation of a ReCl species may be important in Re loss during degassing. Our results confirm this suggestion, and clearly show that Re mobility is increased in the presence of Cl, even in trace amounts (<500 ppm). Cl contents of melt inclusions from arc-type basalts (typically 500-2000 ppm) are consistently higher than their MORB counterparts (<100 ppm) (Wallace, 2005) indicating greater Re loss via degassing from arc-type basalts compared to MORB.

Righter et al. (2002) argue that the low Re contents of arc-type basalts are opposite to that expected by Re behavior in fluids. The high solubility of Re in Cl-rich fluids (Xiong and Wood, 1999) suggest that arc-type magmas, which many believe to have formed by fluids that flux the mantle source region in subduction zones, should have high Re, yet data from arc basalts show the lowest Re concentrations. Given the increased Re diffusivity observed in Cl-bearing silicate liquids (Figure 2.5, Table 2.2), we

hypothesize that the increased mobility and volatility of Re in Cl-bearing silicate liquids, coupled with the increased Cl content in arc-type basalts acts to deplete the magma of Re to a much greater extent than any Re enrichment associated with interaction of subduction derived fluids to the source region of arc magmas.

Significant Re depletion from a lava flow having a thickness of meters would be impossible if it occurred exclusively through a diffusive process. Using the values of D_{Re} we obtain, the time for cooling and solidification of the lava (days) would greatly outpace the rate of diffusion required to deplete the lava (years). Rather, diffusion is only one part of the degassing process. The loss of Re as a volatile species from magma involves: (1) diffusion of Re to a melt/gas interface (gas bubble), (2) the partitioning (solubility) of Re into the gas/fluid phase, and (3) migration of the Re-bearing gas to a surface where it is released. The degree of degassing also depends on the amount of decompression (ascent rate) experienced by the magma. Our study sheds light on the first step in this process, but more experimental data are needed on the latter parts of the process.

2.9. SUMMARY

Volatization experiments performed in basaltic, andesitic and CMAS melts at 0.1 MPa indicate that the diffusivity of Re is strongly affected by melt composition, and its speciation in the melt, and weakly affected by changes in fO_2. The negative correlation of vesicularities and Re concentrations in basalts erupted subaqueously and subaerially suggest that Re can be volatile and strongly partitioned into the gas phase. Re diffusivity in basalt is similar to that of CO_2 and Ar at 500 MPa (Nowak et al., 2004) suggesting no kinetic barrier to Re depletion by gas loss in subaerial eruptions. We therefore argue that

Re depletion in basalts from intra plate and convergent margin tectonic settings does not require the presence of sulfide or garnet in the source regions of these magmas, but rather that Re can be lost as a volatile during ascent and emplacement.

ACKNOWLEDGEMENTS

We thank J. Spence and M. Raudsepp for their able assistance with ICPMS and EMP, respectively. Reviews by R. Linnen, A. Holzheid and an anonymous reviewer and discussions with L. Coogan helped improve the manuscript and are all greatly appreciated. This research was supported by a MAC Foundation Scholarship to JMM and NSERC of Canada Discovery Grant to DC.

Table 2.1: Major and trace element concentration of starting materials. Concentrations are averages of 20 measurements for the MIC99-8 (±Cl) and CMAS compositions. WP1 composition is average of 10 measurements. Measurements were made on randomly selected chips of start glass. 1σ standard deviation for major elements is ± 0.1 wt% unless other wise noted in brackets. 1σ standard deviation for Re in starting glass are shown in brackets. MIC99-8 (Fe^{3+}/Fe^{total} = 0.88), WP-1 (Fe^{3+}/Fe^{total} = 0.79) (calculated after Kress and Carmichael, 1988) Detection limits for Cl and S are 500 and 350 ppm respectively. All Fe reported as Fe_2O_3, b.d. (below detection).

Sample	MIC99-8	MIC99-8 (+Cl)	WP-1	CMAS
Na_2O	2.3	2.7	3.5	-
MgO	8.1	8	2.6	10.8 (0.2)
Al_2O_3	15	14.9	16.6	15.4 (0.2)
SiO_2	48.1 (0.2)	48	64.7 (0.2)	49.1 (0.2)
P_2O_5	0.1	0.1	0.2	-
K_2O	0.1	0.1	1.7	-
CaO	12.2	12.2	5	24.6 (0.2)
TiO_2	1.1	1.1	0.5	-
MnO	0.2	0.2	0.1	-
Fe_2O_3	12.2	12.1	4.7 (0.2)	-
Cl	b.d.	b.d.	-	-
S	b.d.	b.d.	-	-
Re (ppm)	1.0 (0.15)	1.0 (0.15)	1.5 (0.1)	10.0 (0.5)
Total	99.3	99.4	99.5	99.9

Table 2.2: Summary table of run conditions and calculated D values for experiments obtained using the slopes from erf^{-1} versus distance from melt/gas interface demonstrated in Figure 4. *Errors calculated at 1 σ for each experiment based on linear regression statistics of erf^{-1} versus distance from melt/gas interface.

Composition	run#	T	logfO_2	duration (hr)	logD_{Re}	error*
MIC99-8	Re15	1300	-0.68	6	-7.1	0.1
MIC99-8	Re16	1300	-0.68	6	-7.2	0.1
MIC99-8	Re17	1300	-0.68	6	-7.2	0.1
MIC99-8	Re18	1300	-0.68	1	-7	0.3
MIC99-8	Re19	1300	-0.68	3	-7.3	0.2
MIC99-8	Re20	1250	-0.68	6	-7.6	0.2
MIC99-8	Re21	1250	-0.68	1	-7.7	0.2
MIC99-8	Re22	1350	-0.68	6	-6.7	0.1
MIC99-8	Re23	1350	-0.68	1	-6.8	0.2
MIC99-8 + Cl	ReCl1	1300	-0.68	6	-6.5	0.1
MIC99-8 + Cl	ReCl2	1300	-0.68	6	-6.6	0.1
MIC99-8 + Cl	ReCl3	1300	-0.68	3	-6.7	0.1
MIC99-8 + Cl	ReCl4	1300	-0.68	1	-6.4	0.2
MIC99-8	DTRe24	1300	-7.8	24	-7.8	0.1
MIC99-8	DTRe25	1300	-5.1	24	-7.5	0.1
MIC99-8	DTRe26	1300	-10	24	-7.8	0.2
MIC99-8	DTRe27	1300	-6	48	-7.8	0.2
MIC99-8	DTRe28	1300	-2	1	-7.5	0.2
MIC99-8	DTRe29	1300	-2	3	-7.3	0.1
WP-1	ReA-1	1300	-0.68	12	-8.7	0.2
WP-1	ReA-2	1300	-0.68	24	-8.4	0.1
WP-1	ReA-3	1250	-0.68	12	-8.5	0.2
WP-1	ReA-4	1250	-0.68	12	-8.4	0.1
WP-1	ReA-5	1350	-0.68	12	-7.9	0.1
WP-1	ReA-6	1350	-0.68	24	-8	0.1
CMAS	ReCMAS-1	1300	-0.68	23	-7.6	0.1
CMAS	ReCMAS-2	1300	-0.68	23	-7.5	0.1
CMAS	ReCMAS-3	1300	-0.68	1	-7.4	0.2
CMAS	ReCMAS-4	1300	-0.68	4	-7.4	0.2

CHAPTER 3.

VOLATILE HEAVY METAL MOBILITY IN SILICATE LIQUIDS: IMPLICATIONS FOR VOLCANIC DEGASSING AND ERUPTION PREDICTION

Jason M. MacKenzie

Dante Canil

University of Victoria School of Earth and Ocean Sciences

Victoria, BC, Canada,V8W 3P6

3.1. ABSTRACT

The volatilization of Cd, Re, Tl, Pb, Sb and Te from melts in the system CaO-MgO-Al_2O_3-SiO_2 (CMAS) and Na_2O-MgO-Al_2O_3-SiO_2 (NMAS) has been investigated at 0.1 MPa and 1200-1350°C. Experiments were conducted in air using metal-doped melts in Pt crucibles. Analysis of quenched glasses by Laser Ablation Inductively Coupled Plasma Mass Spectrometry (LA-ICP-MS) normal to the melt/gas interface produced concentration profiles for Cd, Re, Tl, Pb, Sb and Te to which a semi-infinite one-dimensional diffusion model could be applied to extract diffusion coefficients (D). The melt was also doped with Cu, Zn, In, Mo, Sn and W but concentration profiles for these metals did not develop. In the CMAS composition at 1300°C, the fastest diffusing element was Cd having a $\log D_{Cd} = -6.5 \pm 0.2$. The slowest element was Re with $\log D_{Re} =$

-7.5 ± 0.3. Diffusivities of Sb, Te, Pb and Tl have intermediate values where $logD_{Sb}$ = -7.1 ± 0.1, $logD_{Te}$ = -7.2 ± 0.3, $logD_{Pb}$ = -7.1 ± 0.2, $logD_{Tl}$ = -7.0 ± 0.2 cm^2/sec. In the NMAS composition, $logD_{Re}$ = -6.5 ± 0.2, $logD_{Sb}$ = -6.0 ± 0.2, $logD_{Pb}$ = -6.1 ± 0.1, $logD_{Tl}$ = -5.8 ± 0.2 cm^2/sec (values for Cd and Te were not determined). Differences in diffusivity of volatile heavy metal ions to a melt-gas interface led to significant fractionation between these metals in magmas during degassing. Given the observed differences in Cd and Re diffusivities in the CMAS composition, we predict an increase in the normalized Cd/Re ratio in the gas phase with increasing bubble growth rate. Monitoring of the Cd/Re ratios in aerosols from degassing volcanoes may provide a tool for predicting volcanic eruptions.

3.2. INTRODUCTION

Volcanic aerosols, plumes and fumarolic gases are considerably enriched in volatile metals such as Cd and Re (Lambert et al., 1986; Crowe et al., 1987; Pennisi et al., 1988; Hinkley et al., 1994; Allard et al., 2000; Nriagu and Becker, 2003; Norman et al., 2004) indicating that vapour transport is an important process by which these metals can be liberated into the environment. Magmatic gases and fluids account for a significant fraction of the flux of these elements into the crust, atmosphere and hydrosphere (Zoller et al., 1974; Lambert et al., 1988; Nriagu, 1989; Rubin, 1997; Norman et al., 2004). For example, Nriagu (1989) has estimated that volcanic emanations may account for as much as 40-50% of the global flux of Cd and Hg into the environment, and 20-40% of other volatile metals (As, Cu, Ni, Pb and Sb). The recognition and quantification of element transport and flux from volcanoes has relied principally on empirical measurements from

plumes (and related fumaroles and condensates) during eruptions and on studies of melt inclusions (Wallace, 2005) and natural glasses (Norman et al., 2004).

While traditionally aqueous fluids have been thought of as the principal transport agent of many important metals (Williams-Jones et al., 2002), the transport of metals by vapour has received renewed attention as a potentially important mechanism in the formation of ore deposits (Williams-Jones and Heinrich, 2005). Monitoring of volcanic gases also has some utility in understanding degassing processes (Miller et al., 1990; Villemant and Boudon, 1999) or to predict volcanic eruption (Aiuppa et al., 2007) and the potential duration of volcanic events (Pennisi and LeCloarec, 1998; Aiuppa et al., 2002; Alletti et al., 2007). Finally, it has been suggested that monitoring trace metal ratios in volcanic fumes from inactive vents could provide a tool for predicting volcanic eruptions (Crowe et al., 1987).

Despite the importance of volcanic degassing to global trace metal inventories and ore genesis, our current understanding of the underlying factors that control the transport of these metals remains in infancy. As a natural system, volcanic eruptions and the resulting metal release are complex, transient phenomenons that are difficult, dangerous, and expensive to measure. It would be beneficial to have complementary experimental constraints on the fundamentals for element mobility, speciation and partitioning to help understand the process, quantity and flux expected for volatile metals liberated during an eruption.

Emanation coefficients (ε_x), which are a measure of the changes in metal concentration of magma as a result of eruption, can be used as a proxy for element

volatility in magmas. The emanation coefficient of an element (x) from magma is defined as:

$$\varepsilon_x = (C_i - C_f) / C_f \qquad \text{(eqn. 3.1)}$$

where C_i and C_f are the concentration in the initial magma and after eruption respectively.

Enrichment factors (EF) have also been used to describe element volatility where the enrichment factor of an element (x) is related to the aerosol and lava concentrations C_x normalized to a single element C_{norm}:

$$EF_x = (C_x/C_{norm})_{aerosol} / (C_x/C_{norm})_{lava} \qquad \text{(eqn. 3.2)}$$

Where C_x is the concentration of element (x) and C_{norm} is the concentration of an element used to normalize the concentrations in the aerosol and lava.

Rubin (1997) compiled volatile emission data for many metals from several basaltic to andesitic volcanoes and calculated their mean ε_x. The calculated values indicate a non-uniform distribution of volatile metals in volcanic gases (Figure 3.1). Calculated EF's (e.g., Hinkley et al., 1994) show a similar trend where chalcophile metals such as Cd and Cu are variably enriched in volcanic plumes. In spite of these empirical observations, the root causes of differences in element enrichment remain unconstrained. Variations in a metal's ε_x and EF may be attributed to intrinsic differences in the concentrations of volatile species in the melt, or to replenishment of volatile metal concentrations through pulses of new (undegassed) magma (Hinkley et al., 1994). Values

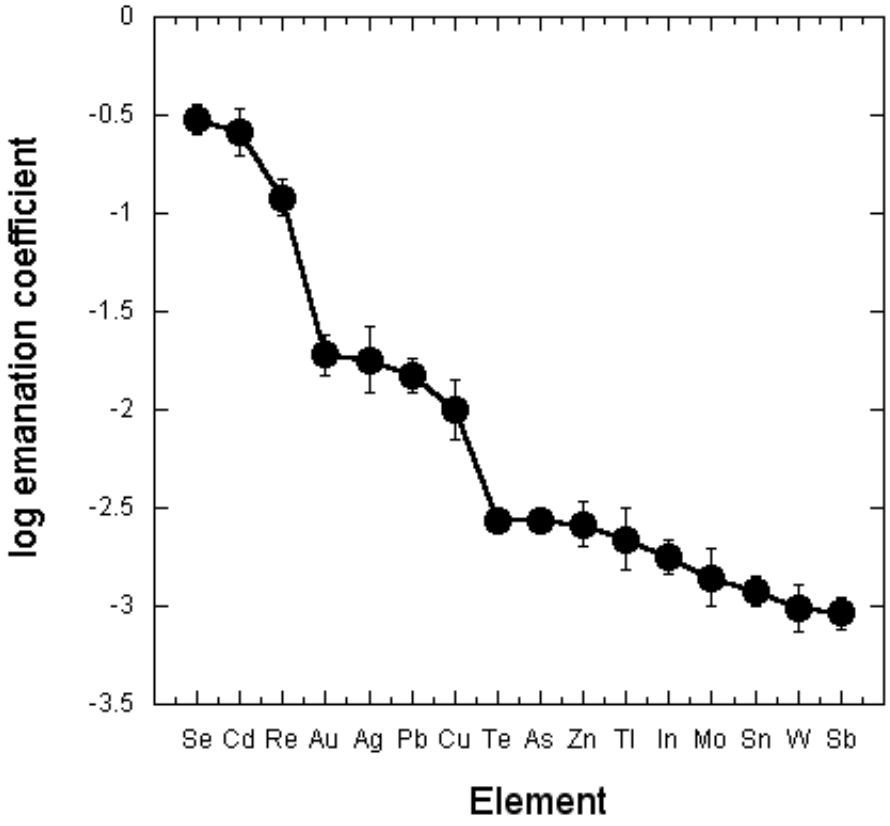

Figure 3.1. Summary of (log) average emanation coefficient for mafic volcanic eruptions worldwide (data from Rubin, 1997). Mean standard deviations shown at 1σ.

of ε_x may also vary according to the ability of a metal to form a volatile species with O, S or halogens (LeGuern, 1988).

Alternatively, different values of ε_x among metals may also depend on an element having variable mobility to migrate and reach a melt/gas interface prior to forming a volatile complex and partitioning into the gas phase during degassing.

Volatile depletion and vapour transport of metals in silicate liquids requires: 1) the exsolution of volatile species from the melt during depressurization and formation of gas bubbles, 2) the diffusion of metal to a melt/gas interface (bubble) and 3) the partitioning of a metal species into the bubble followed by release of this gas. Melt viscosity, oxidation state and the degree of volatile supersaturation are all factors potentially affecting all these processes.

Kinetic processes such as diffusion, likely dominate magma degassing in an open system characterized by disequilibrium fractional distillation. In a closed system under equilibrium, however, partitioning of metals into the gas phase likely controls volatile metal release during magma degassing. Oxide, hydroxide, chloride and sulphide complexation likely also play an important role in metal transport in volcanic gases. Given that diffusivity, partitioning and complexation are all factors in the ultimate release of volatile metals from magma, our study seeks to address the first stage of these processes by measuring the mobility of several volatile metals toward a melt-gas interface in simple silicate melts analogous to natural basaltic magmas. The data is then modeled and compared with empirical measurements of natural samples to establish any correlations between metal mobility and concentrations in naturally degassing volcanoes.

3.3. EXPERIMENTAL METHODS

The mobility of an element in a melt is controlled by its diffusivity, which is dependent on melt composition, temperature and speciation in the melt. To measure diffusion rates of volatile heavy metals, we used metal-doped melts in contact with a gas phase. The technique exploits the volatility of an element to establish a concentration gradient where metals in the melt must equilibrate with the atmosphere above it (MacKenzie and Canil, 2006; Chapter 2). The concentration gradients resulting from volatilization were measured to determine the chemical diffusivity of metals in melts at different temperatures.

A synthetic, CaO-MgO-Al_2O_3-SiO_2 (CMAS "haplobasalt") composition corresponding to the Di_{58}-An_{42} eutectic and a Na_2O-MgO-Al_2O_3-SiO_2 (NMAS) were used as starting materials (Table 3.1). The phase relations in the CMAS system are well studied and CMAS is a good analog for natural basaltic compositions (Presnall et al. 2002). We chose to use the NMAS composition to evaluate the effects of changing melt composition on metal diffusivity because NMAS melts have lower viscosity relative to CMAS thus, our experimental times did not have to be extended.

To prepare starting materials, reagent grade SiO_2, Al_2O_3, MgO and/or Na_2CO_3/$CaCO_3$ powders were ground under alcohol in an agate mortar and dried at 120°C in air for one hour. Once dried, the mixture was decarbonated at 1000°C for 3 hours and then fused at 1500°C in a 25 mm diameter Pt crucible for 4 hours prior to quenching to a glass. The glass was crushed and ground to a powder to which 1000 ppm NIST certified standard solutions of different metals (Cd, Re, Pb, Cu, Te, Zn, Tl, In, Mo, Sn, Sb, W and Yb) were added using a micropipette. The powder and solution were

subsequently ground under alcohol for 10 minutes to homogenize the mixture. After drying under a heat lamp, the mixture was again fused in air at 1500°C for 6 hours prior to quenching to a glass. Quenched glasses were crushed, re-ground and re-melted twice to homogenize the mixture. Analyses of random chips of starting glasses indicate homogeneity in their major and trace element compositions (Table 3.1).

Powdered starting glass was loaded into 10 mm long x 2 mm ID diameter Pt crucibles. The crucible was held in a 3 x 3 x 2 cm ceramic carrier and placed in the pre-heated box furnace. Temperature was measured using a type S ($Pt/Pt_{90}Rh_{10}$) thermocouple immediately above the crucible and controlled to within ± 1°C. Experimental duration was between one and 24 hours and runs were quenched by removal from the furnace and cooling in a stream of dry air (Table 3.2). After each experiment, the charges, composed entirely of quenched glass, were sectioned axially into two pieces. One half was mounted in epoxy, polished and examined in reflected light.

Convection may complicate the transport of diffusing species in diffusion experiments. The Rayleigh number calculated for a melt in our experimental arrangement is less than 10 assuming planar geometry, a thickness of 1 cm and boundary conditions of ΔT (max) = 3°C, which is very low and does not predict convection (Philpotts, 1990). Furthermore, melt convection would distort the shapes of concentration distance profiles, which we do not observe. The lack of a convective driving force, low Rayleigh number and consistency of concentration distance profiles indicate that convection is negligible in our experimental design.

3.4. ANALYTICAL METHODS

Major and minor elements in experimental glasses were determined using a CAMECA SX50 electron microprobe at the University of British Columbia at 15 kV acceleration voltage and beam current of 20 nA, with peak counting times of 30 seconds for Mg, Al, Si and Ca. For analysis of Na in the NMAS composition, the conditions were optimized to reduce Na loss requiring a beam current of 5nA, 10 kV acceleration voltage and a 15 second count time. Major element profiles were collected perpendicular and parallel to the melt/gas interface, and adjacent to the capsule walls and were homogenous throughout the entire charge.

Line profiles of trace element concentrations were collected perpendicular to the melt/gas interface (Figure 3.2) by LA-ICP-MS at the University of Victoria using a Thermo-Instruments X-series II ICP-MS. Laser ablation was conducted using a New Wave Research, solid-state, 213 nm Nd:YAG UV laser pulsed at a frequency of 20 Hz with an energy of ~1.9 mJ. NIST 610 and 613 Standard Reference Materials (SRM) glasses were both used as standards for all metals. The spot size and line scan traverse rate were 20 μm and 5 μm /sec, respectively. Data was collected in peak jumping mode with a dwell time of 10 milliseconds at one point per peak. ^{43}Ca was used as the internal standard for NIST SRM and experimental run products. Data was recorded as time-resolved spectra in counts per second, collected over 360 seconds with 50 seconds allotted to collecting background concentrations. The spectra were then subdivided into 50 time slices, each representing ~30 μm of scan length and each time slice reduced to average concentrations using the Thermo© data reduction software.

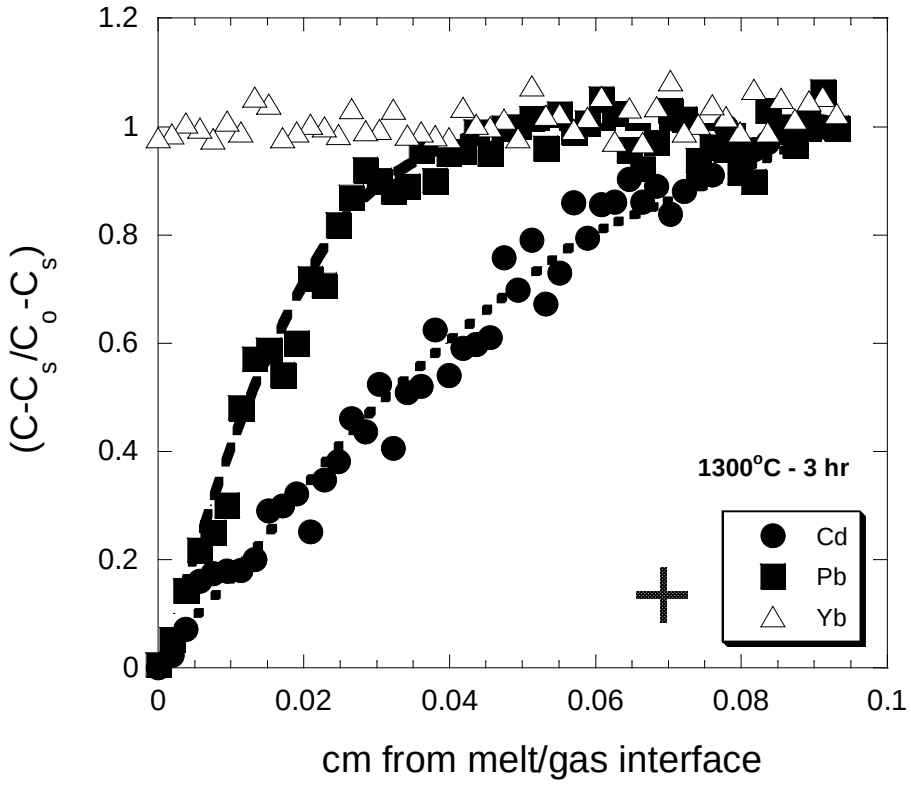

Figure 3.2. Normalized Pb, Cd and Yb concentration versus distance from melt/gas interface in CMAS composition (3 hr run at 1300°C) and modeled diffusion curves. Pb diffusion curve (dashed line) modeled using $\log D_{Pb}$ = -7.2 cm^2/sec and Cd modeled using $\log D_{Cd}$ = -6.5 cm^2/sec. Errors shown as stippled cross. $(C-C_s)/C_o-C_s)$ error bars calculated at 2σ based on counting statistics. Distance error corresponds to the scan distance for each timeslice (~30 μm).

Analysis of separate parallel profiles (perpendicular to the melt/gas interface) near the center and crucible walls showed no difference in the profile shape or location (MacKenzie and Canil, 2006; Chapter 2). We conducted similar line scans ~5 mm from the interface across the charge into the Pt crucible walls and observed no change in metal concentrations within the glass at or near this boundary.

3.5. DATA REDUCTION

In our experimental design, the sample is treated as a one-dimensional, semi-infinite medium (Chakraborty, 1995). We assume the release of a volatile metal from the silicate liquid is limited by its diffusivity (D_x) to the melt/gas interface, where the metal is immediately volatilized as an oxide (e.g., in air). Differences in metal diffusivity are reflected in the curvature of the concentration profile with distance from the interface as shown in Figure 3.2. As expected, non-volatile elements (e.g., Yb) show no change in concentration.

The equation relating the diffusion coefficient (D), distance from the interface (x) and time (t) for diffusion in a one-dimensional, semi-infinite medium (Crank, 1975) is:

$$x/(2\sqrt{Dt}) = erf^{-1}(C - Cs/Co - Cs) \qquad \text{(eqn. 3.3)}$$

Where erf^{-1} is the inverse error function, C is the concentration at distance (x), C_o is the initial concentration and C_s is the concentration at the surface. Plots of erf^{-1} ($C\text{-}C_s/C_o\text{-}C_s$) versus the distance ($x$) from the melt/gas interface yield straight lines with slopes equal to $1/2\sqrt{Dt}$, from which D can be derived (e.g., MacKenzie and Canil, 2006; Chapter 2).

3.6. RESULTS

The experimental results are summarized in Table 3.2 and plotted versus inverse temperature in Figure 3.3 for the CMAS composition. LogD varies linearly with inverse temperature and can be fitted to Arrhenius equations of the form:

$$\log D = \log D_o - E_a/2.303RT \qquad \text{(eqn. 3.4)}$$

where D is the diffusivity at temperature T (K). D_o is the frequency factor, R is the gas constant and E_a is the activation energy. Table 3.2 summarizes the calculated D_o and E_a values for each element in both compositions.

Diffusion profiles only developed for Re, Sb, Cd, Te, Tl, and Pb even though the melts were doped with other "volatile" metals (Cu, Zn, In, Mo, Sn and W). In the CMAS composition, the diffusivity of Re, Sb, Te, Tl, and Pb at 1300°C are similar and, on average, range from $\log D_{Tl} = -7.0 \pm 0.2$ to $\log D_{Re} = -7.5 \pm 0.2$ cm^2/sec. The result for $\log D_{Re}$ is identical to previous work in the CMAS composition of MacKenzie and Canil (2006) ($\log D_{Re} = -7.5 \pm 0.1$ cm^2/sec). The diffusivities of Re, Sb, Te, Tl, and Pb show no correlation with atomic radius or charge of the atoms in their most common oxidation states. At 1300°C, Cd is distinct having a $\log D_{Cd} = -6.5 \pm 0.2$ cm^2/sec nearly an order of magnitude faster than Re, Sb, Te, Tl, and Pb. Diffusion rates vary linearly with inverse temperature for all elements for which D could be derived.

In the NMAS composition, Cd was completely volatilized away during synthesis of the starting material and thus we were not able to calculate D_{Cd}^{NMAS}. The loss of Cd from the starting material can be explained by the very fast diffusion rate determined

(based on the CMAS composition) coupled with the increased temperature (1500°C) used during synthesis of the starting material.

MacKenzie and Canil (2006) (Chapter 2) showed that diffusivity of Re, is most strongly influenced by melt composition and weakly affected by ambient oxygen fugacity. The diffusivities of Re, Sb, Tl and Pb in the NMAS composition are increased by approximately an order of magnitude compared to their CMAS values. While the diffusivities are broadly similar among Re, Sb, Tl and Pb, Re remains the slowest diffusing element with an average $\log D_{Re} = -6.5 \pm 0.2$ cm^2/sec and Tl the fastest having an average $\log D_{Tl} = -5.8 \pm 0.2$ at 1300°C. The increase in diffusivity between CMAS and NMAS compositions reflects the large difference in calculated melt viscosity ($\log\eta^{CMAS} = 2.77$, $\log\eta^{NMAS} = 2.02$ Pa-s). Elements are therefore able to diffuse more rapidly out of a less viscous melt, in agreement with previous findings (MacKenzie and Canil, 2006; Chapter 2).

3.7. DISCUSSION

In addition to the elements noted above, the starting materials were also doped with Cu, Zn, In, Mo, Sn and W but diffusion profiles for these elements were not observed. Because the experiments were performed in air, this observation could indicate that Re, Sb, Cd, Te, Tl, and Pb formed volatile oxides whereas Cu, Zn, In, Mo, Sn and W did not. If diffusion rates for Cu, Zn, In, Mo, Sn and W were very fast, similar to Cd in the NMAS composition, it could be argued that diffusion profiles may not have been preserved. In this case, there would be an overall reduction in the concentration of Cu,

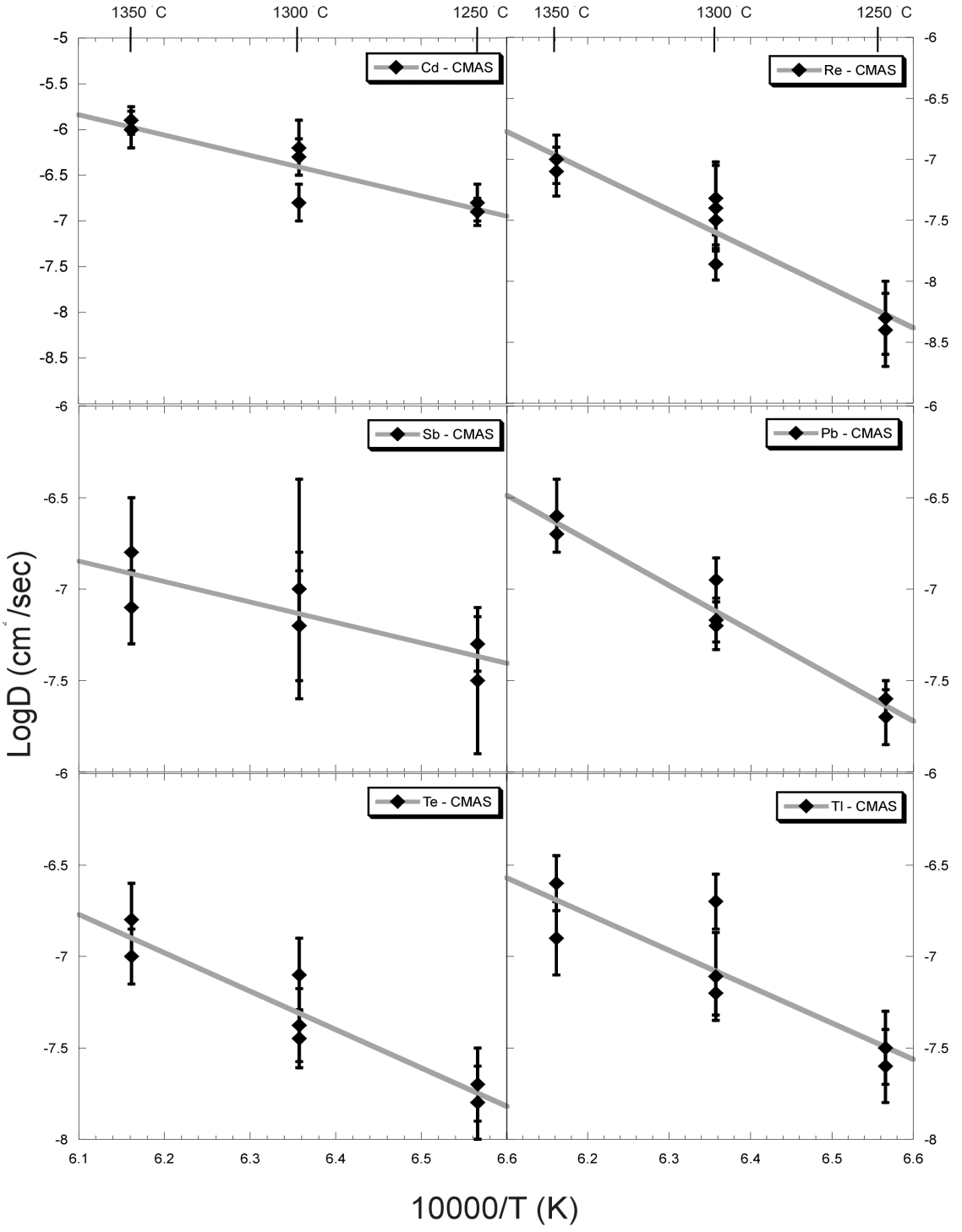

Figure 3.3. Experimental data fitted to Arrhenius functions of absolute temperature for experiments in the CMAS composition. Error bars calculated at 2σ for each data point (experiment) based on linear regression statistics of distance versus concentration (see figure 3.2).

Zn, In, Mo, Sn and W compared to the starting material, but this was not observed. In natural systems, Cu, Zn, In, Mo, Sn and W may volatilize from magma as complex chloride and/or sulphide species, whereas Re, Sb, Cd, Te, Tl, and Pb may also volatilize as a Cl- or S- complex, oxides or hydroxides.

Tellurium was present in the NMAS starting material but diffusion profiles were not observed, unlike in the CMAS composition. Clearly, Te forms volatile oxides reflected by development of diffusion profiles in the CMAS composition. Tellurium may form salts with Na as $Na_2Te_{(x)}$ that are readily oxidized in air (Wells, 1984) explaining the absence of a diffusion profile for this element in the NMAS composition. Because there is no suitable laser standard for Te, we cannot determine the absolute concentration in the melts. For this reason, we cannot determine if Te was lost as fast diffusing $Na_2Te_{(x)}$ resulting in overall Te reduction in the charge relative to the starting material or if Te remained in the melt as a $Na_2Te_{(x)}$ salt.

Studies of volatile diffusion in basaltic melts have focused largely on the most abundant volatiles such as H_2O, CO_2 and SO_2 (Watson et al., 1982; Zhang and Stopler, 1991; Watson et al., 1993; Baker and Rutherford, 1996; Carrol and Blank, 1997; Pineau et al., 1998; Winther et al., 1998; Morizet et al., 2002; Freda et al., 2003; Nowack et al., 2004; Freda et al. 2005) and the halogens (Cl, F, Br and I) (Dingwell and Scarfe, 1984; Dingwell and Mysen, 1985; Watson, 1991; Métrich and Rutherford, 1992; Bai and Koster van Groos, 1994; Lange, 1994; Webster et al., 1999; Bureau et al., 2000; Signorelli and Carrol, 2000; Webster and De Vivo, 2002; Bureau and Metrich 2003; Aiuppa and Federico, 2004; Botcharnikov et al., 2004; Giordano et al., 2004). Although halogens are thought to be important in the transport of metals (Williams-Jones et al.,

2002; Aletti et al., 2007), there are no studies on the diffusivity of volatile *metals* themselves in basaltic compositions.

In the CMAS composition, at 1300°C, the diffusivities of Re, Sb, Te, Tl, and Pb range from $logD_{Tl}$ = -7.0 ± 0.2 cm^2/sec to $logD_{Re}$ = -7.5 ± 0.2 cm^2/sec and $logD_{Cd}$ = -6.5 ± 0.2 cm^2/sec. At the same temperature, water has a diffusion coefficient that is approximately an order of magnitude higher ($logD_{H2O}$ at 1 GPa= -5.6 cm^2/sec (Zhang and Stopler, 1991)). The diffusivity of CO_2 is similar to that of the volatile metals studied here where $logD_{CO2}$ at 500 MPa = -7.2 cm^2/sec (Nowack et al., 2004).

Differences in the diffusivities among volatile components in magma may lead to their fractionation from one another. Considering the evidence that volatile metals are released as complexes with chlorides or S- (Hinkley et al., 1994), they may be even more prone to fractionation by differences in relative diffusivity.

The diffusivities of Re, Sb, Te, Tl, Pb and Cd are similar to halogens and sulphur implicated as important complexing and transport agents (Williams-Jones et al., 2002; Aletti et al., 2007). The diffusivity of S at 1300°C and 0.5-1 GPa are $logD_S$ = -7.2 and -6.5 cm^2/sec (Freda et al., 2005) in dry and wet basalt melts, respectively, similar to that of Re, Sb, Te, Tl, Pb and Cd (figure 3.4). Chlorine diffusivity in dry and wet basalts at 1300°C is $logD_{Cl}$ = -6.7 and –6.3 cm^2/sec respectively (Aletti et al., 2007) which is only slightly higher than Re, Sb, Te, Tl, Pb and, within error, is equivalent to Cd (Figure 3.4). MacKenzie and Canil (2006) (Chapter 2) showed that Re diffusivity increased to $logD_{Re}$ = -6.6 ± 0.3 cm^2/sec when the melt was doped with Cl, suggesting that Re may leave the melt as a Cl- bearing complex and perhaps Sb, Te, Tl, Pb as well in Cl bearing systems.

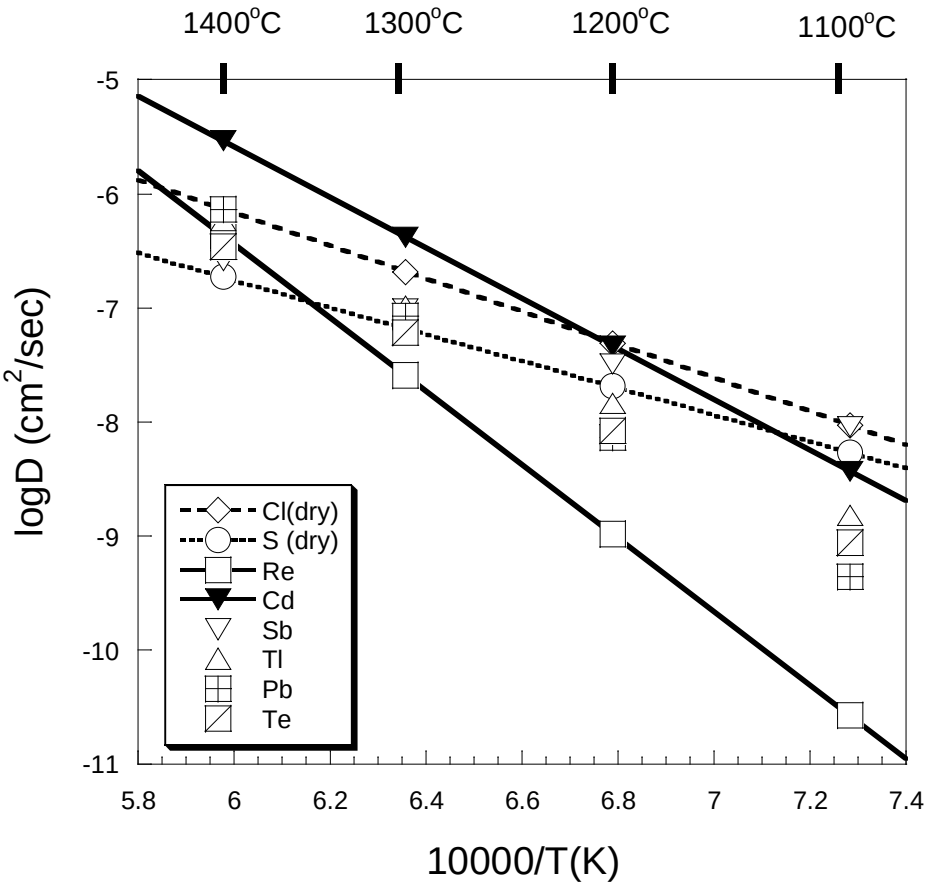

Figure 3.4. Comparison between Cl, S, Re, Cd, Sb, Tl, Pb and Te diffusivity in dry basalts (Cl and S) and haplobasalt (this study). Dashed lines for S and Cl diffusion calculated from equations in Freda et al. (2005) and Aletti et al. (2007) respectively. Data points and solid lines for Cd, Re, Sb, Te, Tl and Pb were calculated using values of Ea and Do from this study (Table 3.2).

If magma degassing is dominated by kinetic processes in an open system, the similarities of diffusivities between metals and halogens and/or sulphur could suggest metals and halogens should correlate in volcanic gases. Crowe et al. (1987) showed that Re and Cl are strongly correlated in Kilauea volcanic gases. The correlation between the two appears to support a kinetic influence on magma degassing. Alternatively, the correlation between Re and Cl correlation may simply reflect their complexation in the volcanic gas.

The comparison between ε_x and the diffusion rates in the CMAS composition at 1300°C for Re, Cd, Te, Pb, Tl and Sb are shown in Figure 3.5. There is no correlation between diffusion rates of all metals and ε_x if Re is included ($R^2 = 0.05$) but a modest correlation is observed if Re is excluded ($R^2 = 0.75$). If we instead use the increased Re diffusivity value reported by MacKenzie and Canil (2006) in Cl bearing melts, diffusivity and ε_x are well correlated ($R^2 = 0.89$). Pennisi et al. (1988) describe ε_x as not a property of metals themselves but rather as being related to the volatility and proportions of different metal compounds existing in the degassing magma as well as its physical properties. Currently, the effect of Cl on the diffusivities of Pb, Tl, Cd, Sb and Te are not known. Given the evidence from Re diffusion, a kinetic (diffusion) control on these metal concentrations (ε_x) in volcanic gases is supported.

3.8. APPLICATION

In our study, we used a simplified basalt composition and the gas phase was dry air, thus metals volatilized from the melt as simple oxides. In real volcanic systems,

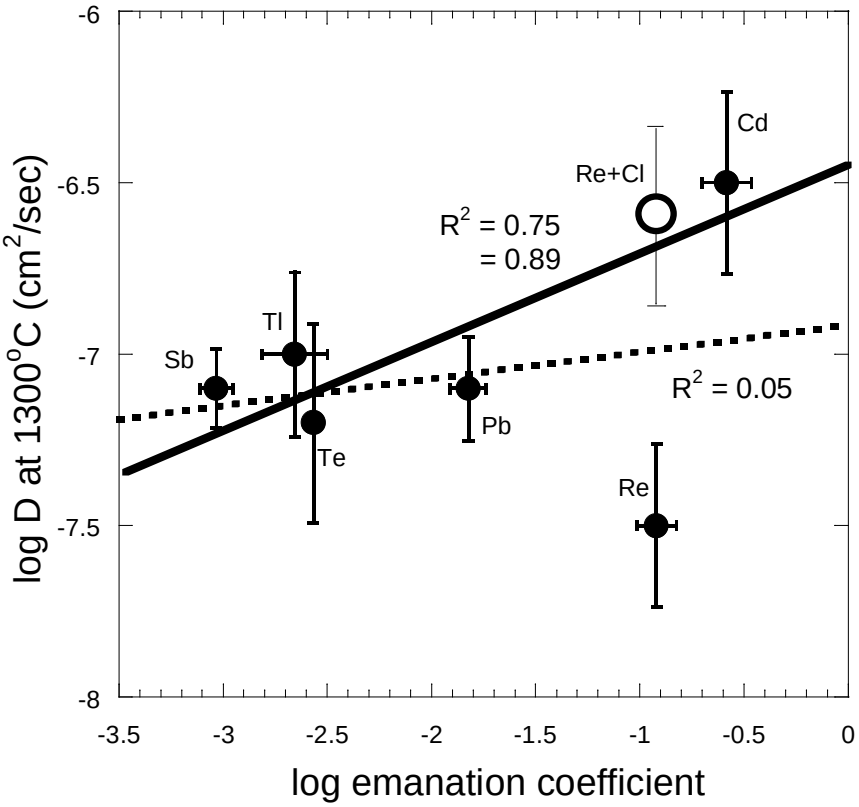

Figure 3.5. log emanation coefficient from volcanic eruptions (data from Rubin, 1997) versus average logD at 1300°C for different metals (solid circles) in the CMAS melt composition from this study. The D_{Re} in Cl-bearing magmas is shown as an open circle. The dashed line shows the relationship between element diffusivity and emanation coefficients if all elements are considered ($R^2 = 0.05$). The solid line shows the same relationship if Re is ignored ($R^2 = 0.75$) or if Re diffusivity in Cl bearing melts is used ($R^2 = 0.89$). Error bars shown at 1σ are based on mean standard deviations.

metals are diffusing toward a hydrous Cl- and S- rich magmatic gas and the composition of the melt is more complex containing H_2O, CO_2, Cl and S among other components. The effects of additional components in the melt act to change the melt structure. Specifically, increasing H_2O depolymerizes the melt and reduces melt viscosity (Lange, 1994). While the role of H_2O on the diffusivities of volatile metals in melts remains unconstrained, Cl and S diffusivities increase with increasing H_2O contents (Watson, 1994).

Our NMAS composition has a lower melt viscosity than our CMAS composition. The diffusivity of all metals studied increased in the NMAS composition. More importantly, the differences in metal diffusivity (e.g., between Tl and Re) in both compositions remained constant (Table 3.2). Consequently, the application of our data, which employs differences in relative metal diffusivity, is not discounted by differences between our simple melt compositions and melts found in nature.

Our calculated diffusivities are chemical diffusivities that reflect a metal's affinity for the gaseous state as an oxide species. We recognize D values may be different if the composition of the gas phase was more similar to a natural magmatic gas as the chemical driving force is likely to be different. Problematically, natural gas compositions, which are constantly changing, are not easily replicated in experiment. However, as a first order approximation, our data likely represent minimum values and cannot address the effects of a metals variable affinities and changing gas compositions for which little is known.

The diffusivities of major volatiles (H_2O, CO_2) are one of the most important processes affecting magma vesiculation and bubble growth (Sparks et al., 1994; Sparks, 2003). Trace metal diffusivities strongly influence the metal content of bubbles and

ultimately, volcanic exhalants. The differences in diffusivities of metals can lead to significant fractionation of these metals during magma degassing.

We attempt to model this fractionation with our diffusion data and assumptions about partition coefficients between melt and gas (*k*), temperature and bubble growth rates. Smith et al. (1955) derived a one-dimensional model that accounts for the relationship between diffusion, partitioning and bubble growth rates:

$$C_b(r) = \frac{1}{2k} C_0 \left\{ 1 + erf\left(\frac{\sqrt{(R/D)r}}{2} \right) + (2k-1) e^{-kq(R/D)r} erfc\left(\frac{(2k-1)\sqrt{(R/D)r}}{2} \right) \right\}$$

(eqn. 3.3)

where C_b is the concentration of a given metal in the bubble at some radius(r). C_0 is the initial concentration in the melt, R is the growth rate, D is the diffusion rate, k is the partition coefficient and q is equal to 1-k. Equation 3.3 can then be used to derive the bubble rim composition under different model conditions which we present as instantaneous concentrations of the bubble.

Our study provides the only measurements of diffusion coefficients of Re, Cd, Te, Tl, Pb and Sb in CMAS and NMAS compositions. The major volatiles H_2O and CO_2 have diffusivities that are orders of magnitude greater than these trace metals. Thus our modeling will assume the concentration of H_2O and CO_2 in the bubbles is constant. As an example, we restrict our model to comparison between Cd and Re as the latter metal has a D value similar to Tl, Pb, Sb and Te. The modeling uses average D values for Re and Cd at 1300°C for the CMAS composition listed in Table 3.2.

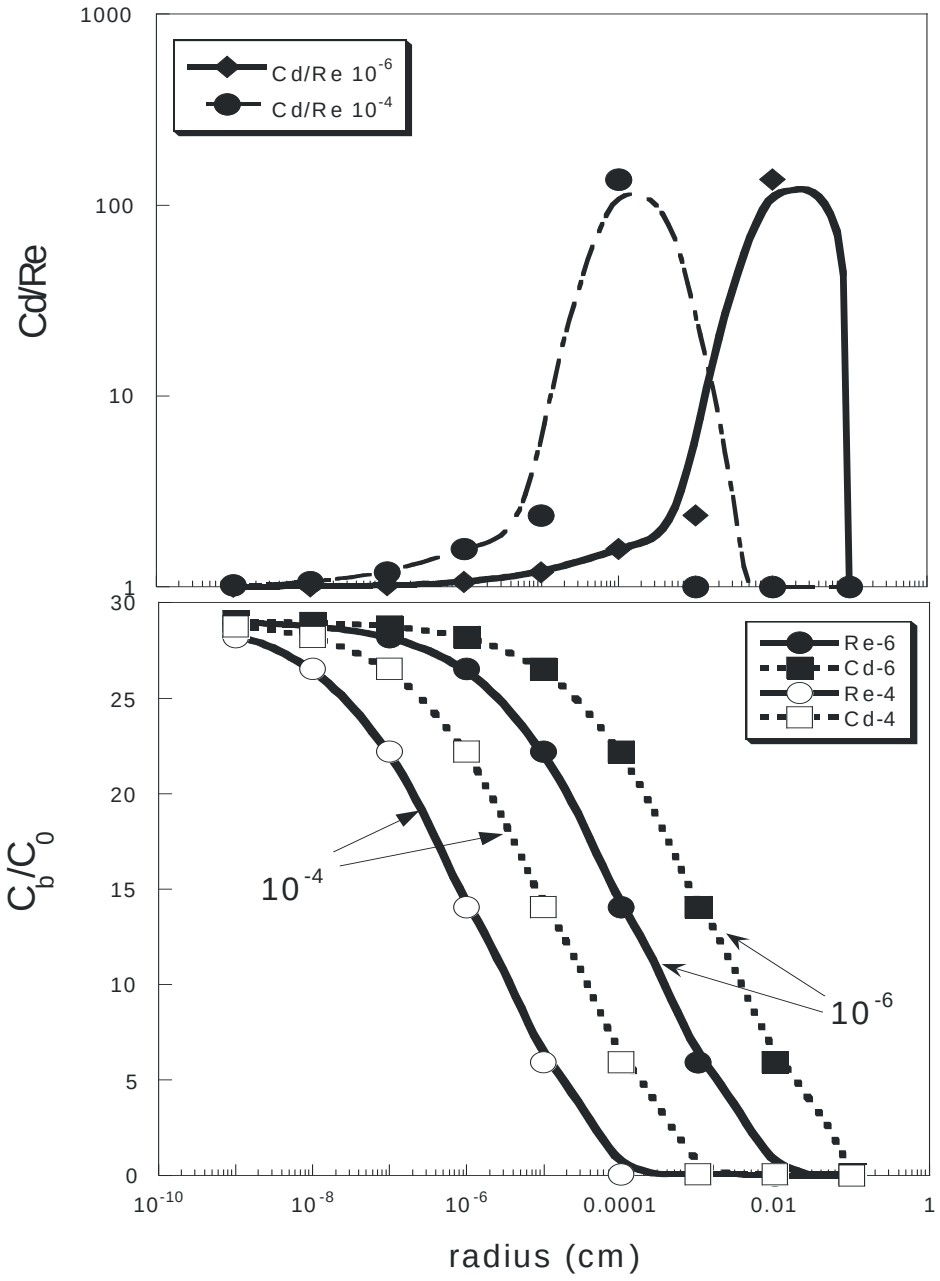

Figure 3.6. Plot showing the change in Re and Cd concentration in bubbles as a function of increasing radius at two different growth rates. As growth rate increases, the bubble becomes more enriched in Cd relative to Re. Open symbols show model data points for Re (circles) and Cd (squares) calculated at a growth rate of 10^{-4} cm^2/sec. Solid symbols show model data points for Re (circles) and Cd (squares) calculated at a growth rate of 10^{-6} cm/sec. The curves are calculated using equation 3 where k_{Re} and k_{Cd} = 15 and at 1300°C, $logD_{Re}$ = -7.5 and $logD_{Cd}$ = -6.5 cm^2/sec.

The effect of changing bubble growth rate on bubble concentration is illustrated in Figure 3.6 showing the calculated concentrations (C_b/C_0) for Cd and Re as the bubble radius increases. At the slowest growth rate (10^{-6} cm/sec), Cd and Re have similar concentrations in the bubble at the inception of the bubble (e.g., nucleation $r = 10^{-9}$ cm) and fractionate little from one another up to a radius of 10^{-3} cm. Over this interval, (C_b/C_0^{Cd} / C_b/C_0^{Re}) (hereafter referred to as Cd/Re) increases from 1.01 to 2.36 as Cd becomes modestly enriched in the bubble relative to Re. At the fastest bubble growth rate (10^{-4} cm/sec), (Cd/Re) increases more rapidly as a function of increasing radius. Overall at both growth rates, the (Cd/Re) ratio changes exponentially with increasing bubble radius. The position of the curve however is shifted to smaller radii at the fastest bubble growth rate.

As temperature decreases in an ascending magma, the diffusivities of Re and Cd also decrease but not at the same rate (figure 3.4). The effect of decreasing temperature therefore is to enhance the fractionation of Re and Cd leading to an increase the ratio (Cd/Re) with decreasing temperature.

During the ascent of magma, bubble growth is governed by the decompression rate in addition to viscous deformation and diffusion (Lensky et al., 2004). The increase in (Cd/Re) with increasing growth rate indicates that volcanic gases released from rapidly ascending magmas should be more enriched in Cd relative to Re compared to magmas that ascend more slowly. Data from volcanic episodes of Kilauea support this contention. Relative to Re, Cd is enriched in volcanic gases in active vents during eruption at times when magma must be ascending more rapidly compared to cooling vents when the magma is rising more slowly or is perhaps stagnant (Crowe et al., 1987). Furthermore,

the higher cooling rate of active vents relative to cooling vents also promotes Cd enrichment over Re in the active vents, which is also consistent with the observations of Crowe et al. (1987).

Currently, there are no high temperature measurements of partition coefficients between melt and gas (*k)* for Re, Cd, Pb, Tl, Sb and Te and thus we can only estimate the effects of changing *k* values within the model. The relationship between the concentration of Re and Cd in a growing bubble as a function of (*k*) is shown in Figure 3.7. As a minimum, *k* must be greater than one to explain the enrichments of these elements in volcanic gases (Crowe et al., 1987) and their depletions in melt (Norman et al., 2004). Using a value for *k* of 1.1, Cd and Re concentrations in the bubble remain at unity until the very largest bubble radius is achieved upon which (Cd/Re) only increases to 1.4. This calculation indicates that differences in diffusion rates of Re and Cd may be unimportant if the partition coefficient is near unity.

Alternatively using *k* values of 15 and 100, (Cd/Re) increases in an exponential fashion. At $k = 100$, (Cd/Re) increases dramatically at a radius of 10^{-5} cm whereas using a k value of 15, a similar increase is not achieved until the bubble radius is 10^{-4} cm. Using a *k* value of 8 (similar to Cl at 1250°C, k = 8.7; Alletti et al., 2006), (Cd/Re) increases more gradually reaching 12.3 at a bubble radius of 10^{-2} cm. As an end-member example, we used different *k* values to see if changes in *k* could offset any diffusion induced fractionation and Cd/Re ratio in the gas. Using $k_{Re} = 100$ and $k_{Cd} = 2$, our modeling still showed an increasing Cd/Re ratio with increasing bubble radii.

This analysis shows that diffusion rates can play a significant role in controlling the concentration of Cd and Re in growing bubbles in magma at *k* values >8. Specifically

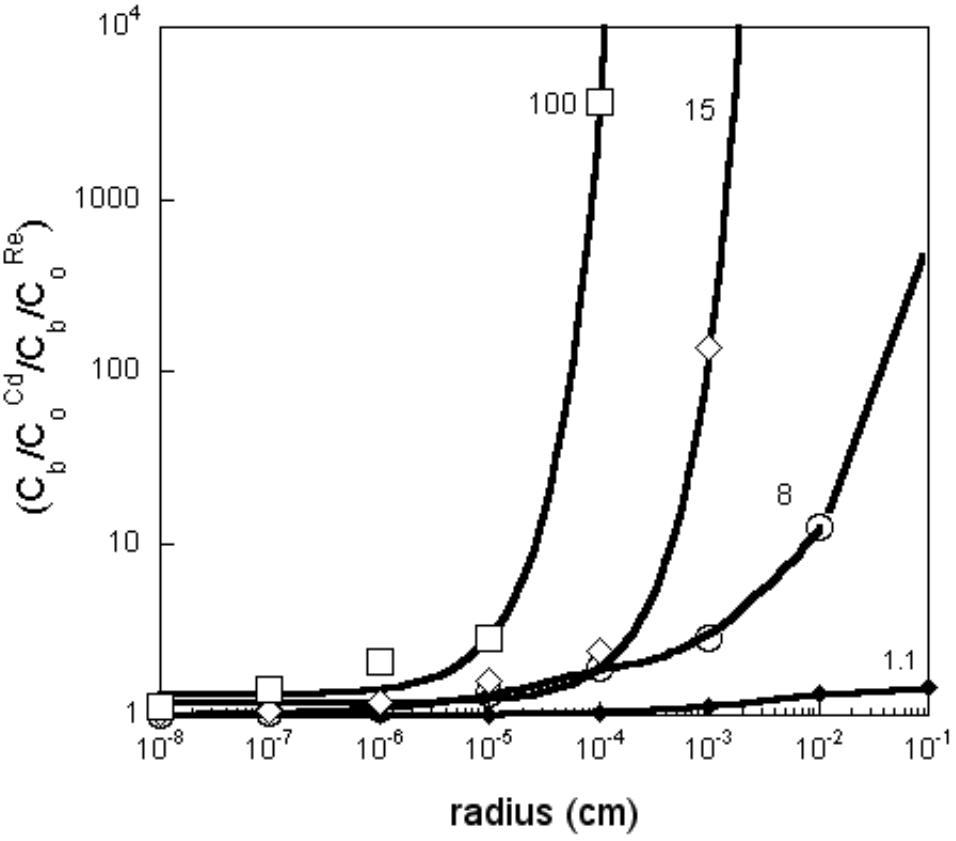

Figure 3.7. Change in Re and Cd concentration in bubbles as a function of increasing radius using *k* values of 1.1, 8, 15 and 100. As *k* increases, the bubble becomes more enriched in Cd relative to Re at progressively smaller bubble sizes. The curves are calculated using equation 3 where at 1300°C, $\log D_{Re} = -7.5$ and $\log D_{Cd} = -6.5$ cm^2/sec and the bubble growth rate is 10^{-5} cm/sec.

Cd and Re will fractionate at smaller bubble sizes with increasing k values. The magnitude of Cd/Re fractionation at *k* values of 15 and 100 is similar but fractionation will occur earlier in the latter. At a *k* value of 8, fractionation is reduced.

Results from the above model indicate the following regarding diffusional fractionation between Cd and Re (and other metals having a similar D value as Re): 1) Cd and Re fractionation in the gas phase increases in fast ascending magmas experiencing increased bubble growth rates, 2) Cd and Re fractionation in the gas phase increases in magmas that cool faster, as may be the case with newly replenished magma because of increased ΔT between the magma and chamber walls, and 3) k values between 100 and 15 have little effect on the magnitude of Cd/Re fractionation in the gas but greatly affect the time when this fractionation occurs; at k = 8 Cd and Re fractionation is reduced and at k = 1.1, there is very little fractionation.

We suggest that Cd/Re ratios in volcanic gases will increase immediately when new magma rises in the conduit or vent and subsequently degases. The magnitude of change of the Cd/Re ratio is affected by bubble growth rate, temperature and partitioning but the ratio will most certainly rise. Given this, it may be possible to predict an approaching volcanic eruption by measuring the Cd/Re ratio of volcanic gases as originally suggested by Crowe et al. (1987). Alletti et al. (2007) have suggested, using a similar model that S/F, Br/F and Cl/F should decrease when new magma rises in the conduit or vent and degasses and that these ratios may also be useful in predicting eruption.

In our model, Cd/Re in volcanic gases should increase during pre-eruptive degassing and after eruption as new (undegassed) magma rises and bubbles grow and are

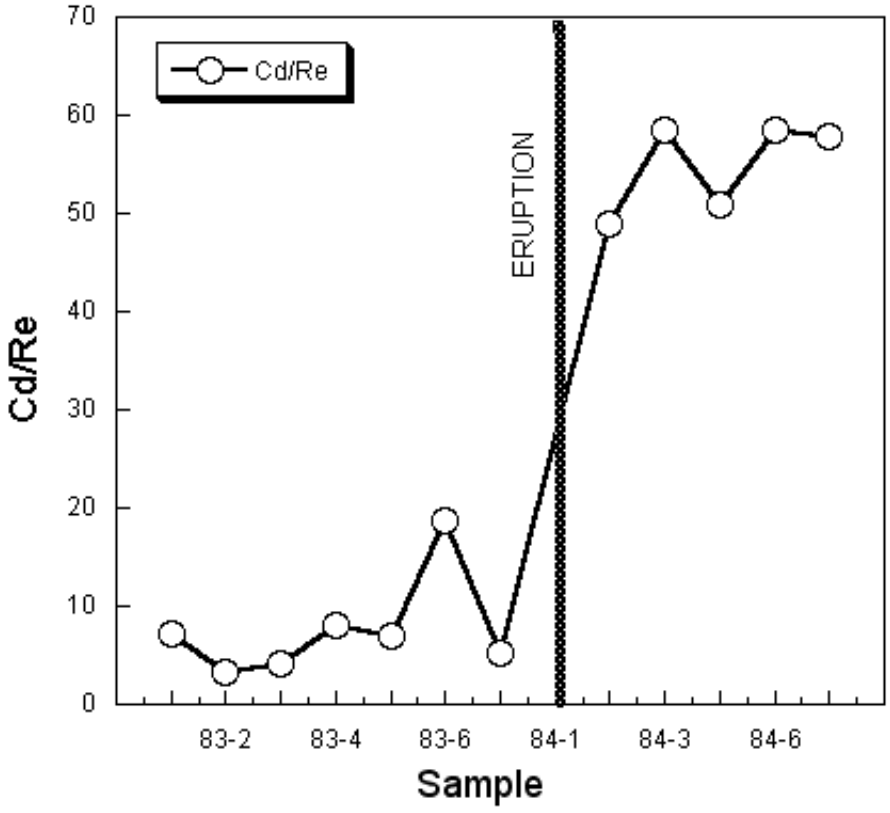

Figure 3.8. Volume normalized Cd/Re versus time for particulate and treated filter sample sets in gasses from Kilauea Volcano sampled between early November 1983 and late January 1984 (data from Crowe et al., 1987). Sample numbers correspond to the year sampled and sample number. Dashed line marks an eruption of lava and the filling of vents. Seep/cool vents were sampled from volcanic vents during quiescent degassing whereas active vent samples are from vents following eruption. Note the increase in Cd/Re ratio prior to and after eruption.

released. There is empirical support for our result. Figure 3.8 shows the Cd/Re ratio of gases released from Kilauea over an eruption cycle from early November 1983 to late January 1984 that ranges from quiescent degassing to active eruption (Crowe et al., 1987). The exact time interval between each sample number in Figure 3.8 was not reported but we assumed the samples were taken at equal intervals (~ 7 days).

Prior to eruption, the Cd/Re ratio in gases is low (5.8 ± 2.1) but nearer to eruption, at sample time 83-6, this ratio more than doubles to 18.8 (Figure 3.8). Immediately prior to eruption, the ratio drops back to the baseline level then increases abruptly to 54.9 ± 4.6 after eruption and this value is maintained during the remaining period.

The changes in Cd/Re throughout an eruption cycle at Kilauea support our model and hypothesis that monitoring Cd/Re may provide a good indication of impending eruption. We also note that Cd/Sb also increases prior to eruption which is predicted in our model given the slower diffusivities of Re and Sb relative to Cd. Changes in Br/F, S/F, Cl/F throughout the eruptive cycle at Kilauea are also consistent with the model of Alletti et al. (2007) suggesting a decrease in these ratios prior to eruption. Ideally, monitoring all these ratios in volcanic exhalants would add confidence to predictions of volcanic eruptions.

3.9. SUMMARY

Volatilization experiments of trace metals, Cd, Re, Pb, Tl, Sb and Te were performed in CMAS and NMAS melts at 0.1 MPa and temperatures between 1200 and 1350°C. Concentration profiles developed as a result of volatilization were measured to provide estimates of metal diffusivity. Although Cu, Zn, In, Mo, Sn and W were also

added to the experiments, concentration profiles did not develop indicating these elements do not form volatile oxides above the melt. The diffusion data was modeled to estimate diffusional fractionation as functions of bubble growth rates, temperature and partitioning. Our model shows that differences in diffusion rates will cause elements to fractionate from one another during magma degassing. Cd/Re ratios should increase during pre-eruptive degassing and remain high throughout the eruption. This result is demonstrated in natural samples providing a compelling method for development in efforts to forecast impending volcanic activity.

ACKNOWLEDGMENTS

We thank J. Spence and M. Raudespp for their able assistance with ICPMS and EMP, respectively and A. Monahan for discussions regarding our mathematical model. We especially appreciate detailed and thoughtful reviews by A. Aiuppa and L. Rose that improved this submission greatly. This research is supported by a MAC Foundation Scholarship to JMM and NSERC of Canada Discovery Grant to DC.

Table 3.1: Major and trace element concentration of starting materials: Concentrations are averages of 15 separate measurements for both compositions. Measurements were made on randomly selected chips of starting glass for trace elements and included run products for major elements. Error shown in brackets at 2σ.

Composition	**NMAS**	**CMAS**
Oxide	wt%	wt%
CaO	0.5 (0.1)	24.6 (0.2)
MgO	12.1 (0.2)	10.7 (0.1)
Na2O	17.6 (0.3)	b.d
Al2O3	15.8 (0.2)	15.6 (0.2)
SiO2	54.5 (0.2)	48.8 (0.3)
TOTAL	**100.5**	**99.8**
Element	ppm	ppm
Cd	b.d	2.8 (0.3)
Re	4.9 (0.4)	2.3 (0.1)
Pb	2.9 (0.3)	3.5 (0.2)
Cu	14.3 (0.2)	6.2 (0.3)
Te	n/a	n/a
Zn	20.5 (1.6)	21.8 (2.1)
Tl	0.9 (0.1)	1.2 (0.2)
In	5.9 (0.3)	9.1 (0.3)
Mo	7.8 (0.3)	10.55 (0.2)
Sn	6.5 (0.2)	7.3 (0.2)
W	6.9 (0.4)	9.4 (0.1)
Sb	4.6 (0.4)	8.3 (0.1)
Yb	16.7 (0.3)	19.5 (0.2)

Table 3.2: Calculated D values for elements in this study. Log D error calculated at 2σ for each experiment based on linear regression statistics of erf-1 versus distance from melt-gas interface. For Ea and Do, 2σ error is shown in brackets calculated using linear regression statistics from the Arrhenius plots.

Comp	Run	Temp	Time	logD (Re)	*(Re)	logD (Sb)	* (Sb)	logD (Tl)	* (Tl)	logD (Pb)	*(Pb)	logD (Cd)	*(Cd)	logD (Te)	*(Te)
	#	(°C)	hrs	cm^2/sec	log	cm^2/sec	log	cm^2/sec	log	cm^2/sec	log	cm^2/sec	log	cm^2/sec	log
CMAS	BM056	1300	12	-7.9	0.1	-7.2	0.3	-7.2	0.1	-7.2	0.1	-6.8	0.2	-7.5	0.2
CMAS	BM055	1300	3	-7.3	0.3	-7	0.6	-7.1	0.2	-7.2	0.1	-6.4	0.2	-7.4	0.2
CMAS	BM052	1300	6	-7.4	0.4	-7.2	0.4	-6.8	0.2	-6.9	0.2	-6.2	0.3	-6.8	0.3
CMAS	BM072	1300	24	-7.5	0.2	-7	0.2	-6.7	0.2	-7	0.1	-6.5	0.3	-7.1	0.2
CMAS	BM067	1350	6	-7.1	0.2	-7.1	0.2	-6.9	0.2	-6.7	0.1	-6	0.2	-7	0.2
CMAS	BM069	1350	6	-7	0.2	-6.8	0.3	-6.6	0.2	-6.6	0.2	-5.9	0.2	-6.8	0.2
CMAS	BM057	1250	1	-8.4	0.3	-7.3	0.2	-7.5	0.2	-7.6	0.1	-6.8	0.2	-7.6	0.2
CMAS	BM065	1250	3	-8.3	0.3	-7.5	0.4	-7.6	0.2	-7.7	0.2	-6.9	0.2	-7.8	0.2
CMAS	*Ea (kJ/mol)*			*617 (92)*		*214 (65)*		*379 (106)*		*472 (58)*		*424 (88)*		*380 (110)*	
CMAS	*logDo (cm^2/sec)*			*12.9 (3.1)*		*0.1(2.2)*		*5.6 (3.3)*		*8.6 (1.9)*		*7.7 (2.9)*		*5.4 (3.6)*	
NMAS	NMAS2	1300	1	-6.6	0.2	-5.9	0.6	-5.6	0.2	-6	0.3				
NMAS	NMAS4	1300	3	-6.3	0.2	-6.3	0.2	-6.2	0.1	-6.1	0.1				
NMAS	NMAS1	1300	6	-6.6	0.1	-5.9	0.3	-5.7	0.3	-6.2	0.3				
NMAS	NMAS5	1200	3	-6.9	0.3	-7.2	0.4	-6.6	0.1	-6.5	0.1				
NMAS	NMAS6	1200	16	-7.1	0.1	-6.8	0.1	-6.7	0.3	-6.8	0.1				
NMAS	*Ea (kJ/mol)*			*218 (122)*		*422 (55)*		*361 (120)*		*239 (56)*					
NMAS	*logDo (cm^2/sec)*			*0.8 (3.1)*		*7.9 (3.3)*		*6.2 (4.0)*		*1.8 (1.9)*					

CHAPTER 4

FLUID/MELT PARTITIONING OF Re, Mo, W, Tl and Pb IN THE SYSTEM HAPLOBASALT-H_2O-Cl AND THE VOLCANIC DEGASSING OF TRACE METALS

Jason M. MacKenzie

Dante Canil

University of Victoria School of Earth and Ocean Sciences

Victoria, BC, Canada, V8W 3P6

4.1. ABSTRACT

The partition coefficients ($Kd_x^{f/m}$) of Re, Mo, W, Tl and Pb between fluid (H_2O + Cl) and a haplobasaltic melt in the CaO-MgO-Al_2O_3-SiO_2 system were measured between 1200 and 1400°C at 1 GPa and fluid chlorine molarities from 7.7 to 27 mol/L. Dissociation of hydroxides added to a trace metal-doped oxide powder, produced a fluid phase in equilibrium with melt at the run conditions. The $Kd_x^{f/m}$ values were determined by mass balance of trace metals added with those determined in glass from the run products. At 1300°C and fluid molarity of 7.7 mol/L, $Kd_{\mathrm{Re}}^{f/m}$ = 9.8 ± 1.8, $Kd_{Mo}^{f/m}$ = 11.8 ± 1.6, $Kd_W^{f/m}$ = 3.7 ± 1.6, $Kd_{Tl}^{f/m}$ = 4.5 ± 1.4 and $Kd_{Pb}^{f/m}$ = 2.4 ± 1.8. Both Mo and Re were shown to partition most strongly into the fluid at all temperatures and fluid chlorinities. At 1400°C, $Kd_{Pb}^{f/m}$ was the only element showing any correlation with fluid chlorinity.

At 1400°C, all Re and Mo completely partitioned into the fluid and thus our calculated $Kd^{f/m}_{\mathrm{Re},Mo}$ are minima. Calculated values of $Kd^{f/m}_{\mathrm{Re},Tl,Pb}$ were combined with the diffusivity of these elements in a 1-D bubble growth model to evaluate the change in metal concentrations and metal ratios expected during the degassing of magma. The model results were compared with emanation coefficients for trace metals from natural volcanoes. The magnitudes of the modeled Re/Tl and Re/Pb in fluids using the diffusivity and partitioning values at 1300°C and the lowest fluid chlorinities were less than that observed from their emanation coefficients. Re and Pb are more sensitive to fluid chlorinity than Tl. The ratios of Re/Tl and Re/Pb expected from emanation coefficients are closely matched if Kd values for experiments having fluid chlorinities of ~16-20 *M*Cl at 1300°C are used.

4.2. INTRODUCTION

Volcanic exhalations are gas and fluid phases originally in contact with melts (Hinkley et al., 1994). Perhaps an under-appreciated aspect of volcanic degassing is that magmatic gases and fluids account for a significant fraction of the flux of trace metals into the crust, atmosphere and hydrosphere (Zoller et al., 1974; Lambert et al., 1988; Nriagu, 1989; Rubin, 1997; Norman et al., 2004). For example, Nriagu (1989) has estimated that volcanic emanations may account for as much as 40-50% of the global inventory of Cd and Hg, and 20-40% of other volatile metals (As, Cu, Ni, Pb and Sb). Secondary processes including condensation on the conduit walls, hydrothermal and groundwater contamination affect the composition of the vapour phase, complicating estimates of volatile metal flux from the volcanoes to the environment.

Volcanoes can significantly fractionate families of metals from one another during degassing (Hinkley et al., 1994) but our knowledge of the underlying causes of element fractionation remain poor. For example, volcanic gases from Kilauea (Crowe et al., 1987) are enriched in chalcophile metals Cd and Cu having enrichment factors that vary over four orders of magnitude. More recently, MacKenzie and Canil (2008) showed differences in metal mobilities in the melt could lead to the fractionation of different metals into the gas phase. They demonstrated that changes in trace metal ratios in gasses over time might provide an indication of impending eruption (Chapter 3).

There are significant limitations in our current understanding of the processes controlling the trace metal concentrations in volcanic gases. The composition of major volatiles (H_2O, CO_2, Cl and S) in volcanic gases in contact with melts is dependent on the composition of the melt, the oxidation state and the degree of volatile supersaturation. The concentration of volatile *metals* such as Cd, W and Re, in volcanic gases is also dependent on metal mobility in the melt and their ability to reach the melt/vapour interface. Once metals arrive at the interface, the fluid-melt partition coefficient ($Kd_x^{f/m}$) between melt and fluid may depend on melt and fluid composition and oxidation state.

It has been suggested that volatile metals are transported as halogen or S complexes in volcanic gases (Hinkley et al., 1994; Williams-Jones et al., 2002; Alletti et al., 2007). Our current understanding of metal complexation, mobility and partitioning is restricted to low temperature studies of metal - fluid solubility relationships (Williams-Jones et al., 2002; Peregoedova et al., 2006) or in high silica granitoid compositions (Keppler and Wyllie, 1991). The reasons for studying fluid/melt partitioning at low temperatures stems from efforts to understand and model the formation of ore deposits

and the ease of experimentation at lower temperature/pressure conditions. Keppler (1996) determined high pressure and temperature fluid/melt partition coefficients for a number of metals (including Pb) and trace elements in one silicate melt and demonstrated that trace element patterns in calc-alkaline magmas in subduction zones can be explained by metasomatism involving an alkali-chloride-rich fluid.

The identity of the magmatic fluid phase controls the concentrations of metals in volcanic exhalents and is affected by processes occurring at depth and as the magma rises. The concentrations of metals in the fluid phase are controlled by element mobility in the melt and the partitioning between fluid and melt. Both of these controls are potentially affected by the composition and oxidation state of the melt and fluid. Our study is an effort to estimate fluid/melt metal partitioning in high temperature, basaltic compositions at 1 GPa in contact with fluid phases containing $H_2O \pm Cl$.

4.3. STARTING COMPOSITIONS

A synthetic, CaO-MgO-Al_2O_3-SiO_2-$H_2O \pm Cl$ and Fe (CMASH "haplobasalt") composition corresponding to the Di_{58}-An_{42} eutectic (Table 4.1) was prepared by grinding reagent grade SiO_2, $Al(OH)_3$, $Mg(OH)_2$ $Ca(OH)_2$ powders in an agate mortar and drying at 120°C in air for one hour. Once dried, the mixture was placed in a closed container and shaken vigorously to homogenize the mixture. NIST certified standard solutions of different metals (Cd, Re, Pb, Cu, Te, Zn, Tl, In, Mo, Sn, Sb, and W) were added using a micropipette in amounts such that the base oxide-hydroxide starting mixture would have ~80 ppm of each metal. The mixture was then ground twice under alcohol, dried at 120°C and stored in an oven at 120°C to keep from it absorbing water (Table 4.1)

To change the Cl/H_2O ratio, Cl was added to the above mixture as $CaCl_2$ and $MgCl_2$ and mixed in a similar fashion. An aliquot of the Ca-$MgCl_2$ mixture was subsequently added to the Cl-free oxide-hydroxide powder in different proportions to provide different levels of Cl in the runs (Table 4.1). In two experiments, Fe was added to the powder and packed into the Pt capsules with a small Pt wire to measure oxygen fugacity (see below).

4.4. METHODS

4.4.1. Experimental Methods

Experiments were performed at 1200-1400°C and 1 GPa in a piston-cylinder apparatus using 12.5 mm NaCl/Pyrex assemblies. Pressure calibration was determined using the transition of Tschermak pyroxene to anorthite-gehlenite-corrundum assemblage at 1300° and 1.3 GPa and 1400°C at 1.4 GPa and the friction correction was found to be less than 5% for this assembly (Fedortchouk et al., 2007). Subsequently, we did not use any friction correction in any experiments and the true pressure is slightly below 1 GPa. Temperature was measured with a $W_{95}Re_5 - W_{74}Re_{26}$ thermocouple and controlled to within ± 2°C by a Eurotherm temperature controller.

For each experiment, the starting powder was loaded and packed into a 3 mm OD x 0.127 mm wall thickness Pt capsule. The capsule was then sealed using an arc welder. The Pt capsule was weighed prior to adding powder and before welding to determine the mass of powder added to the capsule. After welding, the capsule was weighed and placed into a furnace at 140°C for 2 hours to ensure no volatiles were lost.

The loaded capsules were inserted into the pressure media consisting of solid MgO and further packed using MgO powder to reduce distortion of the capsule during heating and pressurization. Pressure assemblies were pressurized to ~30% of the final pressure and heated to 600°C, held for 6 minutes and further pressurized to the final run pressure (~1 Gpa). The charge was then heated to the final run temperature and the pressure adjusted (hot piston in). Quenching was achieved by terminating the power to the graphite furnace upon which the charge cooled to below 100 °C in a few seconds.

The capsule was carefully removed from the pressure assembly, cleaned, weighed and pierced. Visible fluid effervesced out of the charge after piercing. If no fluid was released (e.g., due to capsule failure during pressurization) the run was discarded. The charge was then placed into a furnace at 120°C for 2 hours after which the charge was re-weighed to provide a measure of fluid loss. The dry charge was subsequently mounted and ground to expose the experimental glass for analysis. The run products consisted of glass and a large empty void at the top of the charge where the free fluid phase was present during the run. The glass was cloudy and had many small (<1 um) bubbles that we interpret as exsolution bubbles that formed upon quenching.

4.4.2. Demonstration of equilibrium

In the present study, we use the time invariance of the partition coefficients and the similarity of our calculated $Kd_{Cl}^{f/m}$ (12 ± 4) with those measured by Aletti et al., (2007) ($Kd_{Cl}^{f/m}$ = 14 ± 3) to demonstrate equilibrium. The lack of a significant change in element partitioning behaviour with run times varying from 12-24 hours at 1300 and 1400°C is interpreted to reflect equilibrium among melt and aqueous fluid. At 1200°C, 12

hours does not appear to be sufficient to attain equilibrium but we believe 24 hours is sufficient based on $Kd_{Cl}^{f/m}$.

4.4.3. Mass Balance Calculations

At high temperature during the experiments, the Al, Mg and Ca hydroxides decompose and dissociate producing a CMASH melt in equilibrium with $H_2O \pm Cl$ fluid. Knowing the concentration of an element in the starting powder allows for calculation of the fluid composition by knowing the mass of starting powder added, mass of fluid present and that liberated by the sample (e.g., simple subtraction of element mass that remains in the glass from the mass in the initial starting powder). The calculation procedure is as follows:

1) Concentration in starting powder = µg/g (measured using solution ICPMS)
2) Mass in charge (µg) of element (x) = concentration (x) in powder (µg /g) *x* mass powder (g).
3) Mass (g) of free fluid = mass (g) loss after piercing Pt crucible and heating at 120°C for 2 hours.
4) Melt mass (g) = mass (g) starting powder – mass free fluid (g)
5) Element concentration in melt = measured (µg /g) by LA-ICPMS
6) Mass (µg) of element (x) in melt = concentration in melt (µg /g) *x* mass melt (g)
7) Mass (µg) of element (x) in fluid = mass (µg) in powder – mass (µg) in melt
8) concentration in fluid (µg /g) = mass (µg) of element (x) in fluid / mass fluid (g)
9) $Kd_x^{f/m}$ = µg /g (fluid)/ µg /g (melt)

4.4.4 Sources of Error

The sources of error include: 1) weighing errors, 2) variability in the starting powder composition, 3) variability in the final melt composition and 4) analytical uncertainty. The balance used to weigh the samples is accurate to within 0.00005 g thus the errors associated with weighing amount to ~0.25 and 2.5% relative for the starting powder and fluid, respectively. The 2σ uncertainties for elements in the starting powders are listed in Table 4.1 and range from 4.2 to 8.3% for the trace metals and less than 4% for the major elements. The 2σ standard deviation of elements in the final melt (glass) is less than 8% relative. Finally, the analytical uncertainty is better that 5% on known NIST standard reference materials used for calibration. All these errors were propagated in the mass balance calculations to provide a measure of the uncertainty of calculated $Kd_x^{f/m}$ values listed in Table 4.4.

4.5. ANALYTICAL METHODS

Major and minor elements in experimental glasses and Platinum wire were determined using a CAMECA SX50 electron microprobe at the University of British Columbia at 15 kV acceleration voltage and beam current of 20 nA, with peak counting times of 30 seconds for all elements. Natural standards were used for Mg, Al, Si, Ca, Fe and Cl whereas pure metal standards were used for the Pt metal. While the H_2O content of the melt was not specifically analyzed, we used the ‘by difference’ technique. The accuracy of this technique is discussed further in the results section.

Chlorine concentrations in the starting powder were measured using the Mohr method (Kraemer and Stamm, 1924) which determines the chloride concentration by titration with silver nitrate ($AgNO_3$) where:

$$Ag^{+}_{(aq)} + Cl^{-}_{(aq)} \leftrightarrow AgCl_{(s)} \qquad \text{(eqn. 4.1)}$$

The end point of the titration occurs when all the chloride ions are precipitated. Then additional $Ag^{+}_{(aq)}$ ions react with the chromate ions of the potassium chromate indicator, to produce a red-brown precipitate of silver chromate where:

$$2Ag^{+}_{(aq)} + CrO_4^{2-}{}_{(aq)} \leftrightarrow Ag_2CrO_{4(s)} \qquad \text{(eqn. 4.2)}$$

The molarity of the $AgNO_3$ solution was calibrated by using four solutions incorporating different weights of NaCl dissolved in H_2O and the solution found have a Ag concentration of 0.115 ± 0.002 mol/L. The powders were measured by dissolving 3 aliquots of each powder in D.I. H_2O and titrating with the $AgNO_3$ until the precipitation of $Ag_2CrO_{4(s)}$ was observed. The Cl concentration of each starting powder is listed in Table 4.1↔.

Water in the starting powder was measured using loss on ignition (LOI) whereby an aliquot of starting powder was weighed then placed in a platinum crucible. The powder and crucible were then loaded into a pre-heated box furnace and held at 1000°C for 3 hours prior to quenching in a stream of dry air. The mass of powder was reduced by 17.4 ± 0.4 % and, within error, matches the calculated water contents assuming the starting hydroxides are stoichiometric.

Metals in the starting powder and experimental glasses were determined at the University of Victoria using a Thermo-Instruments X-series II ICP-MS. The starting powders were analyzed by solution nebulisation ICPMS. To prepare the solutions, three

aliquots of each starting powder were dissolved in a mixture of environmental grade HF-HNO_3 acids on a hotplate and dried down three times in sealable Teflon pressure vessels. After the final drying cycle, the powder was finally dissolved in HNO_3. This solution was then diluted using deionised (D.I.) water and spiked with internal standards of Rh, La and Bi. Total procedural blanks and certified reference standards (NIST certified Diabase W-2 and Columbia River basalt BCR2) were also prepared in a similar manner. Data was collected in peak jumping mode with a dwell time of 20 milliseconds at one point per peak. The acquisition time for each sample was 17 seconds in total with a 2.5 minute rinse of 1% environmental grade HNO_3 between each sample.

Synthetic standards were prepared using NIST certified standard solutions using the same internal standards as those used for the unknown samples. All data reduction was done manually offline and concentration of metals in the starting powders closely matches our predicted doping levels. However, Zn, Se and Mo were above the intentional doping level. The increase in these elements is attributed to their presence in the reagent grade oxide/hydroxide mixture, inadvertedly adding more of these metals to the starting powder. While many metals added to our starting powders are not reported in natural rock standard reference materials (W2 and BCR2), the calculated concentrations of Zn and Cu are within error of the reported values.

Metal concentrations in the experimental run product glasses and Pt capsules were measured by Laser ablation (LA-) ICP-MS using a New Wave Research, solid-state, 213

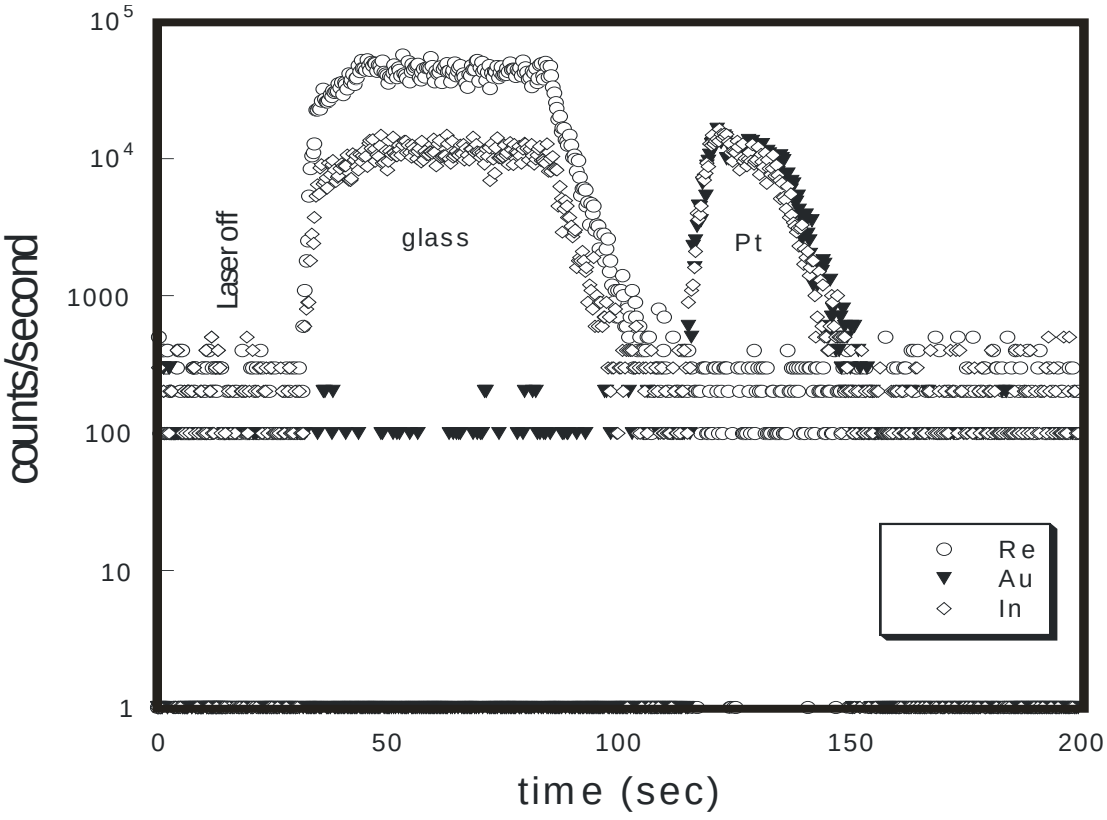

Figure 4.1. Time resolved raw counts/second during laser ablation for experiment P333 (24 hrs, OH-1 composition) showing that all the Au initially added to the starting material has diffused into the Pt. Indium is present in both the glass and Pt and no Re diffused into the Pt capsule

nm Nd:YAG UV laser pulsed at a frequency of 20 Hz with an energy of ~1.9 mJ. NIST 610 and 613 Standard Reference Materials (SRM) glasses were both used as standards for all metals. The spot size and line scan traverse rate were 20 μm and 5 μm /sec, respectively. Data was collected in peak jumping mode with a dwell time of 10 milliseconds at one point per peak. ^{43}Ca was used as the internal standard for NIST SRM and experimental glasses. Data was recorded as time-resolved spectra in counts per second, collected over 200 seconds with 30 seconds allotted to collecting background concentrations. The data was reduced to average concentrations using the Thermo© data reduction software. An example of the raw laser data is shown in Figure 4.1.

It is important to confirm that solution nebulisation and laser ablation return the same concentration for a given sample. We performed this comparison with a homogenous CMAS glass from a previous study (MacKenzie and Canil, 2008, Chapter 3). The CMAS glass contains all the metals investigated in this study. Three samples of the glass were dissolved and analyzed using the solution method described above while three samples of glass were measured using LA-ICPMS. The concentrations of metals in the glasses measured by each method were determined equivalent within error (Figure 4.2).

4.6. OXYGEN FUGACITY

The oxygen fugacity (fO_2) was not explicitly controlled during our experiments. To estimate fO_2 during partitioning experiments, two experiments (P333 and P341) at 1300°C and 1 GPa included adding a small amount of Fe powder and a loop of 0.1 mm diameter Pt wire to the charge. During the course of the experiment, Fe diffused into the

Pt wire. The Fe content in the melt (glass) and wire were determined by microprobe analysis facilitating fO_2 estimates for the experiments from the equilibrium:

$FeO_{(melt)} \leftrightarrow Fe_{(Pt)} + ½\ O_2$ (eqn. 4.3)

from which fO_2 can be determined from the equation:

$\log fO_2 = \Delta G^o/2.303RT + 2\log a_{melt}^{FeO} - 2\log a_{Pt}^{Fe}$ (eqn. 4.4)

where ΔG^o is the free energy change for the reaction and *a* are the activities of FeO and Fe in the melt and Platinum respectively. The activity coefficients for FeO in the melt are given by Holzheid et al. (1997) and Fe in Pt are from Rubie et al. (1993). ΔG^o for reaction (3) is –160.5 kJ/mol as determined by Holzheid et al. (1997). The results of these calculations at 100 kPa yield values of $\log fO_2 = -5.28 \pm 0.15$ for P333 and -5.15 ± 0.23 for P341. These values place the fO_2 of the experiments between 1 to 1.5 log units above the Ni-NiO (NNO) buffer. Increasing pressure from 100 kPa to 1 GPa decreases the Ni-NiO buffers by 0.3 log units. Thus, our fO_2 estimates likely represent minimum values with the true fO_2 within 0.5 log-bar units of the stated values (e.g., $\log fO_2 = -5.2 \pm 0.5$).

In both experiments, the Pt wire showed some compositional zoning from core to rim. This has been also observed by Rubie et al. (1993) and Canil (1994) who used a similar method to estimate fO_2. The concentration gradient indicates that reaction (4.3) did not go to completion but a local equilibrium exists at the contact between the Pt wire and melt. Moreover, the results of Rubie et al. (1993) suggest that the entire charge in our experiments should have equilibrated with respect to fO_2 in our experiments conducted at 1300°C and 24 hours.

4.7. RESULTS

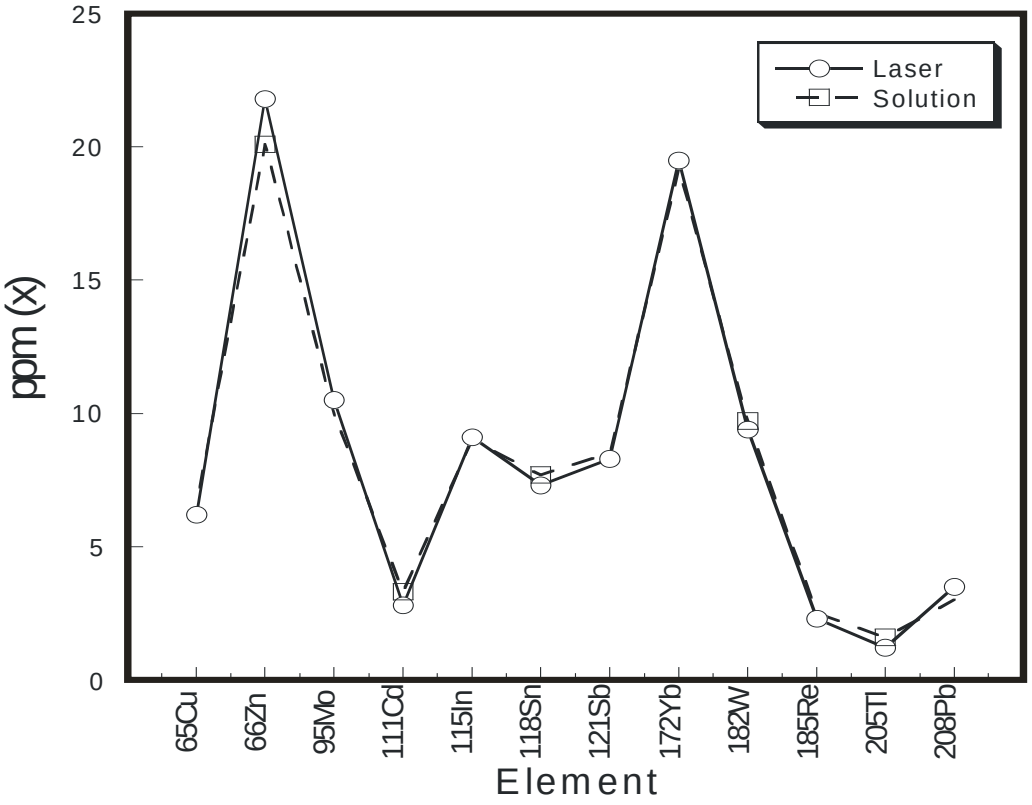

Figure 4.2. Comparison of metal concentrations in CMAS glass determined using solution nebulization and Laser ablation ICPMS.

To calculate $Kd_x^{f/m}$ we used the mass of free fluid liberated at the end of the experiments subtracted from the total mass of the powder added to the capsule to constrain the mass of melt present. This method also provides a measure of the melt H_2O concentration because the water contents of the starting powders are known from LOI measurements; thus the total water content is known in each experiment. Using mass balance, any H_2O that was not liberated at the end of the experiments must have remained dissolved in the melt (Table 4.3).

We also estimated H_2O dissolved in the melt using EMP (by difference approach) assuming water was responsible for the low oxide totals and subtracting this value from 100 wt%. Using the microprobe "by difference" approach, the water contents in the melts are between 9 and 12.5% (Tables 4.2 and 4.3) consistent with those determined in the Diopside-anorthite-H_2O and Diopside-H_2O systems at similar P-T conditions (Yoder, 1965; Eggler and Burnham, (1984).

Figure 4.3 shows a comparison of the melt H_2O contents calculated using both techniques. The H_2O in the melt calculated using the microprobe data is always greater than that determined using the LOI method. This observation indicates either our LOI measurements were not conducted over a long enough period of time or at too low a temperature (incomplete dissociation) or the microprobe (by difference technique) is flawed. The calculated values appear valid using both techniques as evidenced by the consistency with experimental data (e.g., Yoder, 1965) and hydroxide stoichiometry. While the differences in melt water contents have no effect on our calculated partition coefficients, we suggest that the discrepancy between the two techniques is attributable to

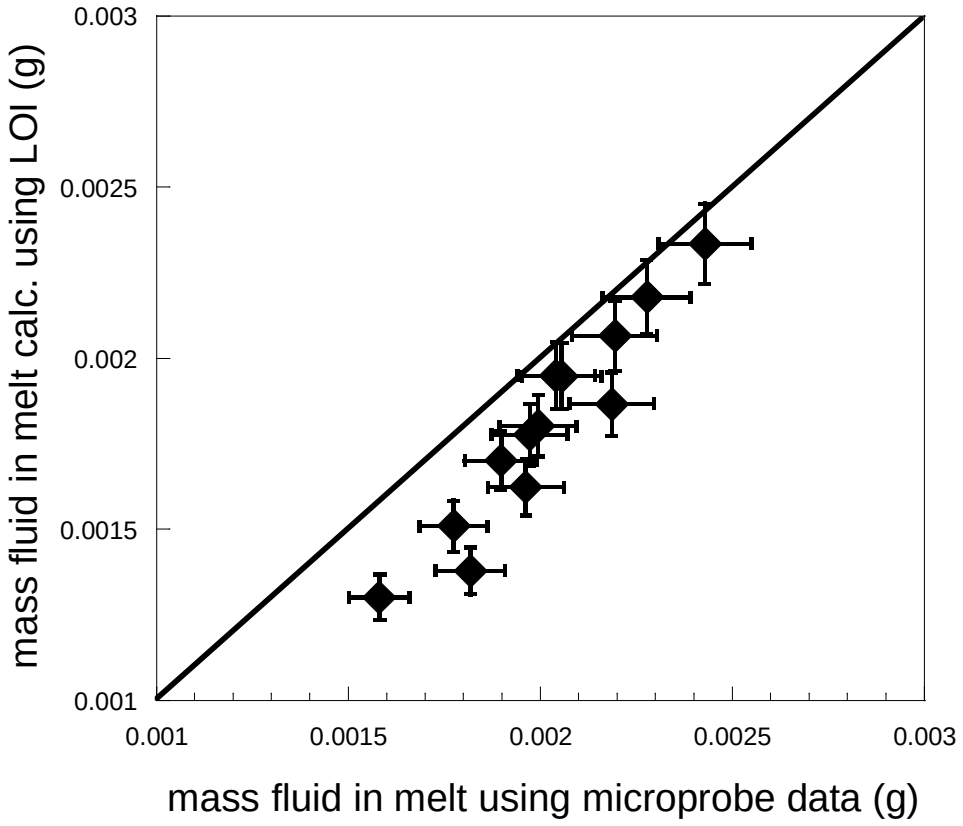

Figure 4.3. Comparison of mass of fluid dissolved in melts estimated using the microprobe data ('by difference' approach) with those determined by LOI. The one to one line is also shown. Error bars shown at 2σ.

the analytical uncertainty associated with using the electron microprobe (by difference) method in melts having water contents above 8 wt% (Nash, 1992).

The experimental results are summarized in Tables 4.3 and 4.4. Although we also doped the starting powders with Cu, Zn, As, Se, In, Sn, Sb, Au and Te, we were only able to determine $Kd_x^{f/m}$ values for Mo, W, Re, Tl and Pb because the former metals diffused either completely (e.g., Au) or partially (e.g., In) into the Pt capsule (Figure 4.1). We made no attempt to quantitatively determine the concentrations in the capsule knowing our mass balance calculations would be completely in error if the metal was in the Pt. Accordingly, we only determined $Kd_x^{f/m}$ for metals that were not present in the Pt capsule at the end of the experiment (Mo, W, Re, Tl and Pb).

Calculated $Kd_{Mo}^{f/m}$ and $Kd_{\mathrm{Re}}^{f/m}$ in experiments at 1400°C in all compositions represent minimum values because all the metal initially added to the starting powder partitioned into the fluid phase. It is unlikely that $Kd_{\mathrm{Re}}^{f/m}$ and $Kd_{Mo}^{f/m}$ are infinite as would be the case if no metal remained in the melt. Rather we are restricted to the limit of detection (LOD) of the glass analysis. We calculated the LOD using the method defined as 3x SD_0, where SD_0 is the value of the standard deviation as the concentration of the analyte approaches zero. For our glass analysis using laser ablation, the LOD for Mo and Re ranges from ~1.2-1.8 ppm for which we use the latter value for calculating minimum $Kd_{\mathrm{Re}}^{f/m}$ and $Kd_{Mo}^{f/m}$.

Figure 4.4 shows the calculated $Kd_x^{f/m}$ for Re, Mo, Tl, Pb and W versus temperature. Between 1200 and 1400°C, $Kd_x^{f/m}$ for Re, Mo, Tl, Pb and W do not change

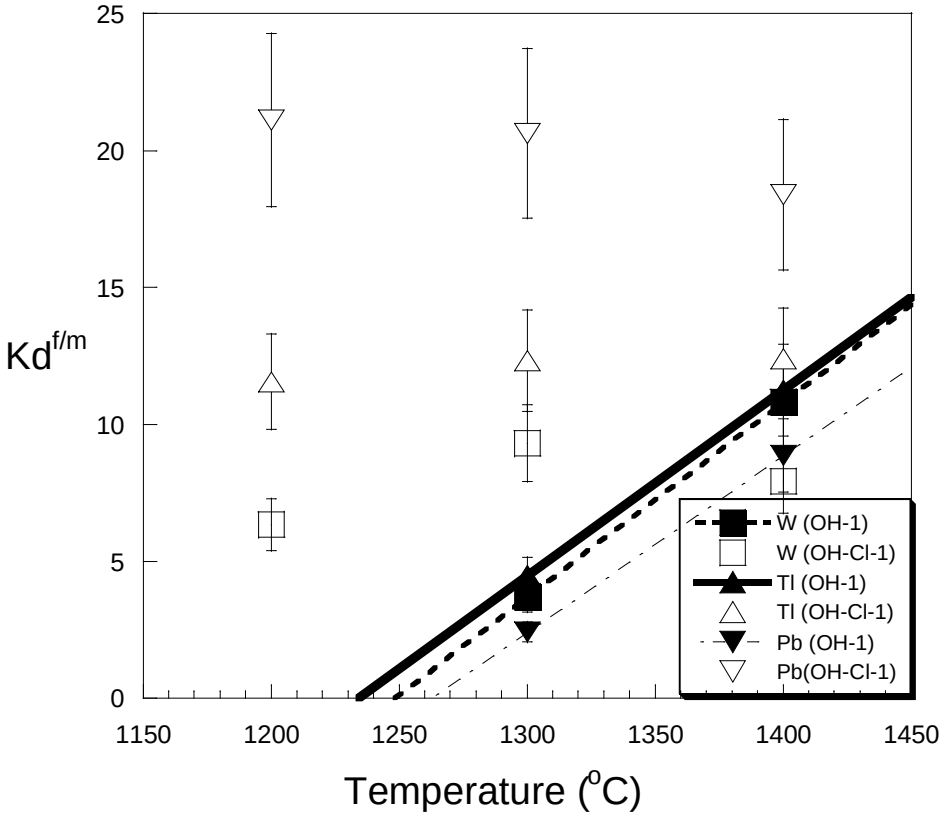

Figure 4.4. $Kd_x^{f/m}$ versus temperature for W, Tl and Pb in OH-1 composition (*M*Cl = 7.7 ± 0.7) and OH-Cl-1 (MCl = 19.2 ± 3.4). Note the temperature dependence of $Kd_x^{f/m}$ only at relatively low fluid chlorinities.

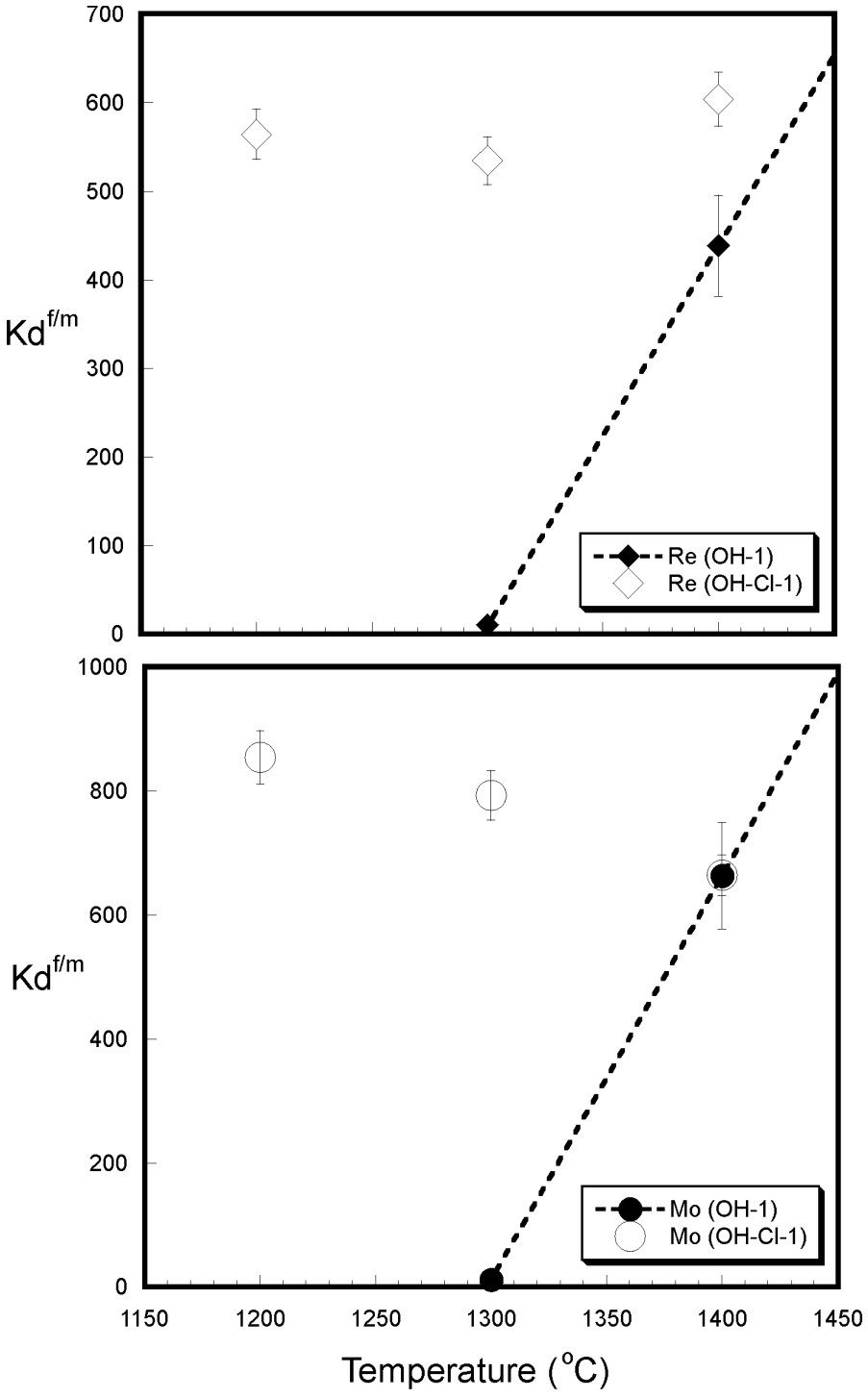

Figure 4.5. $Kd_x^{f/m}$ versus temperature for Mo and Re in OH-1 composition (MCl = 7.7 ± 0.7) and OH-Cl-1 (MCl = 19.2 ± 3.4). Note the temperature dependence of $Kd_x^{f/m}$ only at relatively low fluid chlorinities.

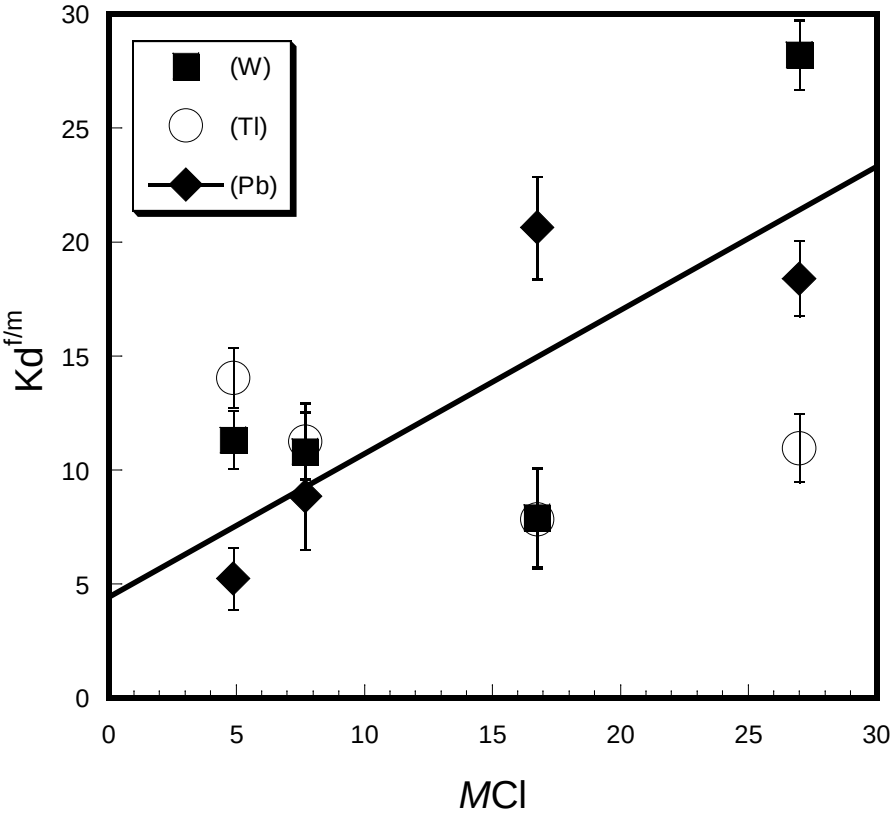

Figure 4.6. Calculated $Kd_x^{f/m}$ versus molarity of Cl in fluid (*M*Cl) for elements at 1400°C.

significantly with changing temperature in the OH-Cl-1 composition having an average fluid Cl molarity (MCl) of 19.7 ± 3.3 mol/L. In the OH-1 composition, however, (MCl = 7.6 ± 0.7), $Kd_x^{f/m}$ for Re, Mo, Tl, Pb and W all increase with increasing temperature from 1300 to 1400°C. In the OH-Cl-1 composition, Re and Mo partitioned completely into the fluid and thus the calculated $Kd_{\mathrm{Re}}^{f/m}$ and $Kd_{Mo}^{f/m}$ represent minimum values.

At temperatures below 1400°C, $Kd_{Pb}^{f/m}$, $Kd_{Tl}^{f/m}$, $Kd_{W}^{f/m}$, $Kd_{\mathrm{Re}}^{f/m}$ $Kd_{Mo}^{f/m}$ all increase with fluid chlorinity from 7.6 ± 0.7 to 19.7 ± 3.3 mol/L. At 1400°C, however, only $Kd_{Pb}^{f/m}$ increases linearly with increasing MCl (R^2 = 0.79) whereas no correlation exists for W and Tl (Figure 4.4). At 1400°C, all the Mo and Re initially added to the powder partitioned into the fluid and thus calculated $Kd_{Mo.\mathrm{Re}}^{f/m}$ are minimum values reflecting the solubility of these elements in the fluid at this temperature (Table 4.4).

4.8. DISCUSSION

Our experiments were aimed at addressing the degassing of metals from magmas at high temperatures, during transit through the crust and upon eruption. There is little data on metal partitioning at the high T, high P systems, especially in more mafic systems like basalt, with which to compare and contrast our results.

Ulrich and Mavrogenes (2008) demonstrate increasing Mo solubility in H_2O-KCl fluids with increasing KCl fluid molarity at constant temperature and increasing temperature at constant KCl fluid molarity. Our experiments show a similar trend at 1300°C where Mo solubility in fluids increases from 812 ± 20 ppm in 7.7 ± 0.7 MCl

fluids to 1478 ± 37 ppm in 19.2 ± 3.4 *M*Cl fluids. It should be noted that, for the latter composition, our data represent only minimum solubility values as all the initial Mo in the starting material partitioned into the fluid. These solubility values are less than Mo solubility values determined from experiments using synthetic fluid inclusions where, at similar Cl molarities, Mo solubility ranges from ~2300 to 5080 ppm at 800°C and 200 MPa (Ulrich and Mavrogenes, 2008).

The increase in Mo partitioning and solubility we observe with increasing Cl concentration in the fluid, however, is contrary to some previous work. In granite-H_2O±Cl systems at 750°C and 140 to 200 MPa pressure, Candela and Holland (1984) observed no change in $Kd_{Mo}^{f/m}$ with changing fluid Cl molarity, and Keppler and Wyllie (1991) measured decreasing $Kd_{Mo}^{f/m}$ with increasing Cl molarity in the fluid. These observations led both authors to suggest Mo dissolves in fluid dominantly as an oxy-hydroxide species.

The contrasting solubility and partitioning behavior of Mo with changing fluid Cl content appear unrelated to temperature as the data from Ulrich and Mavrogenes (2008) span the temperature range (500-800°C) of Candela and Holland (1984) and Keppler and Wyllie (1991). We hypothesize that the contrasting partitioning behavior between these different studies can be explained by a change in speciation of Mo in high Cl fluids. The experiments of Candela and Holland (1984) and Keppler and Wyllie (1991) generally span fluid compositions having <5*M*Cl solutions whereas this study and that of Ulrich and Mavrogenes (2008) extend to much higher (5-27 *M*Cl) fluid compositions. Yokoi et al. (1993) show that, in high Cl fluids (>3*M*HCl), Mo speciation in the fluid may consist of a combined oxide, chloride species such as MoO_2Cl_2. As such, we envision Mo

speciation as an oxide-hydroxide species in low chlorinity (<4 *M*HCl) fluids changing to an oxide-chloride species at higher chlorinities. Furthermore, in supercritical fluids, a temperature dependence of Mo partitioning between fluid and melt is only observed in experiments having low (<7 *M*Cl) fluids. These data provide a measure of the relative influence of temperature and composition on $Kd_{Mo}^{f/m}$.

The $Kd_{\mathrm{Re}}^{f/m}$ is similar to $Kd_{Mo}^{f/m}$ and shows temperature dependence only in runs with low Cl fluids whereas $Kd_{\mathrm{Re}}^{f/m}$ is independent of temperature in runs with high Cl fluids. At 1300°C, $Kd_{\mathrm{Re}}^{f/m}$ increases dramatically with increasing Cl concentration in the fluid, suggesting Re speciation in the fluid is as a ReCl(x) species, as observed by Xiong and Wood (1999) in experiments conducted at 400 and 500°C. Given the similar behavior of Mo and Re in magmatic fluids with respect to temperature and fluid composition, it is not surprising that these elements are concentrated in Cu-Mo ore deposits.

The rhenium contents of mid-ocean ridge (MORB), ocean-island (OIB) and arc-type basalts are non-uniform with the latter having the lowest Re abundance. Righter and Hauri (1998) attributed differences in the Re contents between MORB and OIB to the presence of garnet in the mantle source of the latter magma type whereas others (e.g., Bennett et al., 2000; Lassiter, 2003; Norman et al., 2004; MacKenzie and Canil, 2006) argue that late stage Re degassing is responsible for the differences. At 1300°C and a fluid *M*Cl = 7.7, $Kd_{\mathrm{Re}}^{f/m}$ is ~10, which is an order of magnitude greater than $Kd_{\mathrm{Re}}^{garnet/melt}$ (~ 1.8; Mallmann and O'Neill, 2007) at a similar temperature, thus adding further support

for the hypothesis that volcanic degassing is the cause of lower Re concentrations in OIB and arc-type basalts relative to MORB.

The partition coefficients of Pb, W and Tl are all positively correlated with temperature in our OH-1 composition (fluid = 7.7 ± 0.7 MCl) but independent of temperature in our OH-Cl-1 composition (fluid = 19.2 ± 3.4 MCl) (Figure 4.4). Of these elements, at 1400°C, only Pb shows any correlation with chlorinity of the fluid phase (Figure 4.6). The increase of $Kd_{Pb}^{f/m}$ with increasing fluid chlorinity suggests Pb is dissolved primarily as a chloride complex in the fluid phase, as observed by Candela and Piccoli (1995) and Zajacz et al. (2008) who also noted a positive correlation between $Kd_{Pb}^{f/m}$ and fluid chlorinity.

Zajacz et al. (2008) suggest that the linear correlation for Pb with Cl in the fluid indicates that Pb complexes with only one Cl atom in the fluid producing a charged $PbCl^{+}$ species. Because of the low dielectric constant of water at magmatic temperatures (Holloway, 1987), charged species in the fluid are unlikely. With this in mind, Zajacz et al. (2008) suggest the presence of an additional species in the fluid to balance the charge such as a PbCl(OH) compound. Finally, our calculated $Kd_{Pb}^{f/m}$ at 1300 and 1400°C and in fluids MCL of 7.7 ± 1.2 are $Kd_{Pb}^{f/m}$ = 2.4 ± 0.2 and 8.8 ± 0.5, respectively, are within the range of $Kd_{Pb}^{f/m}$ = 4.2 ± 2 calculated by Keppler (1996) in a andesite-fluid system with 5*M* (Na,K)Cl fluid at 1100°C.

At 1400°C, $Kd_{W}^{f/m}$ does not correlate with increasing fluid Cl molarity at MCl values less than 15 but increases almost three-fold when the MCl of the fluid is ~27. This observation is contrary to the data of Bai and van Groos (1999) and Zajacz et al. (2008)

that show a positive correlation with fluid chlorinity at chlorinities less than *M*Cl = 3. Closer scrutiny of the data of Zajacz et al. (2008) reveals that, at higher fluid chlorinities (12<*M*Cl<14), $Kd_W^{f/m}$ shows significant scatter. The lack of correlation between $Kd_W^{f/m}$ and *M*Cl of the fluid indicates that W dissolves in the fluid as an oxide-hydroxide species in fluids with Cl molarities below 17 but may be present as a chloride species in fluids having Cl molarities above this value.

Unlike W, at 1400°C, $Kd_{Tl}^{f/m}$ is essentially constant at 11 ± 2.5 across the entire range of fluid chlorinities investigated including at the highest fluid MCL (Figure 4.6). This observation indicates that Tl dissolves in fluids as an oxide-hydroxide species and Cl plays no role.

The $Kd_x^{f/m}$ of all metals investigated here increases with increasing fluid MCl, yet only Pb is positively correlated with fluid chlorinity at 1400°C. We can only hypothesize that the wholesale increase in all elements when the fluid MCl increases from 7.6 ± 0.7 to 19.7 ± 3.3 mol/L may be related to complex changes in H_2O and HCl activities for which we have no constraints at the conditions of the experiments. Overall, Pb, Re, and Mo are the most sensitive to fluid chlorinity, W is less sensitive while Tl shows no sensitivity fluid Cl contents.

4.8.1. Geological implications

The emanation coefficient of an element (x) from a degassing magma is defined as:

$\varepsilon_x = (C_i - C_f) / C_f$ (eqn. 4.5)

where C_i and C_f are the concentration in the magma before and after eruption, respectively. The ε_x of metals show a wide range metal enrichment in volcanic gases, and vary over two orders of magnitude for metals investigated in this study (log ε_x(W, Re) = -3.0 and –0.9 respectively) (Rubin, 1997). Factors responsible for the differences in ε_x and the fractionation of metals from one another include the availability of chemical components that act as complexing agents, mineral precipitation prior to eruption, dilution, partitioning and kinetic factors.

Using a 1-D bubble growth model, MacKenzie and Canil (2008) showed that Cd and Re may be fractionated from each other during magma ascent and degassing because of their different diffusion rates in the melt (Chapter 3). However, fluid/melt partitioning data was not available for Cd and Re adding uncertainty to their model. Although, we were unable to obtain fluid/melt partitioning data for Cd, we can estimate the effects of diffusion and fluid/melt partitioning in volcanic gases for Re/Pb, Re/Tl and Tl/Pb for which we have data from this study and MacKenzie and Canil (2008).

Smith et al. (1955) derived a one-dimensional model that accounts for the relationship between diffusion, partitioning and bubble growth rates:

$$C_b(r) = \frac{1}{2k} C_0 \left\{ 1 + erf\left(\frac{\sqrt{(R/D)r}}{2} \right) + (2k-1)\, e^{-kq(R/D)r}\, erfc\left(\frac{(2k-1)\sqrt{(R/D)r}}{2} \right) \right\}$$

(eqn. 4.6)

where C_b is the concentration of the bubble at some radius(r). C_0 is the initial concentration in the melt, R is the growth rate, D is the diffusion rate, k is the partition coefficient and q is equal to 1-k. Equation 6 can be used to derive the bubble rim

composition under different model conditions which we present as instantaneous concentrations of the bubble.

Fundamentally, bubble growth and magma vesiculation occurs at lower pressures than those at which our partitioning values were derived. Thus, it is instructive to compare the nature of fluids at varying pressures and temperatures. At high pressure and temperature, the dielectric constant of water is directly proportional to fluid density and inversely proportional to temperature (Seward and Franck, 1981; Holloway, 1987). The ionization of H_2O generally increases at high temperatures and pressures although the ionization constant decreases exponentially at pressures below 2.5 GPa (Marshall and Franck, 1981). Additionally, ionization constants for alkali and HCl decrease with increasing temperature (Eugster, 1981).

In basaltic systems, the temperatures at which bubbles nucleate and grow are within the range investigated in this study leaving only differences in pressure as controls on fluid properties and subsequent partitioning values. As such, the fluids investigated here are likely to be more ionized with respect to H_2O than at lower pressures. While the increased ionization of HCl at high temperature is known (Eugster, 1981), the effect of pressure is unknown.

Changes in the ionization of H_2O will only effect Tl which we hypothesize only complexes with a hydroxide. We suggest that Tl partitioning will be decreased with decreasing pressure (± temperature). Thus, our partitioning values represent maximum values. Because changes in the ionization of Cl with pressure is not known, it is almost impossible to estimate the effect of changing pressure conditions on the partitioning of Pb, Re, Mo and W that we believe will complex with Cl and hydroxides. It is notable

however, that our experimentally derived partitioning values for W, Mo and Pb fall well within the range of $Kd^{f/m}_{W,Mo,Pb}$ values derived from experimental and natural studies on granitic-fluid systems at lower pressures (e.g., Keppler and Wyllie, 1991; Keppler, 1996; Bai and van Groos, 1999). Keppler (1996) also showed that pressure has little effect on calculated $Kd^{f/m}_{W,Mo,Pb}$ between 0.3 and 2 GPa. For this reason, we feel our data are applicable across a large range of pressures and temperature conditions, certainly those encountered by basaltic magma in the crust and at surface.

By applying equation 4.6, we show the expected enrichment of Re, Tl and Pb in the fluid phase (bubble) relative to their initial concentration in the melt as a function of increasing bubble radius using $Kd^{f/m}_{\mathrm{Re},Tl,Pb}$ values from Table 4.4 at 1300°C in our OH-1 composition and the diffusivity values from MacKenzie and Canil (2008) (Chapter 3). Although Re has a slightly slower diffusivity at 1300°C than Tl and Pb, it is enriched in the bubble until the bubble radius reaches ~1 μm. At 1 μm, Re and Tl are similarly enriched relative to Pb and at ~ 10 μm, Tl is enriched relative to Re and Pb. Finally, as the bubble size increases to 100's of microns, the concentrations of all three elements approach their initial concentrations in the melt (e.g., $C_b/C_o = 1$) (Figure 4.7).

The distribution of concentrations for Re, Tl and Pb in gas bubbles (figure 4.6) can provide some important constraints on magma degassing. The ε_x values for Re, Pb and Tl vary over two orders of magnitude in the order Re>Pb>Tl. Moreover, the ratios of ε_x for Re/Pb, Re/Tl and Pb/Tl are ~ 8, 54 and 7, respectively. Figure 4.8 shows the ratios of Re/Pb, Re/Tl and Pb/Tl modeled using equation 4.6 at the same conditions as those

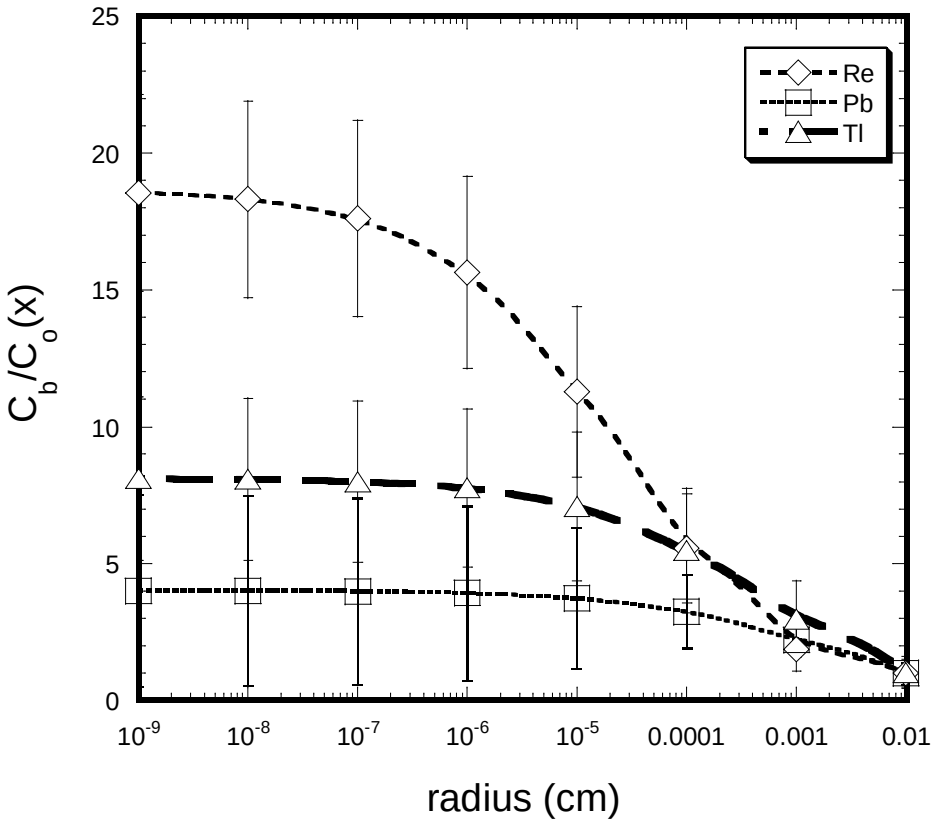

Figure 4.7. Normalized concentration of Re, Tl and Pb as a function of increasing bubble radius modeled using equation 6 at a bubble growth rate of 10^{-5} cm^2/sec and values of $Kd_{\mathrm{Re}}^{f/m} = 9.8 \pm 1.8$, $Kd_{Tl}^{f/m} = 4.5 \pm 1.4$ and $Kd_{Pb}^{f/m} = 2.4 \pm 1.8$ (1300°C, fluid MCl = 7.7 mol/L). Diffusivity values for Re, Tl and Pb used were: $\log D_{\mathrm{Re}} = -7.5 \pm 0.4$, $\log D_{\mathrm{Tl}} = -6.9 \pm 0.2$ and $\log D_{\mathrm{Pb}} = -7.1 \pm 0.2$ cm^2/sec (MacKenzie and Canil, 2008). Error bars calculated at 2σ.

used in Figure 4.7. The expected metal ratios predicted by ratios of ε_x are also shown. We calculate that Re/Pb, Re/Tl and Pb/Tl average 4.5, 2.2 and 0.5 over bubble radii from 10^{-9} to 10^{-7} cm. As the bubble expands, the ratios decrease until radii between 1 and 10 μm's are achieved after which ratios increase.

The magnitude of the Re/Pb and Re/Tl ratios in the gas are lower, and the Pb/Tl ratio has the opposite sense (<1) than what would be expected from ε_x values. Using $Kd^{f/m}_{\mathrm{Re},Tl,Pb}$ for runs with higher chlorinity (Table 4.4) in the model produces an increase in the ratios of Re/Pb and Re/Tl , with Pb/Tl becoming >1. To match the Re/Pb, Pb/Tl and Re/Tl ratios predicted from ε_x values requires a fluid chlorinity of ~16-20 *M*Cl at 1300°C in order to reduce the discrepancy between metal ratios in gases based on ε_x and those calculated using equation 4.6. Our analysis offers only a first order constraint as differences in metal ratios predicted by ε_x values encompass all the metals and complexes therein (e.g., sulphides, chlorides, oxides, and hydroxides) whereas our model only includes the effects of changing Cl concentration in the fluid.

Gases from island arc and intra-plate volcanic settings are important natural sources of metals to the environment and are enriched in Cl relative to other tectonic settings (Perfit et al. 1980). These model results highlight the complexity of fluid and/or gas evolution in magmas as they form and ascend to the surface. Furthermore, as the bubble size increases, the fractionation of metals decreases and approaches their initial melt concentrations. The fact that we do indeed have fractionation in natural volcanic gases could perhaps indicate coalescence of small bubbles is occurring in natural magmas rather than the continuous growth of large ones. That is, the small bubbles in magmas fractionate the metals, and these bubbles coalesce to preserve that fractionation.

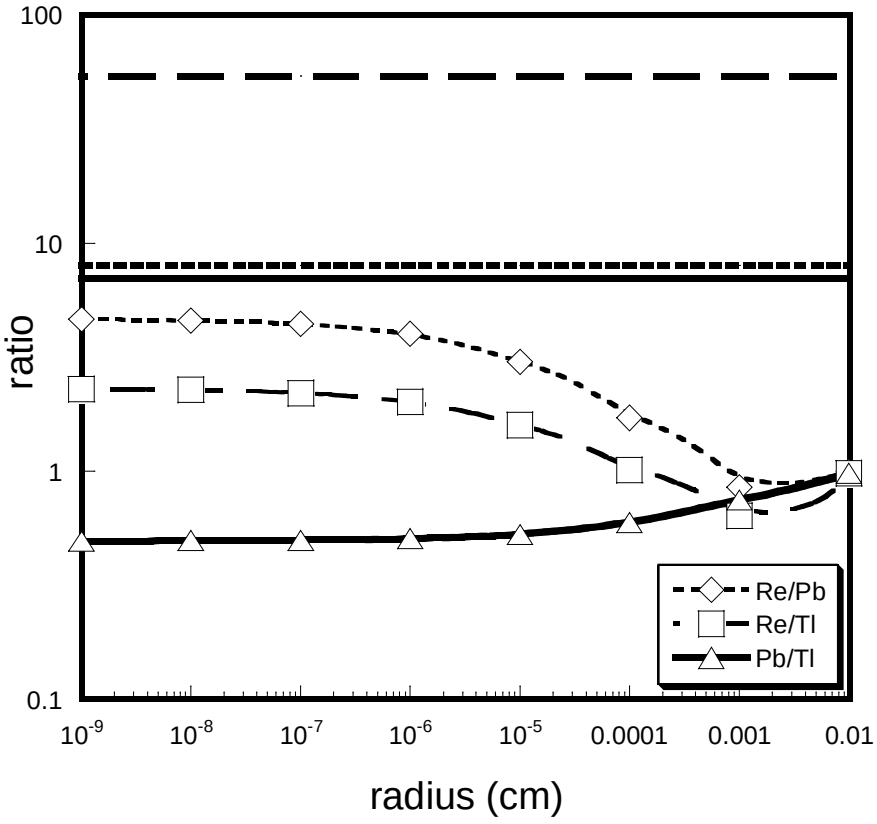

Figure 4.8. Normalized concentration ratios of Re/Pb, Re/Tl and Pb/Tl in growing fluid bubble as a function of increasing bubble radius. Ratios calculated using the data displayed in Figure 4.6 and have similar errors. Metal ratios predicted from values of ε_x are also shown as horizontal lines (line patterns match ratios shown in legend).

4.9. SUMMARY

Partitioning ($Kd_x^{f/m}$) of trace metals Re, Mo, Tl, Pb and W between fluid (H_2O + Cl) and a haplobasaltic melt were measured between 1200 and 1400°C at 1 GPa pressure. Mo and Re were shown to partition strongly into the fluid at all temperatures and fluid chlorinities. At 1400°C, Pb was the only element that showed any correlation with fluid chlorinity but we were unable to evaluate Re and Mo because, at 1400°C, they completely partitioned into the fluid thus our calculated $Kd_{\mathrm{Re},Mo}^{f/m}$ are minimum values. Calculated $Kd_{\mathrm{Re},Tl,Pb}^{f/m}$ were combined with estimates of Re, Tl and Pb diffusivities in a bubble growth model to shows that Re, Tl and Pb will fractionate from one another solely due to differences in $Kd_{\mathrm{Re},Tl,Pb}^{f/m}$. The ratios of Re/Pb, Re/Tl and Pb/Tl in fluids change as bubble diameter increases. Resolving the differences in metal ratios calculated using the model and those expected from ε_x values for these metals in natural volcanoes requires fluid chlorinities of ~16-20 MCl. However values of ε_x include all degassed species of metals and are likely modified en route to the surface. Thus, our modeling offers only a first order constraint that accounts for only changes in fluid Cl concentration in magmas at depth.

ACKNOWLEDGMENTS

We thank J. Spence and M. Raudsepp for their able assistance with ICPMS and EMP. This research is supported by a MAC Foundation Scholarship to JMM and NSERC of Canada Discovery Grant to DC.

Table 4.1. Starting powder compositions. Errors shown in brackets are at 2σ estimated using weighing errors for the major oxides/hydroxides and measurement data for Cl, Mo, W, Re, Tl and Pb.

unit	component	OH-1	OH-Cl-1	OH-Cl-2	OH-Cl-3
wt%	SiO_2	38.4 (0.1)	37.6 (0.1)	37.5 (0.1)	39.0 (0.1)
wt%	$Al(OH)_3$	17.4 (0.1)	16.8 (0.1)	16.2 (0.1)	17.6 (0.1)
wt%	$Mg(OH)_2$	12.3 (0.1)	11.6 (0.1)	11.5 (0.1)	12.2 (0.1)
wt%	$Ca(OH)_2$	25.2 (0.1)	24.3 (0.1)	24.0 (0.1)	25.6 (0.1)
wt%	Cl	6.3 (0.2)	9.7 (0.4)	11.0 (0.4)	5.1 (0.2)
ppm	Mo	121.7 (5.6)	113.8 (4.5)	117.9 (3.7)	120.7 (4.0)
ppm	W	87.2 (7.3)	81.6 (6.5)	84.45 (6.0)	86.5 (4.1)
ppm	Re	81.0 (4.6)	75.7 (3.4)	78.4 (5.1)	80.3 (4.1)
ppm	Tl	78.0 (3.7)	72.9 (4.2)	75.5 (3.5)	77.4 (4.5)
ppm	Pb	81.0 (3.7)	75.8 (2.8)	78.5 (2.1)	80.4 (3.0)

Table 4.2. Major element composition of experimental glasses analysed using electron microprobe. Errors in brackets shown at 2σ standard deviations based on multiple measurements of each glass. n.d. (below detection).

Run #	COMP	T (℃)	Time(hr)	MgO	Al_2O_3	SiO_2	CaO	FeO	Cl	TOTAL
P316	OH-1	1300	6	9.0 (0.1)	12.5 (0.1)	41.9 (0.1)	19.9 (0.1)	n.d	4.7 (0.1)	88.8
P311	OH-1	1300	12	9.1 (0.1)	12.6(0.1)	41.7 (0.3)	19.6 (0.4)	n.d	4.9 (0.6)	88.4
P333	OH-1	1300	24	8.9 (0.1)	12.4 (0.1)	41.7 (0.3)	19.3 (0.3)	1.2 (0.1)	5.3 (0.3)	88.7
P334	OH-1	1400	24	9.0 (0.1)	12.3 (0.1)	41.6 (0.2)	19.9 (0.2)	n.d	4.5 (0.3)	87.4
P335	OH-1	1400	24	8.9 (0.1)	12.7 (0.2)	42.2 (0.4)	19.9 (0.3)	n.d	4.9 (0.2)	88.6
P345	OH-Cl-1	1200	3	9.6 (0.1)	12.6 (0.1)	40.5 (0.3)	19.0 (0.4)	n.d	6.6 (0.6)	88.3
P344	OH-Cl-1	1200	12	9.8 (0.2)	12.7 (0.2)	41.7 (0.5)	18.0 (0.4)	n.d	5.3 (1.2)	87.5
P343	OH-Cl-1	1200	24	9.9 (0.1)	12.3 (0.1)	41.6 (0.5)	18.5 (0.5)	n.d	5.6 (0.5)	87.8
P339	OH-Cl-1	1300	24	9.8 (0.3)	12.4 (0.3)	41.7 (0.5)	18.2 (0.3)	n.d	5.7 (0.9)	87.8
P341	OH-Cl-1	1300	24	8.9 (0.3)	11.7 (0.3)	40.4 (0.6)	17.3 (0.3)	6.8 (1.1)	3.8 (0.2)	88.8
P324	OH-Cl-1	1400	8	9.9 (0.1)	12.3 (0.1)	41.3 (1.2)	18.2 (0.2)	n.d	6.9 (1.2)	88.6
P337	OH-Cl-1	1400	16	9.8 (0.2)	12.2 (0.2)	40.4 (0.8)	18.4 (0.4)	n.d	7.7 (1.0)	88.6
P338	OH-Cl-1	1400	24	10.0 (0.1)	12.4 (0.3)	42.1 (0.6)	18.1 (0.3)	n.d	6.0 (0.8)	88.6
P327	OH-Cl-2	1400	24	10.9 (0.3)	12.3 (0.4)	43.4 (0.8)	19.1 (0.5)	n.d	4.1 (0.6)	89.8
P330	OH-Cl-2	1400	24	9.5 (0.1)	12.5 (0.2)	42.6 (0.5)	20.5 (0.4)	n.d	4.4 (0.5)	89.5
P331	OH-Cl-3	1400	24	9.3 (0.1)	12.7 (0.2)	43.7 (0.4)	20.0 (0.4)	n.d	4.2 (0.3)	90.0
P332	OH-Cl-3	1400	24	9.3 (0.1)	12.8 (0.1)	44.2 (0.2)	20.8 (0.2)	n.d	3.9 (0.1)	91.0

Table 4.3. Summary table of run conditions and masses used in calculation of $Kd_x^{f/m}$. The wt% H_2O (*) content of the glass was calculated by subtracting the wt% total from microprobe analysis. The fluid in the melt (**) was calculated by multiplying the mass of melt (column 6) by the wt% H_2O derived using the microprobe analysis.

Run#	COMP	T	t (hr)	powder (g)	free fluid (g)	melt (g)	% H2O*	fluid added (g)	fluid in melt (g)**	fluid in melt (g)
P316	OH-1	1300	6	0.01700	0.00187	0.01513	11.2	0.00296	0.00169	0.00109
P311	OH-1	1300	12	0.02114	0.00150	0.01964	11.6	0.00368	0.00228	0.00218
P333	OH-1	1300	24	0.01971	0.00148	0.01823	11.2	0.00343	0.00204	0.00195
P334	OH-1	1400	24	0.01798	0.00175	0.01623	11.2	0.00313	0.00182	0.00138
P335	OH-1	1400	24	0.01883	0.00150	0.01733	11.4	0.00328	0.00197	0.00178
P345	OH-Cl-1	1200	3	0.01943	0.00307	0.01636	11.7	0.00338	0.00191	0.00031
P344	OH-Cl-1	1200	12	0.01883	0.00121	0.01762	12.5	0.00328	0.00220	0.00207
P343	OH-Cl-1	1200	24	0.01946	0.00152	0.01794	12.2	0.00339	0.00219	0.00187
P339	OH-Cl-1	1300	24	0.01749	0.00142	0.01607	12.2	0.00304	0.00196	0.00162
P341	OH-Cl-1	1300	24	0.01741	0.00152	0.01589	11.2	0.00303	0.00177	0.00151
P324	OH-Cl-1	1400	8	0.02163	0.00190	0.01973	11.4	0.00376	0.00225	0.00186
P337	OH-Cl-1	1400	16	0.02290	0.00165	0.02125	11.4	0.00398	0.00243	0.00233
P338	OH-Cl-1	1400	24	0.01947	0.00144	0.01803	11.4	0.00339	0.00206	0.00195
P327	OH-Cl-2	1400	24	0.02047	0.00186	0.01861	10.2	0.00356	0.00190	0.00170
P330	OH-Cl-2	1400	24	0.02082	0.00182	0.01900	10.5	0.00362	0.00200	0.00180
P331	OH-Cl-3	1400	24	0.01759	0.00176	0.01583	9.9	0.00306	0.00158	0.00130
P332	OH-Cl-3	1400	24	0.01826	0.00188	0.01638	8.9	0.00318	0.00147	0.00130

Table 4.4. Run summaries and measured trace element concentrations in experimental glasses. Trace element concentrations in fluid and $Kd_x^{f/m}$ are calculated using the mass balance method described in the text. Errors in brackets represent 2σ standard deviations based on counting statistics. * Represents assumed concentration based on Limit of Detection.

Run#	T (℃)	element	glass (ppm)	fluid (ppm)	$Kd_x^{f/m}$	Run#	temp	element	glass	fluid	$Kd_x^{f/m}$
P316	1300	Mo	74.7 (6.1)	501.6 (12.5)	6.7 (1.4)	P341	1300	Mo	1.8*	1375.2 (34.4)	764.0 (18.6)
t (hr)	comp	W	79.9 (3.3)	145.7 (3.6)	1.8 (1.1)	t (hr)	comp	W	53.0 (4.5)	447.5 (11.2)	8.5 (1.1)
6	OH-1	Re	70.1 (5.6)	169.7 (4.2)	2.4 (1.0)	24	OH-Cl-1	Re	1.8*	908.6 (22.7)	504.8 (13.6)
		Tl	73.9 (2.6)	111.2 (2.8)	1.5 (1.2)			Tl	48.4 (15.0)	386.9 (9.7)	8.0 (1.6)
		Pb	80.1 (3.0)	87.8 (2.2)	1.1 (1.2)			Pb	31.5 (8.7)	598.5 (15.0)	19.1 (2.1)
P311	1300	Mo	51.1 (5.7)	577.4 (14.4)	11.3 (1.6)	P324	1400	Mo	14.1 (2.2)	990.2 (24.7)	70.2 (2.1)
t (hr)	comp	W	65.3 (4.7)	225.2 (5.6)	3.4 (1.8)	t (hr)	comp	W	81.0 (11.4)	89.1 (2.2)	1.1 (1.2)
12	OH-1	Re	36.2 (5.1)	372.8 (9.3)	10.3 (1.9)	8	OH-Cl-1	Re	1.8*	727.2 (18.2)	454.5 (9.3)
		Tl	51.5 (4.1)	236.9 (5.9)	4.6 (1.4)			Tl	67.3 (9.2)	122.4 (3.1)	1.8 (1.3)
		Pb	69.2 (4.6)	159.1 (3.9)	2.3 (1.8)			Pb	58.1 (8.5)	231.0 (5.7)	4.0 (1.4)
P333	1300	Mo	65.64 (8.5)	812.6 (20.3)	12.4 (1.7)	P337	1400	Mo	1.8*	1184.0 (29.6)	657.8 (17.8)
t (hr)	comp	W	71.35 (9.2)	282.8 (7.1)	4.0 (1.7)	t (hr)	comp	W	54.0 (10.6)	515.0 (12.9)	9.5 (2.5)
24	OH-1	Re	49.51 (6.8)	468.7 (11.7)	9.5 (1.8)	16	OH-Cl-1	Re	1.8*	1100.8 (27.5)	611.6 (12.6)
		Tl	62.37 (7.4)	270.5 (6.7)	4.3 (1.5)			Tl	49.3 (10.1)	448.6 (11.2)	9.1 (3.0)
		Pb	72.69 (10.9)	183.7 (4.6)	2.(1.9)			Pb	34.3 (6.9)	683.2 (17.1)	19.9 (2.7)
P334	1400	Mo	1.8*	1233.9 (30.8)	685.5 (20.8)	P338	1400	Mo	1.8*	1207.8 (30.2)	671.0 (21.3)
t (hr)	comp	W	42.5 (1.2)	501.5 (12.5)	11.8 (2.1)	t (hr)	comp	W	62.6 (8.8)	395.4 (9.8)	6.3 (1.8)
24	OH-1	Re	1.8*	815.4 (20.4)	452.9 (18.4)	24	OH-Cl-1	Re	1.8*	1072.4 (26.8)	595.8 (12.2)
		Tl	37.5 (5.6)	453.8 (11.3)	12.1 (2.1)			Tl	55.2 (5.7)	364.1 (9.1)	6.6 (1.4)
		Pb	45.1 (2.91)	416.1 (10.4)	9.2 (2.1)			Pb	32.4 (8.2)	690.1 (17.2)	21.3 (1.7)

	T (℃)	element	glass (ppm)	fluid (ppm)	$Kd_x^{f/m}$	Run#	Temp	element	glass	fluid	$Kd_x^{f/m}$
P335	1400	Mo	1.8*	1153.9 (28.8)	641.1 (18.2)	P327	1400	Mo	1.8*	1279.2 (32.0)	710.7 (14.5)
t (hr)	comp	W	45.5 (6.4)	447.6 (11.2)	9.8 (1.3)	t (hr)	comp	W	23.0 (3.0)	699.3 (17.5)	30.4 (1.6)
24	OH-1	Re	1.8*	762.5 (19.0)	423.6 (21.3)	24	OH-Cl-2	Re	1.8*	847.0 (21.2)	529.4 (10.9)
		Tl	39.4 (5.3)	409. (10.2)	10.4 (1.2)			Tl	38.2 (5.2)	449.5 (11.2)	11.8 (1.5)
		Pb	45.4 (2.4)	385.9 (9.6)	8.5 (2.6)			Pb	29.6 (4.4)	567.5 (14.2)	19.2 (1.6)
P345	1200	Mo	60.84 (7.5)	626.9 (15.7)	10.3 (1.1)	P330	1400	Mo	1.8*	1329.6 (33.2)	738.7 (15.1)
t (hr)	comp	W	67.3 (8.8)	252.1 (6.3)	3.7 (1.1)	t (hr)	comp	W	26.5 (9.1)	689.0 (17.2)	26.0 (1.5)
3	OH-Cl-1	Re	80.5 (8.9)	85.0 (2.1)	1.1 (1.0)	24	OH-Cl-2	Re	1.8*	878.3 (21.9)	487.9 (10.1)
		Tl	67.7 (6.7)	162.9 (4.1)	2.4 (0.9)			Tl	42.0 (5.8)	425.5 (10.6)	10.1 (1.5)
		Pb	73.2 (10.6)	146.2 (3.6)	2.0 (1.3)			Pb	32.0 (4.4)	563.2 (14.1)	17.6 (1.7)
P344	1200	Mo	59.2 (8.5)	1031.9 (25.8)	17.4 (2.2)	P331	1400	Mo	1.8*	1190.3 (29.8)	661.3 (16.8)
t (hr)	comp	W	57.3 (6.3)	522.5 (13.1)	9.1 (1.7)	t (hr)	comp	W	45.2 (8.8)	456.5 (11.4)	10.1 (1.3)
12	OH-Cl-1	Re	73.5 (12.5)	188.9 (4.7)	2.6 (2.6)	24	OH-Cl-3	Re	1.8*	786.6 (19.7)	437.0 (9.0)
		Tl	59.8 (9.9)	346.8 (8.6)	5.8 (2.5)			Tl	35.7 (4.9)	451.7 (11.3)	12.6 (1.3)
		Pb	67.8 (9.2)	272.3 (6.8)	4.0 (2.2)			Pb	56.3 (8.3)	297.0 (7.4)	5.3 (1.4)
P343	1200	Mo	1.8*	1537.2 (38.4)	854.0 (21.7)	P332	1400	Mo	1.8	1156.9 (28.9)	642.7 (14.5)
t (hr)	comp	W	61.5 (9.1)	389.8 (9.7)	6.3 (1.8)	t (hr)	comp	W	39.5 (5.3)	495.9 (12.4)	12.5 (1.3)
24	OH-Cl-1	Re	1.8*	1015.6 (25.4)	564.2 (11.6)	24	OH-Cl-3	Re	1.8	764.4 (19.1)	424.7 (8.8)
		Tl	54.1 (9.0)	359.8 (8.9)	6.6 (2.0)			Tl	31.1 (4.3)	480.3 (12.0)	15.4 (1.3)
		Pb	32.1 (5.2)	657.9 (16.4)	20.4 (2.0)			Pb	51.3 (8.3)	333.5 (8.3)	6.5 (1.3)
P339	1300	Mo	1.8*	1478.9 (40.0)	821.6 (18.6)						
t (hr)	comp	W	50.1 (6.4)	509.2 (12.7)	10.12 (1.4)						
24	OH-Cl-1	Re	1.8*	977.1 (24.4)	542.9 (11.1)						
		Tl	46.9 (5.7)	429.1 (10.7)	9.1 (1.5)						
		Pb	28.8 (2.5)	671.2 (16.7)	23.2 (1.2)						

CHAPTER 5.

CONCLUSIONS

The goal of this thesis was to address the dearth of experimental information on kinetic and thermodynamic factors affecting the evolution of volatile trace metals in degassing magmas and use the information to quantify and predict their behaviour in magmas and magmatic gases. To achieve this goal, the diffusivity and fluid/melt partitioning values for eight volatile trace metals (Re, Cd, Tl, Pb, W, Mo, Sb and Te) were determined in 59 high temperature and pressure experiments using nine separate melt compositions. The experiments evaluated metal diffusivity as a function of melt composition, temperature and fO_2 as well as fluid/melt partitioning as a function temperature and fluid composition (chlorinity).

The principal results of this study are:

1) Determination of the diffusivity of Re in silicate melts as a function of temperature, melt composition and fO_2. This value was found to be similar to other volatile diffusivities and indicating little fractionation between Re and other volatile species. The similarities of diffusivity values provided support for a degassing process being responsible for Re depletion in arc-type basalts.

2) Determination of the diffusivity of Cd, Pb, Tl, Te, Sb and Re in a synthetic basalt composition at different temperatures culminating in the development of a degassing (bubble growth) model that predicts fractionation of Cd from the other metals (including Re) due to differences in their mobility. It was shown that this fractionation

leads to changing metal ratios in volcanic gases that may be useful for eruption prediction.

3) Determination of fluid/melt partition coefficients for Re, Tl, Pb, W, and Mo as a function of temperature and fluid composition (chlorinity). The data was combined with diffusivity values for these metals and modeled with the previous bubble growth model. The results showed that natural volcanic gas contents (emanation coefficients) can be matched using our fluid/melt partitioning data calculated for fluids having a fluid Cl molarity between 16 and 20.

To date, this work represents the only known diffusivity measurements for these metals in silicate melts of basaltic composition and the first estimates of high temperature/pressure fluid/melt partitioning for these metals in a basalt/fluid system. The work is important because basalts are formed by melting of the Earth's largest geochemical reservoir, the mantle. Arc basalts are also considered the major building blocks of continental crust (Sun et al., 2003). As such, the metal contents of basalts provide a good measure of the flux of metals across geochemical reservoirs. Problematically, the metal contents of basalts are influenced by degassing processes which lead to underestimates of metal, and other volatile fluxes. The true flux of metals across geochemical reservoirs can only be determined if all the pathways are constrained. This work provides a piece of the puzzle.

Prediction of volcanic eruption is a cardinal goal of volcanic gas studies. Modeling the evolution of metal contents in volcanic gases using the data measured here has provided exciting insight into eruption prediction. This work has shown that monitoring Cd/Re and Cd/Sb ratios in volcanic gases may provide an indication of

impending eruption. Additionally, the mechanism controlling these ratios has been shown to be related to differences in their kinetic behaviours in the melt. Prediction of volcanic eruption is difficult and of utmost importance. This study provides a compelling method for development in efforts to forecast impending volcanic activity. To close the loop, we combined our measured, previously unknown, fluid/melt partition coefficients with our measured diffusion coefficients and showed that ratios of trace metals in volcanic emanations can only be matched using our model if the fluid in equilibrium with the basalt melt has a Cl molarity between 16 and 20. Furthermore, we showed that the fractionation of these metals decrease with increasing bubble radius indicating that small bubbles must coalesce to preserve the observed fractionation.

5.1. Re MOBILITY, PARTITIONING AND THE Re CONTENTS OF BASALTS

Re diffusion experiments in this study show that Re diffusion (D_{Re}) is most strongly influenced by melt composition and speciation in the melt. Oxygen fugacity (fO_2) was found to have less of an influence. Re diffusion was found to be significantly slower in the andesitic (WP-1) composition compared to the basaltic compositions (MIC99-8 and MIC99-8 + Cl). In general, diffusivity decreases with increasing tetrahedral network formers (Si, Al) and decreasing network modifiers (Na, H_2O) (e.g., with decreasing NBO/T). Compared to our basaltic compositions, andesite has a lower ratio of non-bridging oxygen to tetrahedral cations (NBO/T) and thus higher viscosity causing lower diffusivity of Re. At 1300°C, in the lowest viscosity, high NBO/T ratio basalt composition, Re diffusion was $\log D_{Re} = -7.2 \pm 0.3$ cm^2/sec. Re diffusion increased to $\log D_{Re} = -6.6 \pm 0.3$ cm^2/sec in the same composition doped with a small amount of Cl.

The increase in measured diffusion rate in experiments doped with Cl indicate Re complexation with Cl form a more volatile species than a simple Re-oxide as the small amount of Cl present is not believed to change the melt structure significantly.

Fluid/melt partitioning experiments show that Re ($Kd_{\mathrm{Re}}^{f/m}$) is strongly partitioned into the fluid phase in the presence of Cl. Furthermore, Re partitioning increases with increasing fluid chlorine contents suggesting Re speciation in the fluid is as a ReCl(x) species. This observation is confirmed in low temperature experiments of Xiong and Wood (1999) at 400 and 500°C.

This finding is important because arc-type basalts, having the lowest Re contents (0.233 ± 0.170 ppb), also have significantly higher Cl contents (~500-2000 ppm) compared to MORB and OIB. Righter and Hauri (1998) attributed differences in the Re contents between MORB and OIB to the presence of garnet in the mantle source of the latter magma type whereas others (e.g., Bennett et al., 2000, Lassiter, 2003, Norman et al., 2004 and MacKenzie and Canil, 2006) argue that late stage Re degassing is responsible for the differences. At 1300°C and a fluid MCl = 7.7, $Kd_{\mathrm{Re}}^{f/m}$ is ~10 which is an order of magnitude greater than $Kd_{\mathrm{Re}}^{garnet/melt}$ (~ 1.8 – Mallmann and O'Neill, 2007) at a similar temperature.

Increased Re volatility in the presence of Cl combined with increased affinitty for a Cl bearing fluid phase in partitioning experiments strongly favour Re loss as a volatile as the root cause for lower Re concentrations in OIB and arc-type basalts relative to MORB.

5.2. DIFFUSIONAL FRACTIONATION, ERUPTION PREDICTION AND THE EVOLUTION OF VOLCANIC GASES

Diffusion experiments on trace metals Cd, Pb, Tl, Te, Sb and Re in a synthetic basalt melt composition show that at 1300°C, the fastest diffusing element was Cd having a $\log D_{Cd} = -6.5 \pm 0.2$. The slowest element was Re with $\log D_{Re} = -7.5 \pm 0.3$. Diffusivities of Sb, Te, Pb and Tl have intermediate values where $\log D_{Sb} = -7.1 \pm 0.1$, $\log D_{Te} = -7.2 \pm 0.3$, $\log D_{Pb} = -7.1 \pm 0.2$, $\log D_{Tl} = -7.0 \pm 0.2$ cm^2/sec.

Using a similar melt composition in equilibrium with a Cl bearing fluid phase, partitioning values for Re, Mo, W, Tl and Pb were also determined at 1 GPa pressure. At 1300°C and fluid Cl content of 7.7 mol/L, $Kd_{\mathrm{Re}}^{f/m} = 9.8 \pm 1.8$, $Kd_{Mo}^{f/m} = 11.8 \pm 1.6$, $Kd_{W}^{f/m} = 3.7 \pm 1.6$, $Kd_{Tl}^{f/m} = 4.5 \pm 1.4$ and $Kd_{Pb}^{f/m} = 2.4 \pm 1.8$. Diffusion and partitioning data facilitated modeling of the evolution of metals in the volcanic gas phase from initial exsolution through growth and to eventual release at the surface where it may be sampled. The metals were modeled using equation 3.3 in chapter 3.

Problematically, partitioning values were not determined for Cd, Sb or Te as these metals diffused into the Pt during the runs. Cd is the fastest diffusing metal investigated whereas Pb, Tl, Te, Sb and Re had slower diffusivities (Re was the slowest in all compositions). Diffusional fractionation should be most pronounced among metals with the largest differences in diffusivity. As such partitioning values for Cd had to be assumed.

Results from modeling using equation 3.3 and diffusivity/partitioning values measured in this study indicate the following regarding diffusional fractionation between Cd and Re (and other metals having a similar D value as Re): 1) Cd and Re/Sb

fractionation in the gas phase increases in fast ascending magmas experiencing increased bubble growth rates, 2) Cd and Re/Sb fractionation in the gas phase increases in magmas that cool faster, as may be the case with newly replenished magma because of increased ΔT between the magma and chamber walls, and 3) assumed $Kd^{f/m}_{\mathrm{Re}.Cd}$ values between 100 and 15 have little effect on the magnitude of Cd/Re fractionation in the gas but greatly affect the time when this fractionation occurs; at $Kd^{f/m}_{\mathrm{Re}.Cd}$ = 8 Cd and Re fractionation is reduced and at $Kd^{f/m}_{\mathrm{Re}.Cd}$ = 1.1, there is very little fractionation.

$Kd^{f/m}_{\mathrm{Re}}$ is known from partitioning experiments and changes with fluid Cl content and temperature in the lowest Cl fluids. It is recognized that assumptions in $Kd^{f/m}_{Cd}$ may change the model results and Cd/Re fractionation. While these studies are unable to address the shortcomings of $Kd^{f/m}_{Cd}$, as an end-member example, different $Kd^{f/m}_{\mathrm{Re},Cd}$ values were used to see if changes in *k* could offset any diffusion induced fractionation and Cd/Re ratio in the gas. Using $Kd^{f/m}_{\mathrm{Re}}$ = 100 and $Kd^{f/m}_{Cd}$ = 2, the modeling still showed an increasing Cd/Re ratio with increasing bubble radii. This finding adds confidence to the model results and application.

The model indicates that Cd/Re (of Cd/Sb) ratios in volcanic gases will increase immediately when new magma rises in the conduit or vent and subsequently degases. The magnitude of increase of the Cd/Re ratio is affected by bubble growth rate, temperature and partitioning but the ratio will most certainly rise. Given this, it may be possible to predict an approaching volcanic eruption by measuring the Cd/Re ratio of volcanic gases as originally suggested by Crowe et al. (1987).

The model was tested using natural volcanic gas data measured over an eruption cycle at Kilauea that includes quiescent degassing to active eruption (Crowe et al., 1987). Prior to eruption, the Cd/Re ratio in gases is low (5.8 ± 2.1) but nearer to eruption, this ratio more than doubles to 18.8. Immediately prior to eruption, the ratio drops back to the baseline level then increases abruptly to 54.9 ± 4.6 after eruption and this value is maintained during the remaining period.

The changes in Cd/Re (or Cd/Sb) throughout an eruption cycle at Kilauea support our model and hypothesis that monitoring Cd/Re may provide a good indication of impending eruption. We also note that Cd/Sb also increases prior to eruption which is predicted in our model given the slower diffusivities of Re and Sb relative to Cd.

Rubin (1997) compiled volatile emission data for many metals from several basaltic to andesitic volcanoes and calculated their mean emanation coefficients (ε_x). The calculated values indicate a non-uniform distribution of volatile metals in volcanic gases. A principal goal of this work was to determine if the distribution of metals expected from ε_x values could be described with the measured diffusivity and partitioning values using the model. The results will be restricted to Re, Tl and Pb as these are the only metals for which both diffusion and partitioning data were measured.

The ε_x values for Re, Pb and Tl vary over two orders of magnitude in the order Re>Pb>Tl. Moreover, the expected metal ratios predicted by ratios of ε_x for Re/Pb, Re/Tl and Pb/Tl are ~ 8, 54 and 7 respectively. Using the model, and partitioning values in OH-1 composition at 1300 °C (and diffusivity values at 1300 °C) the calculated ratios for Re/Pb, Re/Tl and Pb/Tl average 4.5, 2.2 and 0.5 over bubble radiuses from 10^{-9} to 10^{-7}

cm. As the bubble expands, the ratios decrease until radii between 1 and 10 μm's are achieved after which ratios approach 1.

The distribution of concentrations for Re, Tl and Pb in the fluid can provide some important constraints on fluid composition and magma degassing. Firstly, to match the Re/Pb, Pb/Tl and Re/Tl ratios predicted from ε_x values, the model requires partitioning values for Re, Tl and Pb corresponding to a melt in equilibrium with a of ~16-20 *M*Cl fluid at 1300°C in order to reduce the discrepancy between metal ratios in gases based on ε_x. The Cl content of fluid in composition with basaltic melt is difficult to establish as the initial fluid is generally found separated into a high Cl brine and low Cl vapour. The Cl contents of melt inclusions from basalts range from 0.05 to 0.75 wt% having an average value of ~0.6 wt% (Webster et al., 1999). Using our value for $Kd_{Cl}^{f/m} = 12$, the average fluid in equilibrium with basalt would have 7.2 wt% Cl (*M*Cl = 2.1). This is much less than the model requires to reproduce the ratios expected from ε_x ratios.

To match the ratios expected from ε_x requires a 16-20 MCl fluid phase. Using $Kd_{Cl}^{f/m} = 12$, a 16 MCl fluid would be in equilibrium with a basalt having ~4.7 wt% Cl. Cl solubility in basalt is a dependent temperature, pressure and water content. In general, Cl solubility increases with increasing pressure but decreases with increasing water activity (although the water solubility is also effected by Cl content) (Webster et al., 1999). Although the solubility of Cl in basalt is high enough to meet the model requirements, natural data appear not to support basalts actually having this much Cl in them.

It should be noted that however that differences in metal ratios predicted by ε_x values encompass all the metals and complexes therein (e.g., sulphides, chlorides, oxides,

and hydroxides). The model employed in this work includes the effects only of changing Cl concentration in the fluid. It may very well be that matching the metal ratios predicted by ε_x values requires use of fluid/melt partitioning data for sulphur bearing fluids for which none is available. For example, Re is found as pure Re-sulphide mineral encrustations on the rims of fumarole vents from Kudryavy (Korzhinsky et al., 1994; Taran et al., 1995) thus sulphur complexation is certainly an important process. Mineral/melt partitioning values and partitioning into a residual mineral or sulphide liquid is also envisioned as important in determining metal ratios at the end point of the degassing process.

Gases from island arc and intra-plate volcanic settings are important natural sources of metals to the environment and are enriched in Cl relative to other tectonic settings (Perfit et al., 1980). These model results highlight the complexity of fluid and/or gas evolution in magmas as they form and ascend to the surface and also support an important role for fluid Cl as a partial control on the metal compositions of these gases.

5.3. FUTURE WORK

The concentrations of metals in volcanic gases at the surface represent the endpoint of a long and complex degassing process that initiates when a fluid phase separates from a melt and ends when the fluid/gas phase is released either passively or during active eruption. The results from this work have shown that the concentrations and changes in concentrations of metals in volcanic gases is, in part, controlled by a metals diffusivity in the melt and affinity for the fluid/gas phase.

This work has demonstrated how differences in diffusivity may be responsible for changing metal ratios over an eruption cycle and that these changes may be useful for eruption prediction. With this in mind it is important to note that the calculated diffusivities are chemical diffusivities that reflect a metals affinity for the gaseous state as an oxide species only.

Diffusivity values may be different if the composition of the gas phase was more similar to a natural magmatic gas as the chemical driving force is likely to be different. In nature, melts also contain water and other depolymerising agents changing their viscosity and resulting diffusivity values for the metals. Problematically, natural gas compositions, which are constantly changing, are not easily replicated in experiment.

Having said this, experiments could be developed that use starting compositions having viscosities that replicate those expected in water saturated melts. Diffusion experiments could also incorporate a S, H_2O or Cl bearing gas phase which would serve to change the chemical driving force and may more accurately simulate natural conditions. With the knowledge that metals have different and changing partitioning values in Cl bearing fluids with changing Cl content, it is logical to assume that their diffusivities may scale with changing Cl contents of the gas phase. This work has demonstrated that diffusivity increases when Cl is present in the melt, even at low concentrations. What remains unclear however is if the increase in diffusivity is due to Cl influencing the melt structure or increased volatility of a Cl-bearing species?

Clearly, with respect to Cl, the composition of the fluid phase has an effect on fluid/melt partitioning values for some metals (e.g., Pb) but not others (e.g., Tl). Currently, the effect of other ligands (e.g., S) is unknown but the metal concentrations

measured in volcanic gases at the surface include both of these species in addition to other oxide and hydroxide species. The relative influences of metal complexation with different ligands and the effect on the metal composition of these gases is currently unknown. It is an important issue to resolve because many models that estimate the flux of metals into the environment from volcanic degassing use sulphur as a proxy element (e.g., Pyle and Mather, 2003). If Cl is a much more important complexing ligand than sulphur, these models may be in error. Further study regarding the influence of S in fluid/melt partitioning is warranted.

The thought of conducting more experiments is exciting but it is important to ask the question, what more can be understood from the existing experiments and data? The existing partitioning experiments contain information that is not yet retrieved. In these experiments, it was noted that some metals partitioned into the Pt but also remained in the glass. The fluid/melt partitioning values for these metals (e.g., In) was not determined because we only evaluated metals that resided in the fluid and/or melt using mass balance. It is possible, however, to expand the mass balance to account for metals that partitioned into the fluid and Pt capsule if the concentration in the capsule is known. Determination of metal concentration in the Pt is possible using ICPMS if appropriate standards are incorporated using standard addition techniques.

Modeling of the existing data can also be refined by using a 3-dimensional bubble growth model rather than a 1-D model incorporated here. Preliminary investigation of such a model shows that the concentration of metals in the bubble are significantly higher at the smallest bubble radii but the shape of concentration curves with increasing bubble growth are similar at larger bubble sizes (e.g., $>10^{-6}$ cm). The differences in concentration

distribution may be important when applying the data to different magma types where the bubble sizes and growth rates are likely to be different.

Currently, there are very few measurements that include the metals investigated here. Hopefully the model and predictions herein will promote measurements of trace metals in volcanic gases during eruption cycles to support or refute this work.

REFERENCES

Aiuppa, A., Federico, C., Paonita, A., Pecoraino, G., Valenza, M., (2002) S, Cl and F degassing as an indicator of volcanic dynamics: The 2001 eruption of Mount Etna. Geophysical Research Letters, 29, 54-(1-4).

Aiuppa, A., Federico, C., (2004) Anomalous magmatic degassing prior to the 5th April 2003 paroxysm on Stromboli. Geophysical Research Letters, 31, L14607.

Aiuppa, A., Moretti, R., Federico, C., Giudice, G., Gurrieri, S., Liuzzo, M., Papale, P., Shinohara, H., Valenza, M., (2007) Forecasting Etna eruptions by real-time observation of volcanic gas composition. Geology. 35, 1115-1118.

Alard, O., Griffin, W.L., Pearson N.J., Lorand, JP. O'Reilly, S.Y. (2002) New insights into the Re-Os systematics of sub-continental Lithospheric mantle from in situ analysis of sulphides. Earth and Planetary Science Letters, 203, 651-663.

Allard, P., Aiuppa, A., Loyer, H., Carrot, F., Gaudry, A., Pinte, G., Michel, A., Dongarra, G., (2000) Acid Gas and metal Emission Rates during Long-lived Basalt Degassing at Stromboli Volcano. Geophysical Research Letters 27, 1207-1210.

Alletti, M., Baker, D.R., Freda, C. (2006) Halogen diffusion in basaltic melt. Geophysical Research Abstracts, 8, 05936.

Alletti, M., Baker, D.R., Freda, C., (2007) Halogen diffusion in basaltic melt. Geochimica et Cosmochimica Acta, 71, 3570-3580.

Alves, S., Schiano, P., Allègre, C.J. (1999) Rhenium-osmium isotopic investigation of Java subduction zone lavas. Earth and Planetary Science Letters, 168, 65–77.

Alves, S., Schiano, P., Capmas, F., Allègre, C.J. (2002) Osmium isotope binary mixing arrays in arc volcanism. Earth and Planetary Science Letters, 198, 355–369.

Bai, T.B., van Groos, A.F.K. (1994) Diffusion of chlorine in granitic melts. Geochimica et Cosmochimica Acta, 58, 113–123.

Bai, T.B., van Groos, A.F.K. (1999) The distribution of Na, K, Rb, Sr, Al, Ge, Cu, W, Mo, La, and Ce between granitic melts and coexisting aqueous fluids. Geochimica et Cosmochimica Acta, 63, 1117-1131.

Baker, L., Rutherford, M.J., (1996) Sulfur diffusion in rhyolite melts. Contributions to Mineralogy and Petrology, 123, 335–344.

Becker, H. (2000) Re-Os fractionation in eclogites and blueschists and the implications for recycling of oceanic crust into the mantle. Earth and Planetary Science Letters, 177, 287-300.

Bennett, V.C., Norman, M.D., Garcia, M.O. (2000) Rhenium and platinum group element abundances correlated with mantle source components in Hawaiian picrites: sulfides in the plume. Earth and Planetary Science Letters, 183, 513–526.

Borg, L.E., Brandon, A.D., Clynne, M.A., Walker, R.J. (2000) Re-Os isotopic systematics of primitive lavas from the Lassen region of the Cascade arc, California. Earth and Planetary Science Letters, 177, 301–317.

Borisov A., Jones, J.H. (1999) An evaluation of Re, as an alternative to Pt, for the 1 bar loop technique: An experimental study at 1400°C. American Mineralogist, 84, 1528-1534.

Botcharnikov, R.E., Behrens, H., Holtz, F., Koepke, J., Sato, H. (2004) Sulfur and chlorine solubility in Mt. Unzen rhyodacitic melt at 850 °C and 200 MPa. Chemical Geology 213, 207–225.

Brenan, J.M., McDonough, W.F., Dalpe C. (2003) Experimental constraints on the partitioning of rhenium and some platinum-group elements between olivine and silicate melt. Earth and Planetary Science Letters, 212, 135-150.

Bureau, H., Keppler, H., Metrich, N. (2000) Volcanic degassing of bromine and iodine: experimental fluid/melt partitioning data and applications to stratospheric chemistry. Earth and Planetary Science Letters, 183, 51–60.

Bureau, H., Metrich, N. (2003) An experimental study of bromine behaviour in water-saturated silicic melts.Geochimica et Cosmochimica Acta, 67, 1689–1697.

Burnard, P. (1999) The bubble-by-bubble volatile evolution of two mid-ocean ridge basalts. Earth and Planetary Science Letters, 174, 199-211.

Candela, P.A., Holland, H.D. (1984) The partitioning of copper and molybdenum between silicate melts and aqueous fluids. Geochimica et Cosmochimica Acta, 48, 373-380.

Candela, P.A., Piccoli, P.M. (1995) model ore-metal from melts into vapor and vapor/brine mistures. In. Magmas Fluids and Ore Deposits, v.23 (ed. J.F.H. Thompson). University of British Columbia, Vancouver, BC, pp 101-127.

Canil, D. (1994) An experimental calibration of the “Nickel in Garnet” geothermometer with applications. Contributions to Mineralogy and Petrology, 117, 410-420.

Carmichael, I.S.E. (1991) The redox states of basic and silicic magmas: a reflection of their source regions? Contributions to Mineralogy and Petrology, 106, 129-141.

Carroll, M.R., Webster, J.D. (1994) Solubilities of Sulphur, Noble Gases, Nitrogen, Chlorine and Fluorine in magmas. . In Volatiles in Magmas. Mineralogical Society of America. Reviews in Mineralogy (eds. Carroll M.R. and Holloway J.R.) 30, 231-279.

Carroll, M.R., Blank, J.G., (1997) The solubility of H_2O in phonolitic melts. American Mineralogist, 82, 549–556.

Cashman, K.V., Mangan, M.T. (1994) Physical Aspects of Magmatic Degassing II. Constraints on Vesiculation Processes from Textural Studies of Eruptive Products. In Volatiles in Magmas. Mineralogical Society of America. Reviews in Mineralogy (eds. Carroll M.R. and Holloway J.R.) 30, 447-479.

Chakraborty, S. (1995) Diffusion in silicate melts. In Structure, Dynamics and Properties of Silicate Melts, Mineralogical Society of America (eds. Stebbins J.F., McMillan P.F., Dingwell D.B.) 32, 411-497.

Chebbi, R., Selim, M.S. (2006) The Stefan problem of evaporation of a volatile component from a binary liquid mixture. Journal of Heat and Mass Transfer 42, 238-247.

Chesley, J., Ruiz, J., Righter, K., Ferrari, L., Gomez-Tuena, A. (2002) Source contamination versus assimilation: an example from the Trans-Mexican Volcanic Arc. Earth and Planetary Science Letters, 195, 211–221.

Christie, D.M., Carmichael, I.S.E, Langmuir, C.H. (1986) Oxidation states of mid-ocean ridge basalt glasses. Earth and Planetary Science Letters, 79, 397-411.

Cotton, F.A., Wilkinson, G. (1966) Advanced Inorganic Chemistry: A Comprehensive Text. 2nd ed., Interscience, New York.

Crank, J. (1975) The Mathematics of Diffusion. 2nd ed., Oxford University Press.

Crowe, B.M., Finnegan, D.L., Zoller, W.H., Boynton, W. (1987) Trace Element Geochemistry of Volcanic Gases and Particles From 1983-1984 Eruptive Episodes of Kilauea Volcano. Journal of Geophysical Research, 92, 13708-13714.

Dingwell, D.B., Mysen, B.O., (1985) Effects of water and fluorine on the viscosity of albite melt at high pressure: a preliminary investigation. Earth and Planetary Science Letters, 74, 266–274.

Dingwell, D. B., Scarfe, C. M. (1985) Chemical diffusion of fluorine in melts in the system Na_2O-Al_2O_3-SiO_2. Earth and Planetary Science Letters, 73, 377-384.

Dingwell, D.B., Hess, K.–U. (1998) Melt viscosities in the system Na-Fe-Si-O-F-Cl: Contrasting effects of F and Cl in alkaline melts. American Mineralogist, 83, 1016-1029.

Dixon, J.E., Stopler, E.M. (1995) An experimental study of water and carbon dioxide solubilities in mid-ocean ridge basaltic liquids: Part 2. Applications to degassing. Journal of Petrology, 36, 1633-1646.

Eggler, D.H., Burnham, C.W. (1984). Solution of H_2O in diopside melts – a thermodynamic model. Contributions to Mineralogy and Petrology, 85, 58-66.

Einstein, A. (1956) Investigations on the Theory of Brownian Movement. Dover Publications.

Ertel, W., O'Neill, H. St. C., Sylvester, P.J., Dingwell, D.B., Spettel B. (2001) The solubility of rhenium in silicate melts: Implications for the geochemical properties of rhenium at high temperatures. Geochimica et Cosmochimica Acta, 65, 2161-2170.

Eugster, H.P. (1981) Metamorphic solutions and reactions. Physics and Chemistry of the Earth, 13-4, 461-507.

Fedortchouk, Y., Canil, D., Semenets, E. (2007) Mechanisms of diamond oxidation and their hearing on the fluid composition in kimberlite magmas. American Mineralogist, 92 (7), 1200-1212.

Freda, C., Baker, D. R., Romano, C., Scarlato, P. (2003) Water diffusion in natural potassic melts. In. Oppenheimer, C., Pyle, D. M., and Barclay, J. (Eds.), Volcanic Degassing, vol. 213. Geological Society, London, Special Publication, 53–62.

Freda, C., Baker, D.R., Scarlato, P., (2005) Sulfur diffusion in basaltic melts. Geochimica et Cosmochimica Acta, 69, 5061–5069.

Frost, B.R. (1991) Introduction to oxygen fugacity and its petrologic importance. In Oxide Minerals: Petrologic and Magnetic Significance. Mineralogical Society of America. Reviews in Mineralogy (ed. Lindsley D.H.) 25, 1-9.

Giordano, D., Romano, C., Dingwell, D.B., Poe, B., Behrens, H. (2004) The combined effects of water and fluorine on the viscosity of silicic magmas. Geochimica et Cosmochimica Acta, 68, 5159–5168.

Glasstone, S., Laidler, K.J., Eyring, H. (1941) The Theory of Rate Processes. McGraw Hill, New York-London.

Hauri, E.H., Hart, S.R. (1997) Rhenium abundances and systematics in oceanic basalts. Chemical Geology, 139, 185-205.

Hauri, E.H., Kurz, M.D. (1997) Melt migration and mantle chromatography, 2: a time-series Os isotope study of Mauna Loa volcano, Hawaii. Earth and Planetary Science Letters, 153, 21–36.

Hinkley, T.K., Le Cloarec, M.-F., Lambert, G. (1994) Fractionation of families of major, minor, and trace metals across the melt-vapor interface in volcanic exhalations. Geochimica et Cosmochimica Acta, 58, 3255-3263.

Holloway, J.R. (1987) Igneous fluids. Reviews in Mineralogy, 17, 211-233.

Holzheid, A., Palme, H., Chakraborty, S. (1997) The activities of NiO, CoO and FeO in silicate liquids. Chemical Geology, 139, 21-38.

Jambon, A. (1994) Earth Degassing and Large Scale Geochemical Cycling of Volatile Elements. In Volatiles in Magmas. Mineralogical Society of America. Reviews in Mineralogy (eds. Carroll M.R. and Holloway J.R.) 30, 479-517.

Kiprianov, A.A., Karpukhina, N.G. (2006) Oxyhalide Silicate Glasses. Glass Physics Chemistry, 32, 1-27.

Knacke O., Kubashewski O., Hessekmann K., Eds. (1991) Thermochemical data of pure substances. 2nd ed. Volumes I and II, Springer-Verlag, New York.

Keppler, H., Wyllie, P.J. (1991) Partitioning of Cu, Sn, Mo, W, U, and Th between melt and aqueous fluid in the systems haplogranite-H2O-HCl and haplogranite-H2O-HF. Contributions to Mineralogy and Petrology, 109, 139-150.

Keppler, H. (1996) Constraints from partitioning experiments on the composition of subduction-zone fluids. Nature, 380, 237-240.

Korzhinsky, M.A., Tkachenko, S.I., Shmulovich, K.I., Taran, Y.A., Stienberg, G.S. (1994) Discovery of a pure rhenium mineral at Kudriavy volcano, Nature 369, 51-52.

Kress, V.C., Carmichael, I.S.E. (1988) Stoichiometry of the iron oxidation reaction in silicate melts. American Mineralogist, 73, 1267-1274.

Kraemer, E.O., Stamm, A.J. (1924) Mohr's method for the determination of Silver and Halogens in other than neutral Solutions. Journal of the American Chemical Society 46(12), 2702-2709.

Lambert, G., Le Cloarec, M.-F., Ardouin, B., Le Roulley, J.C. (1986) Volcanic emission of radionuclides and magma dynamics. Earth and Planetary Science Letters, 76, 185-192.

Lambert, G., Le Cloarec, M.F., Pennisi, M. (1988) Volcanic output of SO_2 and trace metals: A new approach. Geochimica et Cosmochimica Acta, 52, 39-42.

Lange, R. A. (1994) The effect of H_2O, CO_2 and F on the density and viscosity of silicate melts. In Carroll, M. R and Holloway, J. R. (Eds.) Volatiles in Magmas, vol. 30. Rev. Miner. 331–369.

Lassiter, J.C., Hauri, E.H. (1998) Osmium-isotope variations in Hawaiian lavas evidence for recycled oceanic lithosphere in the Hawaiian plume. Earth and Planetary Science Letters, 164, 483–496.

Lassiter, J.C. (2003) Rhenium volatility in subaerial lavas: constraints from subaerial and submarine portions of the HSDP-2 Mauna Kea drillcore. Earth and Planetary Science Letters, 214, 311-325.

LeGuern, R. (1988) Ecoulements gazeux reactifs a haute temperature, measures et modelisation. Ph.D. Thesis, Univ. Paris VII.

Lensky, N.G., Navon, O., Lyakhovsky, V. (2004) Bubble growth during decompression of magma: experimental and theoretical investigation. J. Volcano. Geotherm. Res., 129, 7-22.

MacKenzie, J.M., Canil, D. (2006) Experimental constraints on the mobility of Rhenium in silicate liquids. Geochimica et Cosmochimica Acta, 70, 5236-5245.

MacKenzie, J.M., Canil, D. (2008) Volatile heavy metal mobility in silicate liquids: Implications for volcanic degassing and eruption prediction. Earth and Planetary Science Letters, 269, 488-496.

Mallmann, G., O'Neill, H.St.C. (2007) The effect of oxygen fugacity on the partitioning of Re between crystals and silicate melt during mantle melting. Geochimica et Cosmochimica Acta, 71, 2837-2857.

Marshall, W.L., Franck, E.U. (1981) Ion product of water substance. 0°C-1000°C, 1-10000 bars, New international formulation and its background. Journal of Physical and Chemical Reference. 10, v.2, 295-304.

Métrich, N., Rutherford, M.J. (1992) Experimental study of chlorine behavior in hydrous silicic melts. Geochimica et Cosmochimica Acta, 56, 607–616.

Miller, T.L., Zoller, W.H., Crowe, B.M., Finnegan, D.L. (1990) Variations in trace metal and halogen ratios in magmatic gases through an eruptive cycle of the Pu'u O'o vent, Kilauea, Hawaii: July-August 1985. Journal of Geophysical Research, 95, 12607-12615.

Moreira, M., Sarda, P. (2000) Noble gas constraints on degassing processes. Earth and Planetary Science Letters, 176, 375-386.

Morizet, Y., Brooker, R.A., Kohn, S.C. (2002) CO_2 in haplo-phonolite melt; solubility, speciation and carbonate complexation. Geochimica et Cosmochimica Acta, 66, 1809–1820.

Mysen, B.O., Virgo, D., Seifert, F.A. (1982) The structure of silicate melts: implications for the chemical and physical properties of natural magmas. Revues in Geophysics Space Physics, 20, 353-383.

Nash, W.P. (1992) Analysis of oxygen with electron-microprobe – Applications to hydrated glass and minerals. American Mineralogist, 77 (3-4), 453-456.

Norman, M.D., Garcia, M.O., Bennett, V.C. (2004) Rhenium and chalcophile elements in basaltic glasses from Ko'olau and Moloka'I volcanoes: Magmatic outgassing and composition of the Hawaiian plume. Geochimica et Cosmochimica Acta, 68, 3761-3777.

Nowak, M., Schreen, D., Spickenbom, K. (2004) Argon and CO_2 on the race track in silicate melts: A tool for the development of a CO_2 speciation and diffusion model. Geochimica Cosmochimica Acta, 68, 5127-5138.

Nriagu, J., (1989) A global assessment of natural sources of atmospheric trace metals. Nature, 338, 47-49.

Nriagu, J., Becker, C. (2003) Volcanic emissions of mercury to the atmosphere: global and regional inventories. The Science of the Total Environment, 304, 3-12.

Pennisi, M., Le Cloarec, M.F., Lambert, G., Le Roulley, J.C. (1988) Fractionation of metals in volcanic emissions. Earth and Planetary Science Letters, 88, 284-288.

Pennisi, M., Le Cloarec, M.F. (1998). Variations of Cl, F, and S in Mount Etna's plume, Italy, between 1992 and 1995 Journal of Geophysical Research, 103, B3, 5061-5066.

Peregoedova, A., Barnes, SJ., Baker, DR. (2006) An experimental study of mass transfer of platinum-group elements, gold, nickel and copper in sulfur-dominated vapor at magmatic temperatures. Chemical Geology, 235, I. 1-2, 59-75.

Perfit, M.R., Gust, D.A., Bence, A.E., Arculus, R.J., Taylor, S.R. (1980) Chemical Characteristics of Island-Arc basalts – Implications for mantle sources. Chemical Geology, 30 (3), 227-256.

Philpotts, A.R. (1990) Principles of Igneous and Metamorphic Petrology. Prentice Hall, Englewood Cliffs, New Jersey.

Pineau, F., Shilobreeva, S., Kadik, A., Javoy, M. (1998). Water solubility and D/H fractionation in the system basaltic andesite-H_2O at 1250 °C and between 0.5 and 3 kbars. Chemical Geology147, 173–184.

Presnall, D.C., Gudfinnsson, G.H., Walter, M.J. (2002) Generation of mid-ocean ridge basalts at pressures from 1 to 7 Gpa. Geochimica et Cosmochimica Acta, 66, 2073-2090.

Righter, K., Hauri, E.K. (1998) Compatibility of Rhenium in Garnet During Mantle Melting and Magma Genesis. Science 280, 1737-1741.

Righter, K. Chesley, J.T., Ruiz, J. (2002) Genesis of primitive, arc-type basalt: Constraints from Re, Os and Cl on depth of melting and role of fluids. Geology 30, 619-622.

Roy-Barman, M., Allègre, C.J. (1994) $^{187}Os/^{186}Os$ ratios in mid-ocean ridge basalts and abyssal peridotites. Geochimica et Cosmochimica Acta, 58, 5043–5054.

Rubie, D.C., Karato, S., O'Neill, H.StC. (1993) Low differential stress and controlled chemical environment in multianvil high-pressure experiments. Physics and Chemistry of Minerals, 20, 315-322.

Rubin, K. (1997) Degassing of metals and metalloids from erupting seamount and mid-ocean ridge volcanoes: Observations and predictions. Geochimica et Cosmochimica Acta, 61, 3525-3542.

Schiano, P., Birck, J.-L., Allègre, C.J. (1997) Osmium-strontium-neodymium-lead isotopic covariations in mid-ocean ridge basalt glasses and the heterogeneity of the upper mantle. Earth and Planetary Science Letters, 150, 363–379.

Schiano, P., Burton, K.W., Dupré, B., Birck, J.-L., Guille, G., Allègre, C.J. (2001) Correlated Os-Pb-Nd-Sr isotopes in the Austral-Cook chain basalts: the nature of mantle components in plume sources. Earth and Planetary Science Letters, 186, 527–537.

Seward, T.M., Franck, E.U. (1981) The system hydrogen-water up to 440 degrees-C and 2500 bar pressure. Physical Chemistry Chemical Physics, 85, 2-7.

Shirey, S.B., Walker, R.J. (1998) The Re-Os isotope system in cosmochemistry and high-temperature geochemistry. Annual Revues of Earth Planetary Science, 26, 423-500.

Signorelli, S., Carroll, M.R. (2000) Solubility and fluid-melt partitioning of Cl in hydrous phonolitic melts. Geochimica et Cosmochimica Acta, 64, 2851–2862.

Smith, V.G., Tiller, W.A., Rutter, J.W. (1955) A mathematical analysis of solute redistribution during solidification. Canadian Journal of Physics, 33, 723–744.

Sparks, R.S.J., Barclay, J., Jaupart, C., Mader, H.M., Phillips, J.C. (1994) Physical aspects of magmatic degassing, 1. Experimental and theoretical constraints on vesiculation. In Carroll, M. R and Holloway, J. R. (Eds.) Volatiles in Magmas, vol. 30. Rev. Miner. 413–445.

Sparks, R.S.J. (2003) Forcasting volcanic eruptions. Earth and Planetary Science Letters, 210, 1-15.

Sun, W., Bennett, V.C., Eggins, S. M., Kamenetsky, V. S., Arculus, R. J (2003a) Enhanced mantle-to-crust rhenium transfer in undegassed arc magmas. Nature 422, 294-297.

Sun, W., Arculus, R.J., Bennett, V.C., Eggins, S.M., Binns, R.A. (2003b) Evidence for rhenium enrichment in the mantle wedge from submarine arc-like volcanic glasses (Paupa New Guinea). Geology 31, 845-848.

Sylvester, P. J., Eggins, S.M. (1997) Analysis of Re, Au, Pd, Pt and Rh in NIST glass certified reference materials and natural basalt glasses by laser ablation ICP-MS. Journal of Geostandards Geoanalysis, 21, 215-229.

Taran, Y.A., Hedenquist, J.W., Korzhinsky, M.A., Tkachenko, S.I., Shmulovich, K.I. (1995) Geochemistry of magmatic gasses from Kudryavy volcano, Iturup, Kuril Islands. Geochimica et Cosmochimica Acta 59, 1749-1761.

Ulrich, T., Mavrogenes, J. (2008) An experimental study of the solubility of molybdenum in H2O and KCl-H2O solutions from 500°C to 800°C, and 150-300 MPa. Geochimica et Cosmochimica Acta, 72, 2316-2330.

Villemant, B., Boudon, G. (1999) H_2O and halogen (F, Cl, Br) behavior during shallow magma degassing processes. Earth and Planetary Science Letters, 168, 271-286.

Wallace, P.J. (2005) Volatiles in subduction zone magmas: concentrations and fluxes based on melt inclusion and volcanic gas data. Journal of Volcanology and Geothermal Research, 140, 217-240.

Watson, E.B., Sneeringer, M.A., Ross, A. (1982) Diffusion of dissolved carbonate in magmas: experimental results and applications. Earth and Planetary Science Letters, 61, 346–358.

Watson, E.B. (1991) Diffusion of dissolved CO_2 and Cl in hydrous silicic to intermediate magmas. Geochimica et Cosmochimica Acta, 55, 1897–1902.

Watson, E.B., Wark, D.A., Delano, J.W. (1993) Initial report on sulfur diffusion in magmas. EOS Trans of American Geophysical Union, 74, 620.

Webster, J.D., Kinzler, R.J., Mathez, A. (1999). Chloride and water solubility in basalt and andesite melts and implications for magmatic degassing. Geochimica et Cosmochimica Acta, 63, 729–738.

Webster, J.D., De Vivo, B. (2002) Experimental and modeled solubilities of chlorine in aluminosilicate melts, consequences of magma evolution and implications for exsolution of hydrous chloride melt at Mt. Somma-Vesuvius. American Mineralogist, 87, 1046–1061.

Wells, A.F. (1984) Structural Inorganic Chemistry, Oxford: Clarendon Press.

Widom, E., Shirey, S.B. (1996) Os isotope systematics in the Azores: implications for mantle plume sources. Earth and Planetary Science Letters, 142, 451–465.

Williams-Jones, A.E., Migdisov, A.A., Archibald, S.M., Xiao, Z. (2002) Vapor-transport of ore metals. In Water-Rock Interactions, Ore Deposits and Environmental Geochemistry: A Tribute to A. Crerar (eds. Hellmann R. and Wood S.A.), 279-305.

Williams-Jones, A.E., Heinrich, C.A. (2005) 100th Anniversary special paper: Vapor transport of metals and the formation of magmatic-hydrothermal ore deposits. Economic Geology, 100 (7), 1287-1312.

Winther, K.T., Watson, E.B., Korenowski, G.M. (1998) Magmatic sulfur compounds and sulfur diffusion in albite melt at 1 GPa and 1300–1500 °C. American Mineralogist, 83, 1141–1151.

Woodhead, J., Brauns, M. (2004) Current limitations to the understanding of Re-Os behavior in subduction systems, with an example from New Britian. Earth and Planetary Science Letters, 221, 309-323.

Xiong, Y., Wood, S.A. (1999) Experimental determination of the solubility of ReO_2 and the dominant oxidation state of rhenium in hydrothermal solutions. Chemical Geology, 158, 245-256.

Yamamoto, J., Burnard, P.G. (2005) Solubility controlled noble gas fractionation during magmatic degassing: Implications for noble gas compositions of primary melts of OIB and MORB. Geochimica et Cosmochimica. Acta, 69, 727-734.

Yoder, H.S.Jr. (1965) Diopside-Anorthite-water at 5 and 10 kilobars and its bearing on explosive volcanism. Carnegie Institute of Washington Year Book 64, 82-89.

Yokoi, K., Matsubayashi, N., Miyanaga, T., Watanabe, I., Ikeda, S. (1993) Studies on the structure of molybdenum(Vi) in acidic solution by XANES and EXAFS. Polyhedron, 12, 911-914.

Zajacz, Z., Halter, W.E., Pettke, T., Guillong, M. (2008) Determination of fluid/melt partition coefficients by LA-ICPMS analysis of co-existing fluid and silicate melt inclusions: controls on element partitioning. Geochimica et Cosmochimica Acta, 72, 2169-2197.

Zhang, Y., Stolper, E.M. (1991) Water diffusion in basaltic melts. Nature, 351, 306–309.

Zoller, W.H., Gladney, E.S., Duce, R.A. (1974) Atmospheric Concentrations and Sources of Trace Metals at the South Pole. Science, 183, 198-200.

APPENDIX 1 – concentration-distance profiles

TableA1: Concentration (ppb/ppm) versus distance from melt/gas interface (cm from int.) profiles for experiments used to determine Re diffusion coefficients as a function of composition, fO_2 and temperature (Table 2.2).

run#	Re15	Re15	Re16	Re16
time	6 hrs (1300)	6 hrs (1300)	6 hrs (1300)	6 hrs (1300)
log *f*O2	-0.68 (air)	-0.68 (air)	-0.68 (air)	-0.68 (air)
COMPOSITION	**MIC99-8**	**MIC99-8**	**MIC99-8**	**MIC99-8**
	cm from int.	ppb Re	cm from int.	ppb Re
	0.169	730	0.169	743
	0.162	752	0.162	681
	0.154	725	0.154	683
	0.146	724	0.146	702
	0.139	717	0.139	736
	0.131	768	0.131	732
	0.123	729	0.123	711
	0.116	746	0.116	742
	0.108	748	0.108	752
	0.100	710	0.100	709
	0.092	753	0.092	730
	0.085	763	0.085	680
	0.077	744	0.077	737
	0.069	706	0.069	730
	0.062	737	0.062	674
	0.054	712	0.054	708
	0.046	663	0.046	636
	0.039	590	0.039	549
	0.031	515	0.031	486
	0.023	381	0.023	353
	0.015	227	0.015	221
	0.008	123	0.008	122
	0.000	53	0.000	37

Re17 6 hrs (1300) -0.68 (air) **MIC99-8** cm from int.	Re17 6 hrs (1300) -0.68 (air) **MIC99-8** ppb Re	Re18 1 hr (1300) -0.68 (air) **MIC99-8** cm from int.	Re18 1 hr (1300) -0.68 (air) **MIC99-8** ppb Re	Re19 3 hr (1300) -0.68 (air) **MIC99-8** cm from int.
0.169	465	0.095	707	0.132
0.162	452	0.090	721	0.126
0.154	443	0.086	780	0.120
0.146	449	0.082	593	0.114
0.139	458	0.077	707	0.108
0.131	474	0.073	663	0.102
0.123	454	0.069	692	0.096
0.116	470	0.065	656	0.090
0.108	474	0.060	722	0.084
0.100	447	0.056	596	0.078
0.092	468	0.052	655	0.072
0.085	455	0.047	593	0.066
0.077	468	0.043	707	0.060
0.069	453	0.039	663	0.054
0.062	444	0.034	681	0.048
0.054	447	0.030	730	0.042
0.046	407	0.026	721	0.036
0.039	354	0.022	780	0.030
0.031	308	0.017	686	0.024
0.023	219	0.013	629	0.018
0.015	123	0.009	568	0.012
0.008	55	0.004	375	0.006
0.000	4	0.000	199	0.000

Re19	Re20	Re20	Re21	Re21
3 hr (1300)	6 hr (1250)	6 hr (1250)	1 hr (1250)	1 hr (1250)
-0.68 (air)	-0.68 (air)	-0.68 (air)	-0.68 (air)	-0.68 (air)
MIC99-8	**MIC99-8**	**MIC99-8**	**MIC99-8**	**MIC99-8**
ppb Re	cm from int.	ppb Re	cm from int.	ppb Re
837	0.072	446	0.013	805
859	0.069	437	0.012	814
812	0.065	461	0.010	687
870	0.062	451	0.009	633
897	0.059	454	0.007	543
897	0.056	453	0.005	452
890	0.052	463	0.004	416
802	0.049	460	0.004	362
817	0.046	476	0.003	335
870	0.043	453	0.003	271
897	0.039	461	0.003	247
890	0.036	407	0.003	223
926	0.033	405	0.002	190
910	0.029	361	0.002	181
837	0.026	323	0.002	170
859	0.023	260	0.002	162
812	0.020	214	0.001	117
653	0.016	179	0.001	121
529	0.013	116	0.001	81
367	0.010	86	0.001	90
234	0.007	59	0.001	80
158	0.003	39	0.001	53
110	0.000	28	0.000	1

Re22	Re22	Re23	Re23
6 hr (1350)	6 hr (1350)	1 hr (1350)	1 hr (1350)
-0.68 (air)	-0.68 (air)	-0.68 (air)	-0.68 (air)
MIC99-8	**MIC99-8**	**MIC99-8**	**MIC99-8**
cm from int.	ppb Re	cm from int.	ppb Re
0.070	374	0.068	722
0.067	417	0.065	713
0.064	372	0.062	737
0.061	394	0.058	728
0.057	342	0.055	731
0.054	334	0.052	730
0.051	318	0.049	740
0.048	323	0.046	737
0.045	319	0.042	753
0.041	303	0.039	730
0.038	267	0.036	747

0.035	245	0.033	693
0.032	243	0.030	691
0.029	227	0.027	647
0.026	183	0.023	609
0.022	165	0.020	546
0.019	147	0.017	500
0.016	137	0.014	465
0.013	108	0.011	402
0.010	94	0.007	372
0.006	71	0.004	345
0.003	68	0.001	325
0.000	44	0.000	314

ReCl1 6 hrs (1300) -0.68 (air) **MIC99-8+Cl** cm from int.	ReCl1 6 hrs (1300) -0.68 (air) **MIC99-8+Cl** ppb Re	ReCl2 6 hrs (1300) -0.68 (air) **MIC99-8+Cl** cm from int.	ReCl2 6 hrs (1300) -0.68 (air) **MIC99-8+Cl** ppb Re
0.078	304	0.134	404
0.076	315	0.130	412
0.074	340	0.126	400
0.071	303	0.122	399
0.069	285	0.118	405
0.067	276	0.115	411
0.064	285	0.111	402
0.062	263	0.107	384
0.060	246	0.103	342
0.058	249	0.099	328
0.055	215	0.096	349
0.053	203	0.092	328
0.051	201	0.088	349
0.048	197	0.084	345
0.046	185	0.080	303
0.044	176	0.076	276
0.041	150	0.073	299
0.039	142	0.069	267
0.037	125	0.065	260
0.035	115	0.061	229
0.032	109	0.057	238
0.030	88	0.053	204
0.028	84	0.050	191
0.025	68	0.046	167
0.023	63	0.042	156
0.021	44	0.038	130

0.018	38	0.034	112
0.016	41	0.031	101
0.014	28	0.027	67
0.012	17	0.023	54
0.009	18	0.019	35
0.007	11	0.015	30
0.005	12	0.011	26
0.002	9	0.008	21
0.000	6	0.004	12

ReCl3 3 hr (1300 C) -0.68 (air) **MIC99-8+Cl** cm from int.	ReCl3 3 hr (1300 C) -0.68 (air) **MIC99-8+Cl** ppb Re	ReCl4 1 hr (1300) -0.68 (air) **MIC99-8+Cl** cm from int.	ReCl4 1 hr (1300) -0.68 (air) **MIC99-8+Cl** ppb Re
0.017	407	0.032	451
0.016	412	0.031	457
0.016	399	0.029	443
0.015	382	0.027	424
0.015	357	0.026	396
0.014	365	0.024	406
0.014	340	0.023	377
0.013	327	0.021	363
0.013	323	0.020	358
0.012	297	0.018	330
0.012	280	0.016	311
0.011	255	0.015	283
0.011	242	0.013	269
0.010	212	0.012	236
0.010	187	0.010	207
0.009	170	0.009	189
0.009	127	0.007	141
0.009	110	0.005	123
0.008	107	0.004	94
0.008	93	0.004	104
0.007	81	0.003	90
0.007	72	0.003	80
0.006	76	0.003	85
0.006	63	0.003	70
0.005	47	0.002	52
0.005	55	0.002	61
0.004	42	0.002	47
0.004	44	0.002	36
0.003	40	0.001	44

0.003	28	0.001	31
0.002	18	0.001	20
0.002	25	0.001	27
0.001	20	0.001	8
0.001	19	0.001	21
0.000	14	0.000	16

DTRe24	DTRe24	DTRe25	DTRe25
24 hrs (1300)	24 hrs (1300)	24 hrs (1300)	24 hrs (1300)
-7.8	**-7.8**	**-5.1**	**-5.1**
MIC99-8	MIC99-8	MIC99-8	MIC99-8
cm from int.	ppb Re	cm from int.	ppb Re
0.169	445	0.186	787
0.166	437	0.182	851
0.162	430	0.178	847
0.159	425	0.174	896
0.155	456	0.171	838
0.152	434	0.167	852
0.148	428	0.163	795
0.145	430	0.159	862
0.141	415	0.155	856
0.138	407	0.152	877
0.135	451	0.148	840
0.131	388	0.144	855
0.128	383	0.140	908
0.124	397	0.136	859
0.121	391	0.133	848
0.117	400	0.129	822
0.114	404	0.125	816
0.110	407	0.121	815
0.107	415	0.117	858
0.104	396	0.114	862
0.100	425	0.110	826
0.097	404	0.106	839
0.093	413	0.102	858
0.090	396	0.099	826
0.086	403	0.095	879
0.083	410	0.091	863
0.079	422	0.087	783
0.076	404	0.083	768
0.072	424	0.080	755
0.069	409	0.076	725
0.066	410	0.072	720
0.062	392	0.068	753
0.059	402	0.064	732

0.055	409	0.061	736
0.052	425	0.057	674
0.048	406	0.053	682
0.045	400	0.049	625
0.041	376	0.045	634
0.038	376	0.042	594
0.035	337	0.038	541
0.031	332	0.034	471
0.028	324	0.030	404
0.024	301	0.027	339
0.021	261	0.023	330
0.017	230	0.019	261
0.014	196	0.015	221
0.010	142	0.011	159
0.007	92	0.008	117
0.003	37	0.004	95
0.000	24	0.000	63

DTRe26 24 hr (1300 C) **-10** MIC99-8 cm from int.	DTRe26 24 hr (1300 C) **-10** MIC99-8 ppb Re	DTRe27 48 hr (1300) **-6** MIC99-8 cm from int.	DTRe27 48 hr (1300) **-6** MIC99-8 ppb Re
0.136	420	0.221	707
0.133	423	0.216	749
0.130	417	0.212	733
0.127	443	0.207	769
0.125	440	0.203	797
0.122	414	0.198	762
0.119	414	0.194	753
0.116	453	0.189	773
0.114	424	0.185	696
0.111	402	0.180	822
0.108	431	0.176	776
0.105	412	0.171	734
0.102	418	0.167	771
0.100	412	0.162	761
0.097	408	0.158	748
0.094	413	0.153	833
0.091	357	0.149	754
0.089	364	0.144	763
0.086	395	0.140	825
0.083	427	0.135	788
0.080	379	0.131	813
0.078	400	0.126	894

0.075	353	0.122	844
0.072	414	0.117	870
0.069	404	0.113	812
0.066	393	0.108	810
0.064	409	0.104	837
0.061	396	0.099	805
0.058	391	0.095	842
0.055	385	0.090	770
0.053	386	0.086	885
0.050	387	0.081	851
0.047	362	0.077	919
0.044	356	0.072	912
0.042	349	0.068	804
0.039	335	0.063	826
0.036	312	0.059	860
0.033	131	0.054	845
0.030	267	0.050	878
0.028	234	0.045	816
0.025	221	0.041	793
0.022	228	0.036	771
0.019	175	0.032	738
0.017	127	0.027	619
0.014	117	0.023	548
0.011	91	0.018	393
0.008	71	0.014	292
0.006	94	0.009	170
0.003	103	0.005	101
0.000	75	0.000	51

DTRe28 1 hr (1300) **-2** MIC99-8 cm from int.	DTRe28 1 hr (1300) **-2** MIC99-8 ppb Re	DTRe29 3 hr (1300) **-2** MIC99-8 cm from int.	DTRe29 3 hr (1300) **-2** MIC99-8 ppb Re
0.180	465	0.093	516
0.176	452	0.091	476
0.173	443	0.089	516
0.169	449	0.087	504
0.165	458	0.086	479
0.162	400	0.084	507
0.158	454	0.082	495
0.154	470	0.080	493
0.151	449	0.078	481
0.147	458	0.076	538

0.143	474	0.074	505
0.140	454	0.072	512
0.136	466	0.070	492
0.132	487	0.068	510
0.129	444	0.067	569
0.125	465	0.065	551
0.121	452	0.063	587
0.118	443	0.061	623
0.114	449	0.059	582
0.110	458	0.057	486
0.107	474	0.055	557
0.103	454	0.053	496
0.099	470	0.051	506
0.095	561	0.049	501
0.092	570	0.048	486
0.088	449	0.046	562
0.084	513	0.044	432
0.081	490	0.042	501
0.077	477	0.040	492
0.073	445	0.038	482
0.070	426	0.036	520
0.066	482	0.034	524
0.062	431	0.032	505
0.059	477	0.030	498
0.055	464	0.029	516
0.051	467	0.027	463
0.048	429	0.025	457
0.044	428	0.023	520
0.040	397	0.021	533
0.037	346	0.019	450
0.033	330	0.017	444
0.029	300	0.015	463
0.026	278	0.013	342
0.022	256	0.011	360
0.018	213	0.010	345
0.015	173	0.008	320
0.011	157	0.006	226
0.007	106	0.004	228
0.004	84	0.002	171
0.000	65	0.000	176

ReA-1 12 hrs (1300) -0.68 (air)	ReA-1 12 hrs (1300) -0.68 (air)	ReA-2 24 hrs (1300) -0.68 (air)	ReA-2 24 hrs (1300) -0.68 (air)

WP-1	**WP-1**	**WP-1**	**WP-1**
cm from int.	ppb Re	cm from int.	ppb Re
0.189	1675	0.176	1727
0.185	1619	0.172	1678
0.181	1545	0.169	1703
0.178	1324	0.165	1641
0.174	1343	0.162	1621
0.170	1330	0.158	1694
0.166	1343	0.154	1727
0.162	1261	0.151	1678
0.158	1301	0.147	1703
0.154	1230	0.144	1641
0.151	1267	0.140	1621
0.147	1239	0.136	1694
0.143	1184	0.133	1700
0.139	1218	0.129	1727
0.135	1233	0.126	1678
0.131	1231	0.122	1703
0.127	1239	0.118	1641
0.124	1364	0.115	1621
0.120	1338	0.111	1694
0.116	1326	0.108	1454
0.112	1367	0.104	1445
0.108	1285	0.101	1588
0.104	1238	0.097	1632
0.100	1190	0.093	1627
0.097	1213	0.090	1638
0.093	1249	0.086	1724
0.089	1257	0.083	1727
0.085	1281	0.079	1678
0.081	1290	0.075	1703
0.077	1207	0.072	1641
0.073	1294	0.068	1621
0.069	1336	0.065	1694
0.066	1320	0.061	1704
0.062	1412	0.057	1575
0.058	1418	0.054	1533
0.054	1474	0.050	1470
0.050	1445	0.047	1444
0.046	1459	0.043	1414
0.042	1451	0.039	1356
0.039	1429	0.036	1191
0.035	1376	0.032	1207
0.031	1440	0.029	1068
0.027	1472	0.025	975

0.023	1449	0.022	868
0.019	1514	0.018	734
0.015	1410	0.014	652
0.012	1423	0.011	468
0.008	1154	0.007	406
0.004	959	0.004	283
0.000	549	0.000	172

ReA-3 12 hrs (1250) -0.68 (air) **WP-1** cm from int.	ReA-3 12 hrs (1250) -0.68 (air) **WP-1** ppb Re	ReA-4 12 hrs (1250) -0.68 (air) **WP-1** cm from int.	ReA-4 12 hrs (1250) -0.68 (air) **WP-1** ppb Re
0.189	1734	0.189	1680
0.185	1678	0.185	1624
0.181	1604	0.181	1550
0.177	1383	0.177	1329
0.173	1402	0.173	1348
0.170	1389	0.170	1335
0.166	1402	0.166	1348
0.162	1320	0.162	1266
0.158	1360	0.158	1306
0.154	1289	0.154	1235
0.150	1326	0.150	1272
0.146	1298	0.146	1244
0.142	1243	0.142	1189
0.139	1277	0.139	1223
0.135	1292	0.135	1238
0.131	1290	0.131	1236
0.127	1298	0.127	1244
0.123	1423	0.123	1369
0.119	1397	0.119	1343
0.115	1385	0.115	1331
0.112	1426	0.112	1372
0.108	1344	0.108	1290
0.104	1297	0.104	1243
0.100	1249	0.100	1195
0.096	1272	0.096	1218
0.092	1308	0.092	1254
0.088	1316	0.088	1262
0.085	1340	0.085	1286
0.081	1349	0.081	1295
0.077	1266	0.077	1212
0.073	1353	0.073	1299

0.069	1395	0.069	1341
0.065	1379	0.065	1325
0.061	1471	0.061	1417
0.058	1477	0.058	1423
0.054	1533	0.054	1479
0.050	1504	0.050	1450
0.046	1518	0.046	1464
0.042	1510	0.042	1456
0.038	1488	0.038	1434
0.034	1435	0.034	1381
0.031	1499	0.031	1445
0.027	1531	0.027	1477
0.023	1508	0.023	1454
0.019	1573	0.019	1519
0.015	1469	0.015	1415
0.011	1482	0.011	1428
0.007	1213	0.007	1159
0.004	1018	0.004	964
0.000	609	0.000	555

ReA-5 12 hrs (1350) -0.68 (air) **WP-1**	ReA-5 12 hrs (1350) -0.68 (air) **WP-1**	ReA-6 24 hrs (1350) -0.68 (air) **WP-1**	ReA-6 24 hrs (1350) -0.68 (air) **WP-1**
cm from int.	ppb Re	cm from int.	ppb Re
0.108	1476	0.136	1654
0.106	1762	0.133	1667
0.103	1776	0.130	1641
0.101	1786	0.127	1743
0.099	1769	0.125	1731
0.097	1688	0.122	1629
0.095	1542	0.119	1630
0.092	1654	0.116	1782
0.090	1967	0.114	1671
0.088	1846	0.111	1584
0.086	2018	0.108	1696
0.084	1728	0.105	1621
0.081	1717	0.102	1645
0.079	1834	0.100	1623
0.077	1392	0.097	1605
0.075	1674	0.094	1625
0.073	1884	0.091	1407
0.070	2006	0.089	1433
0.068	1951	0.086	1554

0.066	1882	0.083	1682
0.064	1989	0.080	1494
0.062	1810	0.078	1576
0.059	2065	0.075	1391
0.057	2015	0.072	1628
0.055	1557	0.069	1593
0.053	1657	0.066	1548
0.051	1690	0.064	1609
0.048	1705	0.061	1558
0.046	1512	0.058	1539
0.044	1807	0.055	1517
0.042	1960	0.053	1521
0.040	1772	0.050	1524
0.037	1700	0.047	1424
0.035	1986	0.044	1401
0.033	1619	0.042	1373
0.031	1678	0.039	1318
0.029	1643	0.036	1227
0.026	1901	0.033	514
0.024	1595	0.030	1050
0.022	1394	0.028	920
0.020	1383	0.025	872
0.018	1060	0.022	897
0.015	1132	0.019	688
0.013	1105	0.017	500
0.011	946	0.014	462
0.009	859	0.011	360
0.007	599	0.008	278
0.004	750	0.006	370
0.002	533	0.003	405
0.000	441	0.000	295

ReCMAS-1 23 hrs (1300) -0.68 (air) **CMAS**	ReCMAS-1 23 hrs (1300) -0.68 (air) **CMAS**	ReCMAS-2 23 hrs (1300) -0.68 (air) **CMAS**	ReCMAS-2 23 hrs (1300) -0.68 (air) **CMAS**
cm from int.	ppm Re	cm from int.	ppm Re
0.118	9.89	0.121	11.27
0.115	7.56	0.118	8.62
0.113	8.99	0.115	10.25
0.110	7.09	0.112	8.08
0.108	7.01	0.109	7.99

0.106	6.11	0.107	6.97
0.103	8.84	0.104	10.07
0.101	9.86	0.102	11.24
0.098	8.02	0.100	9.14
0.096	9.89	0.097	11.27
0.094	8.44	0.095	9.63
0.091	8.26	0.092	9.42
0.089	8.05	0.090	9.18
0.086	8.80	0.088	10.04
0.084	7.57	0.085	8.64
0.082	10.79	0.083	12.31
0.079	9.89	0.080	11.27
0.077	7.09	0.078	8.08
0.074	7.07	0.076	8.06
0.072	10.76	0.073	12.26
0.070	7.56	0.071	8.62
0.067	8.99	0.068	10.25
0.065	7.50	0.066	8.55
0.062	10.05	0.064	11.46
0.060	10.80	0.061	12.31
0.058	7.09	0.059	8.08
0.055	7.01	0.056	7.99
0.053	6.11	0.054	6.97
0.050	8.84	0.052	10.07
0.048	7.76	0.049	8.84
0.046	8.70	0.047	9.91
0.043	7.75	0.044	8.83
0.041	9.38	0.042	10.69
0.038	9.86	0.040	11.24
0.036	8.02	0.037	9.14
0.034	7.90	0.035	9.00
0.031	8.64	0.032	9.85
0.029	7.29	0.030	8.31
0.026	5.73	0.028	6.53
0.024	6.82	0.025	7.78
0.022	5.00	0.023	5.70
0.019	4.17	0.020	4.75
0.017	3.47	0.018	3.96
0.014	3.20	0.016	3.65
0.012	4.47	0.013	5.10
0.010	2.51	0.011	2.87
0.007	1.97	0.008	2.24
0.005	0.53	0.006	0.61
0.002	0.34	0.004	0.39
0.000	0.80	0.000	0.91

ReCMAS-3 1 hr (1300) -0.68 (air) **CMAS** cm from int.	ReCMAS-3 1 hr (1300) -0.68 (air) **CMAS** ppm Re	ReCMAS-4 4 hrs (1300) -0.68 (air) **CMAS** cm from int.	ReCMAS-4 4 hrs (1300) -0.68 (air) **CMAS** ppm Re
0.056	9.87	0.093	11.30
0.054	8.95	0.091	10.44
0.053	9.13	0.089	11.30
0.051	9.08	0.087	11.04
0.049	9.81	0.086	10.49
0.048	9.33	0.084	11.10
0.046	8.70	0.082	10.86
0.045	9.33	0.080	10.81
0.043	8.70	0.078	10.55
0.042	7.77	0.076	11.79
0.040	8.46	0.074	11.08
0.038	8.79	0.072	11.21
0.037	8.46	0.070	10.79
0.035	8.79	0.068	11.18
0.034	8.10	0.067	12.48
0.032	8.96	0.065	12.07
0.031	8.63	0.063	12.87
0.029	6.87	0.061	13.66
0.027	8.63	0.059	12.76
0.026	8.37	0.057	10.65
0.024	7.94	0.055	12.20
0.023	8.11	0.053	10.87
0.021	7.85	0.051	11.09
0.020	7.77	0.049	10.98
0.018	7.59	0.048	10.65
0.016	6.99	0.046	12.31
0.015	7.25	0.044	9.47
0.013	6.90	0.042	10.99
0.012	6.13	0.040	10.78
0.010	6.04	0.038	10.56
0.009	5.18	0.036	11.40
0.007	4.31	0.034	11.48
0.005	3.62	0.032	11.08
0.004	3.45	0.030	10.91
0.004	2.59	0.029	11.30
0.003	2.17	0.027	10.15
0.003	2.01	0.025	10.02
0.003	1.92	0.023	11.39

0.003	2.38	0.021	11.69
0.002	1.93	0.019	9.86
0.002	2.29	0.017	9.74
0.002	1.73	0.015	10.16
0.002	1.55	0.013	7.50
0.001	1.12	0.011	7.90
0.001	1.29	0.010	7.56
0.001	0.86	0.008	7.01
0.001	0.48	0.006	4.95
0.001	0.01	0.004	5.00
0.001	0.01	0.002	3.75
0.000	0.01	0.000	3.86

TableA2: Concentration (ppb/ppm) versus distance from melt/gas interface (cm from int) profiles for experiments used to determine Re, Pb, Cd, Tl, Sb and Te diffusion coefficients as a function of composition and temperature (Table 3.2).

BM056, 12 hr, 1300°C CMAS

cm from int.	Re (ppm)	Sb (ppm)	Tl (ppm)	Pb (ppm)	Cd (ppm)	Te (ppm)
0.108	0.86	8.01	0.80	8.65	8.68	10.92
0.106	1.02	7.52	0.90	8.87	10.36	10.68
0.103	1.03	8.55	0.89	8.75	8.91	13.60
0.101	1.04	7.73	0.92	10.07	8.59	12.96
0.099	1.03	8.42	0.69	9.88	6.74	13.03
0.097	0.98	8.30	0.89	9.57	6.91	10.85

0.095	0.90	9.00	0.89	10.05	7.76	13.02
0.092	0.96	9.72	0.88	9.18	10.99	15.58
0.090	1.14	7.92	0.82	9.20	6.47	13.54
0.088	1.07	7.67	0.72	9.07	8.45	12.75
0.086	1.17	8.26	0.78	9.49	9.71	14.78
0.084	1.00	8.50	0.92	8.92	7.96	12.84
0.081	1.00	8.33	0.90	9.90	6.57	13.13
0.079	1.07	9.92	1.01	9.12	7.79	14.81
0.077	0.81	7.83	0.78	9.34	6.51	11.95
0.075	0.97	9.48	0.73	9.44	8.57	13.11
0.073	1.10	8.83	0.88	9.77	6.04	13.58
0.070	1.17	8.77	0.90	10.35	6.69	13.55
0.068	1.13	9.17	0.98	9.17	9.24	14.06
0.066	1.09	9.49	0.77	10.17	7.04	13.17
0.064	1.16	9.41	0.88	10.38	7.40	14.48
0.062	1.05	9.35	0.87	9.17	6.34	14.76
0.059	1.20	8.96	0.89	8.47	7.83	13.59
0.057	1.17	8.47	0.79	9.47	6.20	13.98
0.055	0.91	9.67	0.86	8.83	5.94	14.58
0.053	0.96	10.02	0.69	8.20	7.25	17.02
0.051	0.98	9.48	0.69	8.74	6.62	17.11
0.048	0.99	8.15	0.68	8.55	4.70	13.81
0.046	0.88	8.34	0.67	7.32	6.50	13.78
0.044	1.05	9.52	0.67	8.07	4.48	16.83
0.042	1.14	8.92	0.66	7.78	6.85	16.14
0.040	1.03	8.84	0.64	6.59	6.26	15.89
0.037	0.99	9.46	0.67	7.52	6.11	12.99
0.035	1.15	8.43	0.63	6.78	5.52	14.18
0.033	0.94	9.49	0.70	6.42	5.30	14.77
0.031	0.98	8.67	0.63	7.22	4.63	12.63
0.029	0.96	9.98	0.59	7.15	5.64	14.07
0.026	1.11	8.52	0.62	6.32	3.75	11.83
0.024	0.93	9.01	0.55	6.65	5.00	13.52
0.022	0.81	8.11	0.55	6.61	4.83	10.94
0.020	0.80	9.34	0.39	6.96	4.33	11.97
0.018	0.62	7.40	0.42	5.16	5.60	10.54
0.015	0.66	7.10	0.40	4.78	4.30	11.71
0.013	0.64	6.87	0.39	4.73	4.66	9.67
0.011	0.55	7.56	0.34	4.70	2.82	8.09
0.009	0.50	7.21	0.32	4.28	4.09	6.13
0.007	0.35	6.70	0.27	3.91	2.75	5.70
0.004	0.44	5.74	0.21	3.25	2.27	4.80
0.002	0.31	6.26	0.22	3.42	2.06	4.21
0.000	0.26	5.06	0.17	3.32	1.88	3.43

BM055, 3 hr, 1300 °C CMAS

cm from int.	Re (ppm)	Sb (ppm)	Tl (ppm)	Pb (ppm)	Cd (ppm)	Te (ppm)
0.093	1.02	9.60	0.94	11.98	13.14	15.27
0.091	0.94	8.22	1.06	12.51	13.00	15.53
0.089	1.02	9.75	1.07	11.98	13.19	14.51
0.087	1.00	9.51	1.00	11.72	15.35	14.44
0.086	0.95	10.32	1.13	12.73	14.87	16.25
0.084	1.00	7.79	1.24	13.01	14.05	15.66
0.082	0.98	9.72	1.03	11.18	14.47	15.21
0.080	0.98	9.59	0.97	11.32	12.07	14.87
0.078	0.95	7.74	0.75	11.67	15.14	14.60
0.076	1.06	8.29	0.98	11.70	12.45	15.33
0.074	1.00	9.09	0.98	11.50	13.83	15.12
0.072	1.01	9.04	0.90	12.11	11.74	14.81
0.070	0.97	9.15	1.18	13.12	12.99	12.90
0.068	1.01	9.00	1.18	12.76	11.59	14.48
0.067	1.13	8.65	0.78	11.38	13.26	13.47
0.065	1.09	10.43	1.05	11.66	13.78	15.50
0.063	1.16	9.25	0.94	12.19	10.67	14.00
0.061	1.23	8.88	0.96	12.41	13.20	16.00
0.059	1.15	9.52	0.93	12.05	12.44	16.02
0.057	0.96	9.95	1.02	11.19	13.25	14.80
0.055	1.10	8.95	1.06	12.18	11.64	13.80
0.053	0.98	9.03	0.89	10.69	10.93	14.00
0.051	1.00	8.97	0.97	12.12	12.39	13.90
0.049	0.99	9.09	0.88	10.58	11.24	13.30
0.048	0.96	9.55	0.95	11.98	11.99	13.47
0.046	1.11	8.06	0.84	10.99	8.56	12.56
0.044	0.85	8.44	1.01	10.88	9.99	11.59
0.042	0.99	8.88	1.02	11.63	9.90	13.40
0.040	0.97	9.49	0.97	10.62	9.27	14.10
0.038	0.95	10.02	0.90	10.15	10.33	12.27
0.036	1.03	8.71	0.88	11.66	7.30	13.93
0.034	1.04	9.50	0.86	9.86	8.89	13.59
0.032	1.00	10.97	0.86	10.07	7.61	15.02
0.030	0.98	10.38	1.06	11.96	9.08	15.89
0.029	1.02	8.76	0.94	11.75	7.99	13.29
0.027	0.92	10.16	0.73	10.96	8.30	14.53
0.025	0.90	9.38	0.68	10.55	7.31	13.36
0.023	1.03	9.86	0.87	9.66	6.89	13.82
0.021	1.05	10.07	0.71	9.76	5.68	14.11
0.019	0.89	8.08	0.66	8.32	6.56	12.05
0.017	0.88	9.07	0.68	8.33	6.28	10.83
0.015	0.92	8.92	0.68	8.70	7.58	12.29

0.013	0.68	8.21	0.63	8.56	6.12	10.38
0.011	0.71	8.91	0.47	7.85	6.19	9.18
0.010	0.68	8.32	0.44	5.75	4.78	7.56
0.008	0.63	7.75	0.36	5.71	4.73	7.26
0.006	0.45	6.77	0.38	5.74	4.55	6.36
0.004	0.45	7.15	0.30	5.15	3.46	5.83
0.002	0.34	7.02	0.28	4.43	2.85	5.00
0.000	0.35	6.28	0.20	4.05	2.56	3.38

BM052, 6 hr, 1300°C CMAS

cm from int.	Re (ppm)	Sb (ppm)	Tl (ppm)	Pb (ppm)	Cd (ppm)	Te (ppm)
0.176	0.89	9.33	1.04	10.94	9.85	11.69
0.173	0.77	10.34	1.06	11.12	11.10	11.22
0.169	0.69	10.11	1.10	11.45	9.40	13.16
0.166	0.84	10.33	1.11	10.91	9.99	11.90
0.162	1.03	10.16	1.16	10.74	10.10	10.49
0.158	0.82	10.05	1.00	11.66	10.10	11.01
0.155	0.92	9.74	0.97	10.48	10.93	12.20
0.151	0.85	9.66	1.11	11.14	11.28	12.96
0.148	0.74	10.70	1.01	10.95	9.81	13.65
0.144	0.87	8.97	0.78	9.75	9.91	10.99
0.140	0.91	10.44	0.94	10.29	9.18	11.37
0.137	0.80	9.17	0.95	10.71	9.66	13.03
0.133	0.83	10.79	1.07	10.77	10.64	8.92
0.130	0.85	9.84	0.91	11.45	9.02	14.32
0.126	0.71	10.32	1.07	10.94	11.14	13.05
0.122	0.82	8.96	0.88	10.17	10.63	12.59
0.119	0.95	10.13	1.07	10.63	7.47	13.32
0.115	0.78	9.04	0.94	10.48	8.18	14.71
0.112	0.86	11.16	1.13	11.08	9.78	11.17
0.108	0.73	10.26	0.94	9.51	9.56	13.44
0.104	0.86	9.77	0.84	9.03	9.14	13.21
0.101	0.93	9.76	0.92	10.01	8.72	12.99
0.097	1.01	12.13	1.08	10.77	10.11	16.41
0.094	0.97	9.88	1.02	10.45	10.07	12.50
0.090	0.88	9.66	0.82	9.30	6.81	14.75
0.086	0.96	11.09	0.96	10.80	8.99	14.14
0.083	0.88	10.79	0.91	10.77	9.03	14.84
0.079	0.80	9.47	0.77	9.04	6.47	12.92
0.076	0.81	9.78	0.98	9.13	9.72	12.60
0.072	0.97	10.01	0.99	9.95	7.71	14.97

0.068	0.92	10.66	0.85	8.94	8.10	14.53
0.065	0.90	11.45	0.88	8.98	7.51	13.73
0.061	0.64	9.61	0.82	9.39	6.60	12.91
0.058	0.91	11.13	0.89	8.88	5.75	13.41
0.054	0.99	11.11	0.83	8.99	7.92	14.62
0.050	0.78	9.76	0.69	7.70	5.30	12.06
0.047	0.98	9.95	0.70	7.30	6.43	11.81
0.043	0.83	9.92	0.73	8.05	6.91	11.38
0.040	0.70	10.95	0.78	7.69	7.21	12.84
0.036	0.77	9.02	0.59	7.91	6.03	9.67
0.032	0.70	9.65	0.55	7.36	6.67	10.04
0.029	0.82	10.28	0.63	6.61	6.42	11.42
0.025	0.71	10.35	0.60	6.53	5.78	10.18
0.022	0.70	8.02	0.48	6.13	4.65	9.93
0.018	0.70	8.47	0.44	6.33	5.69	10.35
0.014	0.65	8.72	0.40	6.35	5.11	7.87
0.011	0.56	9.55	0.42	5.40	3.96	7.63
0.007	0.48	8.50	0.40	5.03	4.14	7.08
0.004	0.61	7.30	0.31	4.66	4.57	6.49
0.000	0.29	6.59	0.30	4.38	3.59	6.21

BM072,24 hr,1300°C CMAS

cm from int.	Re (ppm)	Sb (ppm)	Tl (ppm)	Pb (ppm)	Cd (ppm)	Te (ppm)
0.118	1.26	10.69	1.55	13.64	9.23	31.56
0.115	0.97	9.93	1.58	15.20	7.56	35.79
0.113	1.15	9.74	1.40	14.33	8.08	28.15
0.110	0.91	10.74	1.42	13.18	6.59	30.88
0.108	0.90	9.40	1.43	13.63	5.24	29.42
0.106	0.78	10.17	1.37	13.93	5.08	31.53
0.103	1.13	10.15	1.51	14.68	7.43	35.04
0.101	1.26	9.55	1.54	13.80	8.55	28.96
0.098	1.02	9.95	1.37	14.43	6.03	30.74
0.096	1.26	10.38	1.58	14.60	7.42	37.25
0.094	1.08	9.68	1.53	13.26	5.15	35.19
0.091	1.06	9.70	1.39	13.42	5.31	33.94
0.089	1.03	9.26	1.16	14.08	5.13	35.23
0.086	1.12	9.13	1.30	13.18	6.69	31.10
0.084	0.97	9.76	1.47	13.67	7.76	32.37
0.082	1.38	10.11	1.29	12.69	3.97	29.46
0.079	1.26	9.52	1.46	12.81	6.45	38.58

0.077	0.91	10.28	1.33	13.33	5.98	34.05
0.074	0.90	9.99	1.32	13.45	5.64	35.26
0.072	1.37	12.18	1.69	17.16	5.51	54.13
0.070	0.97	12.19	1.79	16.68	3.55	57.37
0.067	1.15	10.72	1.20	12.11	3.90	36.17
0.065	0.96	10.00	1.39	11.14	3.27	29.31
0.062	1.28	9.97	1.32	12.47	6.08	36.31
0.060	1.38	10.85	1.14	11.11	5.83	31.52
0.058	0.91	10.06	1.03	12.10	2.41	30.04
0.055	0.90	9.73	1.27	11.41	4.15	28.93
0.053	0.78	10.65	1.32	10.10	4.94	30.30
0.050	1.13	9.67	1.12	10.19	4.65	26.61
0.048	0.99	10.88	0.84	9.50	4.03	35.70
0.046	1.11	9.28	1.18	9.98	4.10	27.09
0.043	0.99	8.44	0.80	8.94	2.42	27.35
0.041	1.20	8.80	0.87	9.20	4.48	14.85
0.038	1.26	7.88	0.77	7.93	3.72	14.84
0.036	1.02	7.88	0.52	8.71	2.17	10.95
0.034	1.01	8.02	0.69	8.15	3.42	14.84
0.031	1.10	7.11	0.57	7.47	4.15	11.32
0.029	0.93	6.87	0.64	7.64	4.20	14.75
0.026	0.73	6.05	0.51	6.51	2.05	8.64
0.024	0.87	6.68	0.38	6.57	1.93	9.64
0.022	0.64	6.75	0.56	5.98	4.29	4.44
0.019	0.53	5.23	0.46	5.74	2.53	6.60
0.017	0.44	5.36	0.45	4.97	2.00	3.70
0.014	0.41	5.42	0.47	4.93	2.58	6.71
0.012	0.57	5.88	0.20	4.18	1.07	4.34
0.010	0.32	5.87	0.27	5.47	2.34	7.08
0.007	0.25	5.28	0.23	4.28	2.89	3.41
0.005	0.07	5.09	0.11	4.13	3.03	6.64
0.002	0.04	4.42	0.01	3.46	1.16	3.55
0.000	0.10	4.63	0.11	3.33	1.66	2.15

BM067, 6hr, 1350°C CMAS

cm from int.	Re (ppm)	Sb (ppm)	Tl (ppm)	Pb (ppm)	Cd (ppm)	Te (ppm)
0.127	1.10	11.09	0.98	12.36	6.81	22.24
0.125	1.12	10.23	1.08	10.94	6.51	22.62
0.122	1.21	10.70	1.28	11.73	9.62	20.79
0.120	1.17	11.70	0.97	11.50	6.60	22.29

0.117	1.09	10.71	0.90	10.85	6.11	18.92
0.114	1.11	9.78	0.94	12.10	8.44	22.14
0.112	1.00	8.78	0.89	11.27	8.83	24.73
0.109	1.03	10.70	1.01	10.93	6.97	27.29
0.107	1.12	11.06	0.91	10.63	5.82	19.61
0.104	1.14	10.12	0.90	10.57	8.46	22.37
0.101	1.16	10.88	0.77	9.79	5.85	22.47
0.099	1.10	10.52	0.83	10.09	5.97	20.33
0.096	1.04	9.77	0.85	10.56	9.72	23.74
0.094	1.00	10.78	0.83	9.96	7.85	19.23
0.091	1.02	11.46	1.01	9.59	6.30	21.26
0.088	1.06	11.99	0.92	10.56	7.08	22.16
0.086	1.12	11.19	1.00	12.16	6.45	22.25
0.083	1.10	11.31	0.80	9.21	8.17	21.17
0.081	1.18	10.77	0.87	11.35	7.18	21.37
0.078	1.07	11.13	1.15	9.36	5.26	21.29
0.075	1.11	12.38	0.91	10.05	5.67	22.03
0.073	1.07	9.22	0.93	9.00	5.39	23.76
0.070	1.19	10.30	0.81	10.83	5.18	20.51
0.068	1.08	10.24	0.79	9.20	6.08	19.80
0.065	1.11	10.54	0.76	6.81	5.82	24.83
0.062	1.20	10.00	0.76	8.47	5.94	18.96
0.060	1.26	10.61	0.86	8.03	4.50	21.68
0.057	1.06	9.45	0.76	7.59	4.35	22.18
0.055	0.91	10.76	0.75	6.85	5.01	18.25
0.052	0.88	10.65	0.58	6.79	4.53	18.05
0.049	0.96	9.44	0.63	6.08	3.79	16.24
0.047	1.01	9.99	0.56	7.39	3.74	20.00
0.044	0.91	8.60	0.65	6.09	5.22	15.47
0.042	0.74	9.24	0.43	6.71	5.65	15.07
0.039	0.72	8.63	0.43	5.25	4.97	14.56
0.036	0.87	7.65	0.51	5.22	2.59	14.40
0.034	0.87	8.68	0.46	5.34	2.09	13.88
0.031	0.69	6.98	0.45	4.85	2.25	11.54
0.029	0.63	7.44	0.39	4.85	2.90	11.80
0.026	0.53	6.53	0.33	4.30	2.17	15.05
0.023	0.57	6.55	0.40	4.11	3.41	9.21
0.021	0.52	6.99	0.28	3.76	1.90	9.49
0.018	0.55	6.42	0.24	3.34	2.77	12.45
0.016	0.57	5.50	0.25	3.43	2.04	8.60
0.013	0.47	5.56	0.24	3.56	3.55	8.54

0.010	0.41	6.47	0.22	3.43	0.92	7.68
0.008	0.32	6.82	0.25	2.52	1.69	5.88
0.005	0.25	4.51	0.15	2.40	2.79	4.56
0.003	0.23	5.11	0.13	2.95	2.04	6.48
0.000	0.19	5.10	0.17	2.48	1.13	4.79

BM069, 6 hr, 1350°C CMAS

cm from int.	Re (ppm)	Sb (ppm)	Tl (ppm)	Pb (ppm)	Cd (ppm)	Te (ppm)
0.093	0.99	9.78	0.84	11.78	6.62	21.57
0.091	1.01	8.92	0.94	10.36	6.32	21.95
0.089	1.10	9.39	1.14	11.15	9.43	20.12
0.087	1.06	10.39	0.83	10.92	6.41	21.62
0.086	0.98	9.40	0.76	10.27	5.92	18.25
0.084	1.00	8.47	0.80	11.52	8.25	21.47
0.082	0.89	7.47	0.75	10.69	8.64	24.06
0.080	0.92	9.39	0.87	10.35	6.78	26.62
0.078	1.01	9.75	0.77	10.05	5.63	18.94
0.076	1.03	8.81	0.76	9.99	8.27	21.70
0.074	1.05	9.57	0.63	9.21	5.66	21.80
0.072	0.99	9.21	0.69	9.51	5.78	19.66
0.070	0.93	8.46	0.71	9.98	9.53	23.07
0.068	0.89	9.47	0.69	9.38	7.66	18.56
0.067	0.91	10.15	0.87	9.01	6.11	20.59
0.065	0.95	10.68	0.78	9.98	6.89	21.49
0.063	1.01	9.88	0.86	11.58	6.26	21.58
0.061	0.99	10.00	0.66	8.63	7.98	20.50
0.059	1.07	9.46	0.73	10.77	6.99	20.70
0.057	0.96	9.82	1.01	8.78	5.07	20.62
0.055	1.00	11.07	0.77	9.47	5.48	21.36
0.053	0.96	7.91	0.79	8.42	5.20	23.09
0.051	1.08	8.99	0.67	10.25	4.99	19.84
0.049	0.97	8.93	0.65	8.62	5.89	19.13
0.048	1.00	9.23	0.62	6.23	5.63	24.16
0.046	1.09	8.69	0.62	7.89	5.75	18.29
0.044	1.15	9.30	0.72	7.45	4.31	21.01
0.042	0.95	8.14	0.62	7.01	4.16	21.51
0.040	0.80	9.45	0.61	6.27	4.82	17.58
0.038	0.77	9.34	0.44	6.21	4.34	17.38
0.036	0.85	8.13	0.49	5.50	3.60	15.57
0.034	0.90	8.68	0.42	6.81	3.55	19.33

0.032	0.80	7.29	0.51	5.51	5.03	14.80
0.030	0.63	7.93	0.29	6.13	5.46	14.40
0.029	0.61	7.32	0.29	4.67	4.78	13.89
0.027	0.76	6.34	0.37	4.64	2.40	13.73
0.025	0.76	7.37	0.32	4.76	1.90	13.21
0.023	0.58	5.67	0.31	4.27	2.06	10.87
0.021	0.52	6.13	0.25	4.27	2.71	11.13
0.019	0.42	5.22	0.19	3.72	1.98	14.38
0.017	0.46	5.24	0.26	3.53	3.22	8.54
0.015	0.41	5.68	0.14	3.18	1.71	8.82
0.013	0.44	5.11	0.10	2.76	2.58	11.78
0.011	0.46	4.19	0.11	2.85	1.85	7.93
0.010	0.36	4.25	0.10	2.98	3.36	7.87
0.008	0.30	5.16	0.08	2.85	0.73	7.01
0.006	0.21	5.51	0.11	1.94	1.50	5.21
0.004	0.14	3.20	0.01	1.82	2.60	3.89
0.002	0.12	3.80	0.00	2.37	1.85	5.81
0.000	0.08	3.79	0.03	1.90	0.94	4.12

BM057, 1 hr, 1250°C CMAS

cm from int.	Re (ppm)	Sb (ppm)	Tl (ppm)	Pb (ppm)	Cd (ppm)	Te (ppm)
0.056	0.93	10.74	0.85	11.08	8.64	22.14
0.054	0.99	9.74	0.83	10.48	8.25	18.92
0.053	1.05	9.93	0.77	10.63	5.92	21.62
0.051	1.03	9.88	1.01	9.21	9.72	20.12
0.049	1.01	10.68	0.83	12.16	5.97	21.95
0.048	0.92	10.15	0.85	10.56	5.85	23.09
0.046	0.96	9.47	0.83	9.59	8.46	21.36
0.045	1.07	10.15	0.77	9.96	5.82	20.62
0.043	0.99	9.47	0.90	10.56	6.97	26.62
0.042	1.01	8.46	0.76	10.09	8.83	24.06
0.040	0.95	9.21	0.83	9.79	8.44	21.47
0.038	0.93	9.57	1.14	10.57	6.11	18.25
0.037	0.99	9.21	0.94	10.63	6.60	21.62
0.035	1.05	9.57	0.80	11.58	9.62	20.12
0.034	0.94	8.81	1.00	9.98	6.51	21.95
0.032	1.01	9.75	0.92	9.01	6.81	23.09
0.031	0.92	9.39	1.01	9.38	6.90	21.36
0.029	0.89	7.47	0.83	9.98	6.68	20.62
0.027	1.00	9.39	0.85	9.51	6.40	20.70

0.026	0.98	9.11	0.83	9.21	5.97	20.50
0.024	1.06	8.64	0.77	9.99	6.11	21.58
0.023	0.95	8.83	0.90	10.05	5.69	21.49
0.021	1.01	8.54	0.91	10.35	5.47	20.59
0.020	0.91	8.45	1.01	10.69	5.40	18.56
0.018	0.89	8.26	0.89	11.52	4.98	23.07
0.016	0.93	7.61	0.11	10.21	4.69	20.65
0.015	0.99	7.89	0.93	10.14	4.27	22.21
0.013	1.05	7.51	0.83	9.02	4.05	19.77
0.012	1.03	6.67	0.84	9.12	3.56	19.99
0.010	1.01	6.57	0.71	7.71	3.13	16.88
0.009	0.92	5.63	0.65	7.10	2.84	16.30
0.007	0.98	4.70	0.56	6.08	2.13	13.33
0.005	0.93	3.94	0.47	5.07	1.85	11.11
0.004	0.86	3.76	0.43	4.66	1.42	10.22
0.004	0.83	2.82	0.37	4.06	1.56	8.88
0.003	0.76	2.36	0.34	3.75	1.35	8.22
0.003	0.66	2.19	0.28	3.04	1.21	6.00
0.003	0.68	2.08	0.25	2.77	1.28	5.97
0.003	0.64	2.59	0.23	2.49	1.06	10.66
0.002	0.59	2.10	0.20	2.13	0.78	4.89
0.002	0.63	2.49	0.19	2.03	0.92	4.44
0.002	0.49	1.88	0.18	1.91	0.71	3.98
0.002	0.46	1.69	0.17	1.81	0.54	4.00
0.001	0.39	1.22	0.12	1.31	0.67	2.89
0.001	0.34	1.41	0.12	1.36	0.47	3.50
0.001	0.31	0.94	0.08	0.91	0.31	2.44
0.001	0.24	0.53	0.09	1.01	0.41	2.22
0.001	0.20	0.01	0.08	0.89	0.11	1.10
0.001	0.26	0.01	0.05	0.60	0.31	1.40
0.000	0.10	0.01	0.00	0.01	0.23	0.10

BM065, 3 hr, 1250°C CMAS

cm from int.	Re (ppm)	Sb (ppm)	Tl (ppm)	Pb (ppm)	Cd (ppm)	Te (ppm)
0.024	1.00	12.21	0.88	11.93	10.29	23.83
0.023	1.07	11.07	0.85	11.28	9.82	20.37
0.023	1.12	11.29	0.80	11.44	7.05	23.27
0.022	1.10	11.23	1.04	9.91	11.58	21.66
0.022	1.08	12.14	0.85	13.09	7.12	23.63
0.021	0.99	11.54	0.88	11.37	6.97	24.85

0.021	1.03	10.77	0.85	10.32	10.07	22.99
0.021	1.15	11.54	0.80	10.72	6.93	22.20
0.020	1.06	10.77	0.93	11.37	8.30	28.65
0.020	1.09	9.62	0.78	10.86	10.52	25.90
0.019	1.03	10.47	0.85	10.54	10.05	23.11
0.019	1.00	10.88	1.18	11.38	7.28	19.64
0.018	1.07	10.47	0.97	11.44	7.86	23.27
0.018	1.12	10.88	0.83	12.47	11.45	21.66
0.017	1.01	10.02	1.03	10.74	7.76	23.63
0.017	1.08	11.09	0.95	9.69	8.11	24.85
0.016	0.99	10.68	1.04	10.10	8.21	22.99
0.016	0.95	8.49	0.85	10.74	7.96	22.20
0.015	1.07	10.68	0.88	10.24	7.62	22.28
0.015	1.05	10.36	0.85	9.92	7.11	22.07
0.014	1.14	9.82	0.80	10.75	7.28	23.23
0.014	1.02	10.04	0.93	10.82	6.77	23.13
0.013	1.09	9.72	0.94	11.14	6.52	22.16
0.013	0.98	9.61	1.05	11.51	6.44	19.98
0.012	0.96	9.39	0.92	12.40	5.93	24.83
0.012	1.00	8.65	0.12	10.99	5.59	22.23
0.011	1.07	8.97	0.96	10.91	5.08	23.91
0.011	1.12	8.54	0.86	9.71	4.83	21.28
0.010	1.10	7.58	0.87	9.82	4.23	21.52
0.010	1.08	7.47	0.73	8.29	3.73	18.17
0.009	0.99	6.41	0.67	7.64	3.39	17.55
0.009	1.05	5.34	0.58	6.55	2.54	14.34
0.009	1.00	4.48	0.48	5.46	2.20	11.95
0.008	0.93	4.27	0.44	5.02	1.69	11.00
0.008	0.89	3.20	0.39	4.37	1.86	9.56
0.007	0.82	2.68	0.36	4.04	1.61	8.85
0.007	0.71	2.49	0.29	3.27	1.44	6.46
0.006	0.74	2.37	0.26	2.98	1.52	6.43
0.006	0.68	2.95	0.24	2.68	1.26	11.48
0.005	0.63	2.39	0.20	2.29	0.93	5.26
0.005	0.68	2.83	0.19	2.18	1.10	4.78
0.004	0.53	2.14	0.18	2.05	0.85	4.28
0.004	0.50	1.92	0.17	1.95	0.64	4.30
0.003	0.42	1.39	0.12	1.41	0.80	3.11
0.003	0.37	1.60	0.13	1.46	0.56	3.77
0.002	0.33	1.07	0.09	0.98	0.36	2.63
0.002	0.26	0.60	0.10	1.09	0.49	2.39

0.001	0.21	0.01	0.08	0.96	0.14	1.18
0.001	0.28	0.01	0.06	0.64	0.37	1.51
0.000	0.11	0.01	0.00	0.01	0.28	0.11

NMAS1, 6 hr, 1300°C **NMAS**

cm from int.	Re (ppm)	Sb (ppm)	Tl (ppm)	Pb (ppm)
0.074	2.36	3.43	0.26	3.08
0.072	2.51	3.64	0.14	3.09
0.071	3.58	5.49	0.52	3.56
0.069	2.25	4.23	0.19	3.13
0.068	2.98	3.53	0.42	3.23
0.066	1.99	2.81	0.33	3.33
0.065	2.56	3.47	0.33	3.00
0.063	2.09	2.83	0.51	2.74
0.062	2.38	3.59	0.19	2.39
0.060	3.73	4.41	0.27	3.75
0.059	2.01	2.70	0.32	2.79
0.057	2.52	4.31	0.41	3.06
0.056	2.48	4.51	0.40	2.47
0.054	2.39	2.90	0.33	3.32
0.053	2.70	3.43	0.47	3.01
0.051	2.70	4.23	0.11	2.64
0.050	3.18	4.19	0.37	3.59
0.048	2.04	4.21	0.19	3.59
0.047	2.38	3.16	0.29	2.21
0.045	1.38	2.46	0.06	2.56
0.044	2.57	2.21	0.15	2.98
0.042	2.21	2.12	0.19	2.09
0.041	2.49	3.62	0.23	2.43
0.039	1.94	3.50	0.29	2.41
0.038	1.71	2.76	0.30	2.81
0.036	1.21	3.12	0.17	2.27
0.035	1.18	3.20	0.12	1.57
0.033	2.92	2.91	0.27	2.68
0.032	1.42	2.74	0.31	2.81
0.030	2.16	3.06	0.11	2.73
0.029	1.04	1.98	0.32	3.06
0.027	2.28	2.78	0.20	1.99
0.026	1.73	3.81	0.17	2.63
0.024	2.16	3.10	0.16	3.45
0.023	1.48	2.69	0.22	2.81
0.021	2.79	2.81	0.13	1.95
0.020	1.60	2.79	0.03	3.72
0.018	1.07	2.76	0.15	2.90

0.017	1.67	3.07	0.09	2.40
0.015	1.33	3.21	0.15	2.18
0.014	1.09	2.56	0.09	2.63
0.012	1.01	2.42	0.06	3.02
0.011	0.88	2.97	0.05	2.47
0.009	1.00	3.48	0.10	2.53
0.008	1.00	2.61	0.06	1.94
0.006	0.51	2.43	0.12	2.93
0.005	1.26	2.99	0.04	2.33
0.003	0.53	2.39	0.15	1.43
0.002	0.78	2.11	0.03	2.27
0.000	0.68	1.84	0.04	1.39

NMAS2, 1 hr, 1300°C **NMAS**

cm from int.	Re (ppm)	Sb (ppm)	Tl (ppm)	Pb (ppm)
0.078	7.56	6.78	1.05	8.79
0.077	6.65	7.60	1.45	8.30
0.075	6.12	6.86	1.38	6.52
0.074	7.15	6.03	1.38	5.60
0.072	6.66	8.43	1.08	6.88
0.070	7.91	5.94	0.89	7.24
0.069	9.98	10.39	1.81	8.69
0.067	8.45	8.91	1.00	7.38
0.066	7.84	9.10	0.96	6.86
0.064	5.71	6.20	0.85	6.08
0.062	6.44	6.05	0.77	7.87
0.061	7.29	6.15	1.40	7.51
0.059	8.23	6.36	0.85	5.87
0.058	11.14	6.77	1.41	6.92
0.056	6.96	6.94	0.79	5.29
0.054	8.03	6.88	1.09	6.66
0.053	6.53	6.55	0.84	4.41
0.051	6.54	6.39	0.68	6.29
0.050	7.39	6.74	0.95	6.53
0.048	7.16	6.60	1.45	6.49
0.046	7.27	6.31	0.95	6.36
0.045	8.66	6.11	0.82	6.80
0.043	7.19	5.75	0.93	5.66
0.042	6.00	6.25	1.16	5.22
0.040	6.87	5.84	0.99	7.09
0.038	6.32	4.78	0.61	4.41
0.037	5.73	4.49	0.99	5.43
0.035	8.17	5.11	1.11	6.24
0.034	8.07	6.14	0.79	5.36

0.032	6.71	4.90	0.57	4.98
0.030	5.96	4.36	0.61	4.65
0.029	7.65	5.33	0.56	5.37
0.027	6.28	6.33	0.42	3.83
0.026	6.62	4.51	0.61	4.38
0.024	4.96	4.53	0.28	3.24
0.022	5.51	5.11	0.70	2.95
0.021	5.77	4.87	0.27	3.63
0.019	4.10	3.22	0.76	2.65
0.018	5.00	4.74	0.39	3.34
0.016	4.55	3.97	0.37	3.20
0.014	4.29	4.18	0.66	2.57
0.013	4.30	5.09	0.34	4.48
0.011	2.97	3.83	0.10	2.73
0.010	3.73	4.33	0.16	3.22
0.008	3.65	3.65	0.11	2.65
0.006	2.39	3.77	0.32	2.37
0.005	2.69	4.05	0.15	2.22
0.003	2.13	2.78	0.32	2.50
0.002	1.75	3.48	0.09	2.04
0.000	1.41	1.93	0.08	1.90

NMAS4, 3 hr, 1300°C		**NMAS**		
cm from int.	Re (ppm)	Sb (ppm)	Tl (ppm)	Pb (ppm)
0.093	4.84	4.74	0.91	2.91
0.091	4.58	5.06	0.78	3.08
0.089	4.44	4.68	0.75	3.12
0.087	4.77	4.82	0.79	2.59
0.085	4.47	5.48	0.76	2.91
0.083	4.81	4.37	0.74	2.58
0.081	4.58	5.19	0.84	2.76
0.079	4.64	5.00	0.81	2.88
0.077	4.99	4.84	1.01	2.58
0.076	4.29	4.87	0.86	2.53
0.074	4.52	5.07	0.76	2.73
0.072	5.34	4.94	0.70	2.85
0.070	4.20	4.90	0.95	2.51
0.068	3.97	4.48	0.73	2.23
0.066	4.64	3.92	0.63	2.29
0.064	4.25	4.18	0.64	2.34
0.062	4.17	4.65	0.57	2.33
0.060	4.30	4.49	0.72	2.40

0.059	4.23	4.14	0.63	2.26
0.057	4.43	4.43	0.66	2.16
0.055	4.23	4.29	0.59	2.24
0.053	4.25	4.82	0.62	2.12
0.051	4.06	4.12	0.57	2.13
0.049	4.63	4.84	0.53	2.24
0.047	3.99	4.35	0.60	2.05
0.045	3.85	3.91	0.57	1.79
0.043	3.25	3.65	0.40	1.54
0.042	3.46	3.77	0.49	1.99
0.040	3.47	4.06	0.43	1.96
0.038	3.26	3.63	0.40	1.97
0.036	3.64	3.75	0.45	1.92
0.034	2.92	3.36	0.44	1.47
0.032	3.17	3.73	0.45	1.71
0.030	2.94	3.15	0.45	1.48
0.028	3.01	3.12	0.37	1.59
0.026	3.37	3.66	0.39	1.46
0.025	3.19	3.68	0.36	1.34
0.023	2.94	3.44	0.28	1.21
0.021	3.35	3.43	0.40	1.41
0.019	2.97	2.78	0.25	1.32
0.017	2.67	3.05	0.26	1.33
0.015	2.70	2.43	0.30	1.04
0.013	2.01	2.94	0.26	1.22
0.011	2.26	2.55	0.33	1.15
0.009	2.04	2.48	0.21	1.02
0.008	1.89	2.67	0.19	0.90
0.006	1.74	1.97	0.20	0.75
0.004	1.63	2.14	0.10	0.67
0.002	1.61	2.11	0.18	0.72
0.000	1.15	1.39	0.09	0.58

NMAS5, 3 hr, 1200°C		**NMAS**		
cm from int.	Re (ppm)	Sb (ppm)	Tl (ppm)	Pb (ppm)
0.090	5.12	6.46	1.33	6.24
0.088	4.81	5.92	1.05	5.25
0.086	5.37	5.73	1.09	5.65
0.084	5.11	6.11	1.09	5.58
0.082	5.31	5.80	1.04	5.50

0.081	5.40	6.31	1.12	5.42
0.079	6.15	6.92	1.00	5.83
0.077	5.32	6.77	1.00	5.51
0.075	5.46	6.36	0.93	5.26
0.073	5.68	6.58	1.10	5.45
0.071	5.42	5.50	0.93	4.99
0.070	5.06	6.11	1.02	5.21
0.068	5.63	6.52	0.96	5.16
0.066	5.54	6.13	0.84	4.83
0.064	5.64	6.14	0.82	4.89
0.062	5.81	6.01	0.88	4.87
0.060	5.22	6.40	0.79	4.54
0.059	5.07	5.97	0.88	4.72
0.057	5.02	6.88	1.07	5.34
0.055	5.35	6.77	0.93	5.33
0.053	5.15	6.18	0.77	4.47
0.051	4.94	6.27	0.78	4.75
0.049	5.22	6.59	0.77	4.57
0.048	5.20	6.32	0.70	4.46
0.046	5.41	7.65	0.82	5.10
0.044	5.63	7.85	0.79	4.38
0.042	4.93	6.90	0.74	4.99
0.040	5.79	7.26	0.73	4.69
0.038	5.54	8.10	0.80	4.99
0.037	5.75	7.49	0.84	4.69
0.035	5.98	7.87	0.71	4.52
0.033	5.34	7.51	0.65	4.35
0.031	5.47	6.83	0.62	4.05
0.029	4.92	7.19	0.48	4.19
0.027	4.87	6.44	0.48	3.94
0.026	4.64	6.40	0.42	3.45
0.024	4.90	6.62	0.50	3.64
0.022	4.31	6.50	0.60	3.74
0.020	4.52	5.83	0.44	4.02
0.018	4.02	5.31	0.39	3.33
0.016	3.81	5.91	0.40	2.90
0.015	4.43	5.94	0.39	3.11
0.013	3.94	5.78	0.32	2.95
0.011	3.86	4.95	0.37	2.82
0.009	3.74	4.52	0.27	2.41
0.007	3.08	4.76	0.27	2.51
0.005	3.24	4.53	0.16	2.36
0.004	3.33	4.82	0.25	2.31

0.002	3.32	5.37	0.24	2.63
0.000	3.41	4.65	0.24	2.51

NMAS6, 16 hr, 1200°C NMAS

cm from int.	Re (ppm)	Sb (ppm)	Tl (ppm)	Pb (ppm)
0.098	4.17	4.77	0.19	2.90
0.096	4.49	5.98	0.10	3.24
0.094	4.00	4.56	0.12	3.08
0.092	4.59	5.60	0.12	3.10
0.090	4.52	4.97	0.19	3.43
0.088	4.63	4.91	0.16	2.85
0.086	4.47	5.00	0.26	2.76
0.084	4.37	4.85	0.17	2.75
0.082	4.50	5.34	0.21	3.04
0.080	4.29	5.51	0.11	2.59
0.078	4.27	5.06	0.14	2.90
0.076	3.98	4.98	0.17	2.92
0.074	4.20	5.47	0.16	2.93
0.072	4.68	5.61	0.17	2.99
0.070	3.73	4.86	0.17	2.66
0.068	4.07	4.30	0.14	2.93
0.066	3.44	4.32	0.15	2.67
0.064	4.15	5.55	0.06	2.82
0.062	3.55	4.40	0.13	2.48
0.060	3.70	4.49	0.12	2.29
0.058	3.67	4.04	0.16	2.36
0.056	3.43	4.62	0.08	2.36
0.054	2.96	3.93	0.14	2.41
0.052	3.01	4.16	0.12	2.18
0.050	2.79	4.67	0.12	2.16
0.048	2.68	4.01	0.07	2.07
0.046	2.42	3.75	0.15	1.99
0.044	2.59	4.30	0.12	2.13
0.042	2.49	4.16	0.09	2.14
0.040	2.28	3.54	0.10	1.55
0.038	2.06	3.04	0.04	1.83
0.036	2.28	3.58	0.08	1.99
0.034	2.23	3.31	0.05	1.62
0.032	2.29	3.55	0.07	1.72
0.030	2.05	3.90	0.07	1.71

0.028	1.65	2.97	0.08	1.75
0.026	1.61	2.76	0.05	1.66
0.024	1.76	2.85	0.11	1.80
0.022	1.70	3.01	0.08	1.58
0.020	1.47	2.48	0.04	1.33
0.018	1.47	2.82	0.03	1.39
0.016	1.44	2.75	0.06	1.61
0.014	1.20	2.51	0.09	1.31
0.012	1.15	2.84	0.07	1.08
0.010	1.07	2.62	0.04	1.17
0.008	0.90	1.79	0.04	0.96
0.006	0.76	2.50	0.07	0.90
0.004	0.68	1.92	0.07	1.00
0.002	0.51	1.90	0.02	0.74
0.000	0.47	1.90	0.05	0.92